Stable thrombus formation on irradiated microvascular endothelial cells using vascular targeting agents under pulsatile flow: pro-thrombotic treatment for brain arteriovenous malformations

Sinduja Subramanian

(M. Tech, Biotechnology)

A thesis submitted in fulfillment of the requirements for the degree of

Doctor of Philosophy

Supervisor: Prof. Marcus Stoodley

Associate supervisor: Dr Zhenjun Zhao

Co-supervisor: Dr Lucinda McRobb

Department of Clinical Sciences

Faculty of Medicine and Health Sciences

MACQUARIE University

Declaration of originality

I hereby declare that the work presented in this thesis has not been submitted for a higher degree to any other university or institution. To the best of my knowledge this submission contains no material previously published or written by another person, except where due reference is stated otherwise. Any contribution made to the research by others is explicitly acknowledged.

Sinduja Subramanian

Department of Clinical Sciences

Faculty of Medicine and Health Sciences

Macquarie University

27 November 2018

Abstract

Background: Brain arteriovenous malformations (AVMs) are a leading cause of intracranial haemorrhage in children and young adults. Limitations of current treatment approaches leave one third of AVM patients at risk. The overall goal of this work is to develop a radiation-guided vascular targeting treatment for AVMs. Externalised phosphatidylserine and alpha-crystallin B (CRYAB) have been identified as potential biomarkers on the endothelium of irradiated AVM blood vessels. It was hypothesised that these molecules could be selectively targeted after AVM radiosurgery with ligand-directed pro-thrombotic vascular targeting agents (VTAs) to achieve localised thrombosis and rapid occlusion of pathological AVM vessels. Pre-testing of novel VTAs may be more economically and ethically performed *in vitro.*

Aim 1: To establish an *in vitro* parallel-plate flow chamber system using whole blood for VTA testing.

Aim 2: To develop and test the efficacy of pro-thrombotic VTAs targeting phosphatidylserine and CRYAB on irradiated endothelial cells under flow.

Methods: Conjugates were prepared by Lys-Lys cross-linking of thrombin with annexin V targeting phosphatidylserine, or with an anti-CRYAB antibody. Cerebral microvascular endothelial cells were irradiated (5 Gy, 15 Gy, and 25 Gy) and after 1 or 3 days assembled in a parallel-plate flow chamber containing whole human blood and conjugate (1.25 µg/mL or 2.5 µg/mL). Confocal microscopy was used to assess thrombus formation after flow via binding and aggregation of fluorescently-labelled platelets or fibrinogen.

Results and conclusions: Both annexin V-thrombin and anti-CRYAB-thrombin VTAs induced rapid thrombosis on irradiated endothelial cells under flow. Thrombosis was greatest at the highest combined doses of radiation and conjugate. Annexin V-thrombin induced

moderate thrombus stimulation even at the lowest radiation dose. These molecules and their developed VTAs appear suitable for further testing in animal models. The parallel-plate flow chamber proved to be a simple and cost-effective method to pre-test pro-thrombotic vascular targeting agents prior to preclinical studies.

List of Abbreviations

ALK-1	Activin receptor-like kinase (ALK-1 genes)
AVMs	Arteriovenous malformations
BSA	Bovine serum albumin
CLU	Clusterin
CRYAB	Alpha-B Crystallin
CT	Computed tomography
EBM-2	Endothelial basal medium
ELISA	Enzyme-linked immunosorbent assay
ENG	Endoglin
ENPP3	Ectonucleotide Pyrophosphatase/ pyrophosphodiesterase
FDP	Fibrin degradation product
FITC	Fluorescein isothiocyanate
HCMEC	Human cerebral microvascular endothelial cells
HHT	Hereditary haemorrhagic telangiectasia
ICAM-1	Intercellular cell adhesion molecule 1
IFN-γ	Interferon-gamma
IL-2	Interleukin-2
LINAC	Linear accelerator
MMP	Matrix metalloprotease
MRI	Magnetic resonance imaging
MUH	Macquarie university hospital
PBS	Phosphate buffered saline
PDIA6	Protein disulphide isomerase

PFA	Paraformaldehyde
PS	Phosphatidylserine
R6G	Rhodamine 6G
SDS-PAGE	Sodium dodecyl sulfate polyacrylamide gel electrophoresis
SRS	Stereotactic radiosurgery
TCO	Trans-cyclooctene
TF	Tissue Factor
TM	Thrombomodulin
TFPI	Tissue factor pathway inhibitor
TNF-α	Tumour necrosis factor- alpha
Tz	Tetrazine
VCAM	vascular cell adhesion molecules
VEGF	Vascular endothelial growth factor
vWF	von Willebrand Factor
VTA	Vascular targeting agents
VT	Vascular targeting
WSS	Wall shear stress

List of publications/presentations

Publications

S. Subramanian, S. O. Ugoya, Z. Zhao, L. S. McRobb, G. E. Grau, V. Combes, D. W. Inglis, A. J. Gauden, V. S. Lee, V. Moutrie, E. D. Santos and M. A. Stoodley. Stable thrombus formation on irradiated human cerebral microvascular endothelial cells under pulsatile flow: pre-testing annexin V-thrombin conjugate for treatment of brain arteriovenous malformations. (Thrombosis Research, accepted on May 2018).

S. Subramanian, L. S. McRobb, Z. Zhao, G. E. Grau, V. Combes, D.W. Inglis, A.J. Gauden, V.S. Lee, V. Moutrie, E.D Santos and M.A Stoodley. Validation of new molecular targets on irradiated endothelial cells: development and testing of an anti-CRYAB antibody-thrombin conjugate under flow for the treatment of brain arteriovenous malformations. (In preparation).

L.S. McRobb, M. J. McKay, A. J. Gauden, V. S. Lee, **S. Subramanian**, S. G. Thomas, M. Wiedmann, V. Moutrie, E. D. Santos, Z. Zhao, M. P. Molloy, M. A. Stoodley. Radiation- stimulated markers on the endothelial surface provide potential vascular targets in brain arteriovenous malformations. (In Preparation).

A. J. Gauden, V. S. Lee, L. S. McRobb, Z. Zhao, G. E. Grau, **S. Subramanian**, V. Moutrie, M. A. Stoodley. Vascular targeting of phosphatidylserine causing occlusion in an arteriovenous malformation animal model. (In preparation).

Conference and Symposia Presentations

S. Subramanian, Z. Zhao, L. McRobb, V. Moutrie, M. Stoodley. Pro-thrombotic treatment for brain arteriovenous malformations: *in vitro* testing of conjugate. Innovations in Radiation Applications, University of Wollongong, 2017.

S. Subramanian, Z. Zhao, L. McRobb, A. Gauden, V. Moutrie, G. Grau, M.A. Stoodley. Vascular targeting as a new approach for the treatment of brain arteriovenous malformations. XIII World Congress of Neurology, Kyoto, 2017.

S. Subramanian, Z. Zhao, L. McRobb, A. Gauden, V.S. Lee, V. Moutrie, D. Inglis, V. Combes, G. Grau, M. A. Stoodley. Developing a new treatment for brain arteriovenous malformations. 12th International Conference on Cerebral Vascular Biology, Melbourne, 2017.

A. J. Gauden, V.S. Lee, **S. Subramanian,** V. Moutrie, Z. Zhao, L. McRobb, M. A. Stoodley. Vascular targeting of phosphatidylserine translocation causing thrombosis in an arteriovenous malformation animal model. Neurological Society Annual Scientific Meeting, Adelaide, 2017.

A. J. Gauden, V. S. Lee, **S. Subramanian**, V. Moutrie, Z. Zhao, L. McRobb, M. A. Stoodley. Ligand vascular targeting of phosphatidylserine translocation in an arteriovenous malformation animal model. Australian Vascular Biology Society, Queensland, 2017.

S. Subramanian, Z. Zhao, L. McRobb, A. Gauden, V.S. Lee, V. Moutrie, D. Inglis, V. Combes, G. Grau, M.A. Stoodley. Vascular targeting treatment for brain arteriovenous malformations: *in vitro* testing of conjugates. Early Career Research Symposia, Macquarie University, 2017.

Acknowledgments

I would like to express my sincere gratitude to my supervisor Professor Marcus Stoodley for providing me with a great opportunity to work on this project. His valuable advice and continuous encouragement have motivated me to work with great freedom in a friendly environment to share my thoughts and ideas more conveniently. I feel very great and thankful for his continuous support, guidance and patience, throughout my candidature that strengthened my knowledge and skills.

I would like to thank my Associate Supervisor, Dr Zhenjun Zhao for his patience, kind support and guidance in this project. His constant feedback and direction to the approach was very helpful in facilitating the experiments. He has always been so kind in supervising and sharing his thoughts.

I would like to express my gratitude to my Co-Supervisor Dr Lucinda McRobb for her kind support and continuous encouragement throughout my candidature which has helped me to gain more confidence in completing this project. She has spent her valuable time discussing my findings and carefully reviewing the manuscript/thesis. Her moral support and positive feedback has greatly influenced me to improve the depth of knowledge in the subject area and to stand up as a well-recognised researcher.

I would also like to thank Professor Georges Grau, Dr David Inglis, and Dr Valery Combes for their valuable feedback and suggestions with the experimental methods and techniques. Their constant support was highly useful in bringing up this project in a good shape and take forward to a next level more easily.

I would like to thank Dr Sarah Hemley, Dr Magdalena Lam, Joel Berliner and Shinuo Liu for helping me with imaging techniques and analysis. Also, they were so helpful in giving valuable

suggestions and ideas during trouble-shooting. Thanks also go to Vivienne Lee and Andrew Gauden for their kind help and assistance in the lab with more sharing of thoughts and information.

I would like to extend my thanks to Vaughan Moutrie and Daniel Santos for their kind help in radiating my cells throughout this project. The way they gave preference to the research team by booking special sessions apart from their busy schedule with patients was highly appreciated.

I would like to thank all the blood donors for their kindness and patience in spending their valuable time to give blood for my experiments. It would not be possible to progress this work without their help and support.

Also, I would like to acknowledge the entire Macquarie Neurosurgery team for their support. My special thanks to Kate Morkel for her moral support and patience in booking appointments with my Professor whenever I wanted, without any hesitation.

I would like to thank everyone in FMHS for helping me at various times. Thanks to Viviana Bong, Collette Tosen, Laura Newey, Lucy Lu, Tamara Leo, Louise Marr and Mitchell Borton for administering and organising the office/lab very well. I greatly appreciate their helping tendency at any time that made me to work in a more convenient way. Also, I would like to thank Sumudu Gangoda, Anna Guller, and Jude Amalraj, for their help, motivation and support.

I would like to acknowledge Macquarie University for providing me with such a great opportunity and excellent infrastructure to carry out my research. Thanks to Macquarie University research training scholarship for providing me with a stipend for living expense and National Health Medical Research Council (NHMRC) their financial support of this project.

Last but not least, my Special thanks to my loving parents Meenakumari and Subramanian and my grandparents Srinivasan and Rajeswari who encourage me with their great affection throughout that helped me to pursue this PhD. I would like to thank my loving husband Pradeep who cared about me and shared some of the household responsibility to reduce my burden. Special thanks to my daughter Kethana Pradeep who unknowingly supported me in this PhD journey by making me smile and laugh during the stressful conditions. Also, I would like to extend my thanks to my respectful in-laws Ananthi, Rajendran, Prashanth, Niveditha and baby Kridyuth for their kindness and support.

Overall, I completely enjoyed this journey with all the support and blessings from everyone. It is not that easy to express my feeling and happiness. Thanks to everyone who made this journey more valuable and memorable.

All the figures in the Chapter 1 thesis were professionally created for Prof Stoodley's group to communicate the research work. I would like to acknowledge Stoodley's group for giving me the permission to use these figures in my thesis.

Table of Contents

Chapter 1

1. Introduction

1.1 Preface

Brain arteriovenous malformations (AVMs) are vascular malformations associated with a major risk of haemorrhage in younger members of the population. Current treatments can be effective but for various reasons leave one-third of patients at risk. Vascular targeting (VT) was proposed in this study as a possible approach to AVM treatment with radiation as a priming mechanism to induce endothelial surface changes, since AVM themselves have no distinct molecular features for targeting. VT in AVMs requires initial identification of radiation-induced target proteins on the endothelial surface that discriminate these vessels from normal vasculature, and the development of VT agents that combine a ligand or antibody to such target molecules, with pro-thrombotic factors (eg, thrombin, the effector). The overall goal is being to induce thrombosis selectively in these abnormal vessels to create occlusion and AVM cure.

Having previously identified a series of radiation-stimulated targets, the aim of the current study was to develop new pro-thrombotic ligand/antibody conjugates specific to identified targets and to develop and optimise an *in vitro* parallel-plate flow system that would allow pre-testing of each agent's efficacy in endothelial binding and thrombus formation under high flow conditions in the presence of whole blood. This would allow more economical, ethical, and efficient assessment of novel conjugates prior to pre-clinical animal studies. Hence, the purpose of this research is to develop and test the efficacy of pro-thrombotic conjugates in inducing thrombosis on irradiated brain microvascular endothelial cells using an *in vitro* parallel-plate flow chamber. In this chapter, AVMs are introduced as a clinical problem and the literature reviewed with respect to the development of VT with radiation priming as an approach to AVM treatment.

1.2 Brain AVMs

1.2.1 Pathology and pathophysiology

AVMs can occur in all parts of the central nervous system but larger ones most frequently occur in the brain in the area supplied by the middle cerebral artery [1]. AVMs consist of direct connections between arteries and veins without an intervening capillary network resulting in tangled collections of abnormal blood vessels called the "nidus" (Figure 1.1), which involve complex twists connected by one or more fistulae [2]. This causes dynamic changes where relatively weak-walled veins are unable to resist the high pressure from arterial blood resulting in progressive venous dilation from arterial pulsation [3]. McCormick described large AVMs as a "bag of worms", with markedly thick-walled and dilated venous channels projecting into the parenchyma [1]. Observation of AVMs shows the thickening of veins with no damage to the elastic lamina of the arterial intimal layer [4] and other studies have demonstrated microvessel accumulation, disordered collagen, intimal hyperplasia, and venous enlargement [5, 6]. Dural feeding arteries can be twisted and enlarged showing fibrous thickening in the intima and adventitia where artery-like thickening of venous walls occurs due to internal high pressure of arterial blood flow directly to the veins [7]. Brain AVMs are often described as complicated or poorly developed blood vessels in which there are also many cases of multiple brain AVMs with multiple nidi containing either deep or cortical lesions [8].

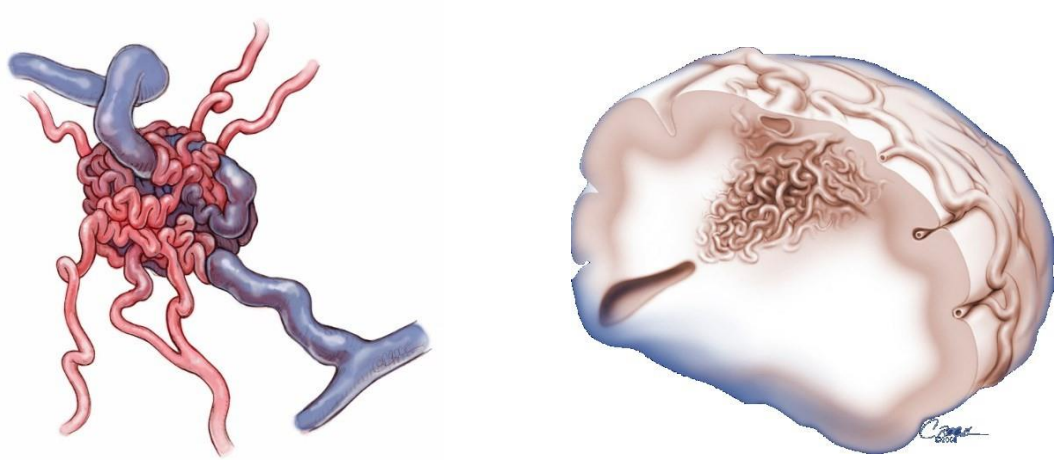

Figure 1.1: Arteriovenous malformations. Direct connection of arteries and veins without intervening capillaries forming tangled collections of abnormal vessels. Figure courtesy of Professor Marcus Stoodley.

Some studies have examined the haemodynamic derangements in AVMs and their association with clinical outcomes, in particular the issue of arteriovenous shunting of blood in which the arterial pulses are mediated directly to the venous side [9]. Various AVM animal models have been developed to study the blood flow, intracranial hypoperfusion, and the role of venous hypertension. From a clinical point of view, venous hypertension in AVMs is more likely to be associated with the occlusion of venous outflow compared to arteriovenous shunting [10-12]. Many recent studies have focused attention on venous drainage, AVM size, feeding arterial pressure and their significance on the pathophysiology of haemorrhage. Both deep venous drainage and size are considered as independent predictors of haemorrhage [13-16]. In contrast, some authors report that haemorrhage is more likely with superficial rather than deep venous drainage [17, 18]. Though feeding arterial pressure has a weak correlation with the size of a lesion, higher arterial pressure appears to be associated with a high risk of bleeding compared to lower arterial pressure [19]. Aneurysms are often associated with AVMs, resulting from the haemodynamic changes in AVM vessels that weaken the arterial wall [20]. The annual risk of haemorrhage has been reported to be 8.3% for patients with associated aneurysms and 2.4% for patients without associated aneurysms [21].

1.2.2 Aetiology

The cause of AVMs remains poorly understood. They are thought to be congenital in origin with the potential to grow and progress with time, with the vessels maintaining a form of vascular immaturity. Although AVMs may be present at birth, symptoms usually do not become evident until the second decade of life [22]. This suggests that either these lesions actually develop after birth or have not grown sufficiently before birth to be detectable or induce symptoms [23, 24]. There are cases reported of *de novo* development of AVMs with no abnormal vascularity observed on prior MRI [25, 26] and some cases with pre-existing vascular abnormalities that developed into full AVMs later in life [27, 28]. One interesting case report revealed the development of a de novo AVM in a 9-year old girl within 4 years of experiencing mild head injury [29]. These findings indicate that lesions may appear and develop de novo. AVMs may be present but sometimes remain undetected suggesting that either they are too small for detection or current diagnostic methods might be too insensitive to detect AVMs during the early stages of development [24, 30].

Recent studies have reported genetic factors in AVM development that have a role in vascular remodeling and vasculogenesis [31-33]. Hereditary haemorrhagic telangiectasia (HHT) is an autosomal dominant genetic disorder with clinical manifestations resulting in formation of AVMs that can occur anywhere in the body. The estimated prevalence in the general population is reported to be one or two cases per 100,000, with a mutation rate of 2 to 3 per million [34-36]. As described previously, multiple AVMs have been reported in many cases [8, 37-39], but are most commonly associated with HHT [40-42]. Patients with HHT are at increased risk of developing brain AVMs, with an incidence of 7.9% brain AVMs noted out of 215 cases of HHT in one study [43]. Mutations in endoglin (ENG) and activin receptor-like kinase (ALK-1) genes, that are part of the transforming growth factorβ (TGF-β) signaling pathway, cause HHT type 1 (HHT1) and HHT type 2 (HHT 2), respectively, where TGF-ß plays an important

role in angiogenesis and vasculogenesis [44-47]. HHT with associated juvenile polyposis has also been associated with mutations in SMAD4, also an important component in TGF-ß signaling [48, 49]. Impairment of these genes also leads to abnormal angiogenesis resulting in HHT angiodysplasia where factors such as vascular endothelial growth factor (VEGF) and angiopoietin-2 (Ang-2) play important roles [50].

Studies on AVM phenotypes in non-HHT patients also suggest an aberrant angiogenic-like phenotype with overexpression of VEGF, a growth factor responsible for vasculogenesis and angiogenesis [51, 52], consistent with abnormal vessel development or maturation that may be inherent or instigated by injury and sustained by haemodynamic or hypertensive forces. On comparing AVM endothelial cells with normal endothelial cells, it was found that they have active vascular remodeling with a higher Ki-67 proliferative index and endothelial cell turnover [53]. Proliferation of AVM endothelial cells was greater with over-expressing pro-angiogenic growth factors compared to normal brain endothelial cells (BECs) with highly activated AVM endothelium expressing high levels of VEGF-A with overexpressed VEGF receptors 1 and 2. Further, functional angiogenesis assays using AVM-derived BECs show the development of shorter, dysfunctional tubules compared to normal BECs [52]. Other immunohistochemical studies have reported higher levels of AVM endothelial proliferation and angiogenesis with an increased level of angiogenesis in partially obliterated AVMs, as well as strong expression of VEGF in brain AVMs [54]. VEGF is also found to have association with regrowth of AVMs post radiosurgery [55]. Surgical specimens from 10 AVMs out of 112 patients showed strong expression of integrin αß1 in endothelium and sub-endothelium with moderate expression of integrin αß3 and αß5 on analysis by immunohistochemical staining [56]. These integrins are also commonly associated with angiogenic vessels.

The Notch signaling pathway is a fundamental pathway also with an important role in vascular development and physiology [57, 58]. To date, four Notch family receptors and five ligands

have been identified in mammals where specific expression of Notch pathways ligands and receptors in vascular endothelium confirm its role in vascular development and haemostasis [59-61]. Upregulation of Notch4 was reported in endothelial cells and smooth muscle cells of human adult brain AVMs suggesting that this signalling is involved at some stage of the development of human brain AVMs [62]. This was further confirmed using mouse embryos with conditional activation of the Notch I gene in endothelial cells which has exhibited abnormal vascular remodelling resulting in AVMs [63].

Genetic studies in non-HHT patients have identified the influence of single nucleotide polymorphisms (SNPs) in several genes associated with risk of AVM rupture resulting in intracranial haemorrhage (ICH) [64-66]. Achrol et al. reported the involvement of SNPs in the increased risk of ICH after brain AVMs diagnosis [32]. Other studies have associated tumour necrosis factor- alpha-238G>A (TNF-α-238G>A) and apolipoprotein E2 (ApoE e2) genotypes with 3.5-fold and 3.2-fold increases in the risk of post-treatment ICH [67]. Many of these SNPs associate with rupture risk but do not necessarily contribute to our understanding of initial formation of AVMs [68].

1.2.3 Epidemiology

The incidence of AVMs is reported to be 0.89 – 1.34 cases per 100,000 persons per year with a prevalence of less than 0.1% of the population [69-71] and a mortality rate ranging from 6% to 20% [72-74]. The annual rate of bleeding in AVM patients ranges from 2 to 4% with a mean age of patients dying from AVM-related haemorrhage of 44.4 years [75]. Haemorrhage occurs most commonly between the ages of 10 and 40 [37]. Life survival analyses in 217 with a mean follow up of 10.4 years reported a 42% risk of haemorrhage, 29% risk of death, 18% risk of epilepsy, followed by 27% risk of other neurological deficits by 20 years after diagnosis [72]. Brown and colleagues studied the natural history of a patient population with unruptured intracranial AVMs and reported that 11% of patients with AVMs

less than 3.4 cm ruptured, compared to 18% and 19% of patients with 3.4 – 5 cm and more than 5.5 cm, respectively. They also reported 2.2% mean risk of hemorrhage per year with increase in recurrent hemorrhage over time [76]. Several studies have reported that patients who initially present with haemorrhage have a higher risk of subsequent haemorrhage [15, 72, 73].

1.3 Clinical presentation

Haemorrhage, headache and seizure are the most common initial presentations of patients with brain AVMs [77]. Patients with an initial haemorrhage symptom also followed with seizure, headache and other neurological deficits [78] with the chances of developing residual epilepsy [79]. Previous studies associated the greater likelihood of patients with small AVMs presenting with haemorrhage and patients with large lesions presenting with epilepsy [80]. Seizure is a common symptom which is not included as morbidity, but patients with preoperative seizures are more likely to have them continue after surgery [81]. The association of AVMs with headache is not yet understood but occipital AVMs carry a high risk for migraine-like headache with visual symptoms [82]. The risk of other neurological disorders varies from 8% to 17% after 10 years which may develop as an immediate neurological handicap resulting from an initial haemorrhage or a late progressive consequence [80].

1.4 Diagnosis

Brain AVMs can be diagnosed by cerebral angiography, CT (Computed Tomography) scanning, and MRI (Magnetic Resonance Imaging). Angiography is required for evaluating the angioarchitectural characteristics of AVMs [2]. The extent of haemorrhage and specific anatomical position of AVMs are well determined on CT [83]. MRI is useful in assessing the morphology of specific lesions and demonstrates the relationship of small cerebral AVMs with the surrounding brain and ventricles (Figure 1.2) [84]. Brain AVMs can be completely

asymptomatic in some patients but are detected incidentally after imaging for other medical reasons.

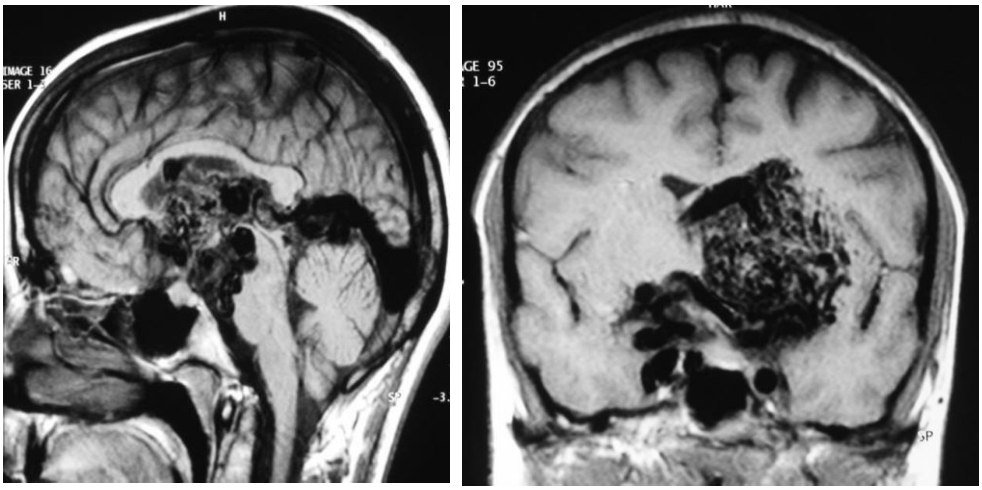

Figure 1.2: MRI image of a Grade V AVM. Figure courtesy of Professor Marcus Stoodley.

1.5 Classification of AVMs

To predict the risk of morbidity and mortality of AVM patients undergoing surgery, a grading system is currently in use called 'Spetzler-Martin grading system' [85]. According to the system, the lesions are classified from Grade I to Grade V based on their size, pattern of venous drainage and neurological eloquence of the brain regions adjacent to them [85]. Grade I and II have low risk and can be handled with microsurgery alone [86-88] whereas Grade IV and V are associated with higher morbidity and mortality rates [85, 89, 90]. Lesions of 3 – 6 cm diameter in eloquent locations have morbidity rates higher than expected for other Grade III and more likely Grade IV AVMs, while AVMs of <3 cm diameter with deep venous drainage in eloquent locations have lower morbidity rates than expected for Grade III lesions [91, 92]. No treatment was recommended for 75% of the patients with Grade IV and Grade V AVMs because of the high risk [93].

Some of the other proposed grading scales include Lawton's modified Spetzler-Martin Grading Scheme [94], AVM related intracerebral haemorrhage (AVICH) [95], Lesion-to-Eloquence (LED) [96], and Buffalo score [97]. However, the Spetzler-Martin scheme is most frequently used to predict outcomes after AVM surgery [85]. Then, to predict the complication and risk of AVM radiosurgery, Pollock and Flickinger in 2002 proposed Radiosurgery Based AVM Score (RBAS) to predict the chances of complete AVM obliteration without any risk of acquiring new deficits which was later modified based on AVM volume, patient age and location [98, 99]. Some of the other grading scales are Heidelberg score [100], Virginia Radiosurgery Score (VRAS) [101], and Proton Based Stereotactic Radiosurgery Score (PBAS) [102]. A comparative study of 5 different grading scores (RBAS, PBAS, VRAS, Heidelberg Score and Spetzler-Martin) was made with respect to their ability to predict the functional outcome after SRS without any risk. RBAS and PBAS proved successful in predicting the radiosurgical outcome by considering possible neurological conditions compared to other scales [103].

Overall, grading scale has proven to be a simple and accurate approach to predict the risk from surgical/radiosurgical morbidity and mortality rates before considering the treatment.

1.6 Current treatments for AVMs

Brain AVMs are currently treated with microsurgery, radiosurgery or endovascular embolisation. The main aim of treatment is to prevent haemorrhage. Choice of treatment is based on the nidus size, eloquence of adjacent brain and the presence of deep venous drainage [104].

1.6.1 Microsurgical resection

Microsurgical resection remains the gold standard technique for small and easily accessible AVMs by dissecting the nidus along with direct feeders thereby removing the lesions completely [105]. Surgical resection provides complete protection against further haemorrhage [77, 106, 107]. Small AVMs can typically be safely operated using surgery with low mortality and morbidity. Factors that are significant in determining the surgical accessibility of the AVM lesion include size, pattern of venous drainage, and eloquence of the adjacent brain regions to the AVM [85]. A study examining 110 patients reported that complete obliteration was achieved in 99% of patients with small AVMs with 17% moderately disabled [87]. Whereas with 320 patients, 19% underwent surgery with lesion size less than 3 cm in diameter, regardless of their location, and 45% of the lesions present in the surgically inaccessible areas of the brain. Angiographic results revealed complete obliteration in 94% of these patients with a surgical morbidity of 1.5% with no mortality [88].

1.6.2 Endovascular embolisation

Endovascular embolisation is a treatment to occlude blood flow in AVM vessels using catheters that deposit occlusive materials into the feeding arteries and nidus. This can be carried out alone but may typically be used before surgery or radiosurgery as an adjunctive treatment to shrink the AVM nidus and prevent bleeding [108]. Embolic liquids such as isobutyl-2-cyanoacrylate (IBCA), N-butyl cyanoacrylate (NBCA) ethylene vinyl alcohol copolymer, histoacryl, and onyx are commonly used agents [109-112]. A successful embolisation reduces the size of the lesion, occludes deep feeding vessels, and reduces intraoperative haemorrhage [113]. Though most AVMs can be embolised, partial embolisation with combined surgery or radiosurgery has more convincing functional outcomes except for AVMs with small size nidus [114]. Some post- embolisation results correlate with intra-embolic recanalisation followed

by melting of the clots trapped with the glue of isobutyl-2-cyanoacrylate (IBCA) [115]. The key factor in the prevention of nidus recanalisation is the ability of the embolic agent to penetrate deep into the nidus rather than just occluding its feeders [110].

1.6.3 Stereotactic radiosurgery (SRS)

In general, radiation causes damage to living tissues by changing cellular structure and damaging DNA thereby leading to prolonged cell injury and death [116]. This procedure is widely utilised in cancer therapy for causing tumour necrosis [117]. However, it also carries a high risk of affecting surrounding healthy cells by causing severe injury and inflammation [118]. Hence, stereotactic radiosurgery gamma unit was first installed with cobalt 60 as an efficient way to deliver a narrow-focused beam of radiation to a precise target volume [119].

In AVM treatment, SRS is considered as an effective alternative to microsurgery in treating small AVMs [120]. This technique is characterised by accurate delivery of high doses of radiation with a sharp dose fall-off outside the target volume using various technologies such as gamma knife, linear accelerators and proton beam (Figure 1. 3) [121, 122]. AVM obliteration is achieved by radiosurgery via endothelial cell proliferation, increasing vessel wall thickening, and eventual luminal closure [123-125]. Vaso-occlusive effects of radiosurgery are believed to slowly initiate from endothelial proliferation, progressive wall thickening, and luminal closure [126]. The primary change in AVMs after standard radiation treatment is the endothelial damage which includes separation of the endothelial lining from the vessel wall which creates a subendothelial space containing proteinaceous material [125, 127]. Irradiated endothelial cells have also been observed to contain numerous filopodia, abundant lysosomes and other cytoplasmic vesicles with a hyalinised basement membrane and smooth muscle cells showing bundles of proliferating microfilaments [128]. Both proliferative and degenerative

changes have been observed in irradiated AVM vessels with spindle-shaped cell populations resembling myofibroblasts following tissue granulation [127]. A rodent model of AVMs was developed recently to study the morphological changes in AVM vessels after irradiation which showed increased collagen layering and fibro-hyalinised internal elastic lamina in the model nidus [129]. These radiation-induced changes resulted in upregulation of cellular pro-coagulant activity and tissue factor expression following re-endothelialisation, platelet activation, and fibrin deposition thereby leading to post-irradiation thrombosis [130].

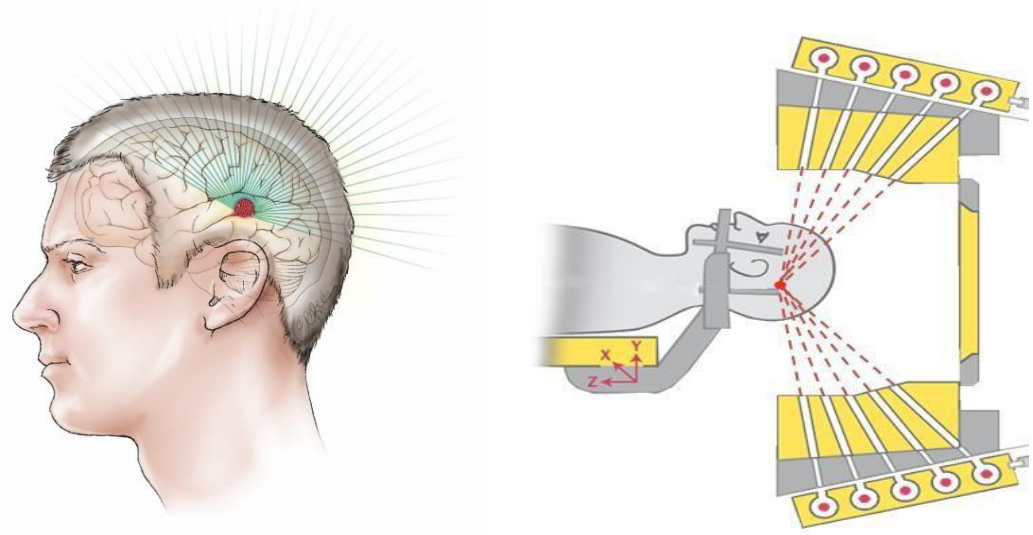

Figure 1. 3: Radiosurgery of AVM vessels: focused beam of radiation from multiple directions. Figure courtesy of Professor Marcus Stoodley. (Simonian et al, 2004, MOJ Proteomics & Bioinformatics)

It is possible to achieve complete obliteration using SRS with a latency period of around 2 – 3 years where some studies reported complete obliteration rates of more than 90% in small AVMs and 30% in large AVMs during the latency period of 1 – 3 years [131, 132]. For Spetzler-Martin Grade II – IV AVMs, radiosurgery is considered a treatment option with 43 – 85% of obliteration rates at 4 years after a single treatment [133-136]. Deeply located AVMs of <4 cm^3 can be treated safely and effectively using radiosurgery with low morbidity but may require repeated treatments for complete obliteration [137].

1.7 Limitations and risks of current AVM treatment

1.7.1 Limitation of microsurgery

Although surgical resection of AVM lesions can be effective, surgery remains challenging for lesions in eloquent regions [138]. Surgical risk for large and deeply located lesions involves reoccurrence of arterial bleeding from the nidus even after all major feeders are thought to have been occluded [33]. Hence not all AVMs can be safely treated by surgery [90].

1.7.2 Limitation of endovascular embolisation

Endovascular therapy carries a risk of causing infarction of normal brain parenchyma distal to the AVM nidus. The most common cause of complications associated with embolisation is ischemia due to occlusion of normal vessels [139]. Further, there is possibility of post-embolised recanalisation with the evidence of 2 to 19% reported where the rate of recanalisation was related to the type of embolic agents, method of embolisation, and type of vascular lesion [140-144] In one study of 233 patients treated with endovascular procedures, 14% had neurological deficits with 2% being continuous disabling deficits, while 1% died after the treatment [145]. It is possible for a patient to have an additional risk when undergoing pre-operative embolisation where worsening of a pre-existing deficit is evaluated as a new deficit. The proposed Spetzler-Martin grading scheme has also been applied to assess complication risk from embolisation. It is also important to note that the risk-to-benefit ratio for pre-operative embolisation may vary for high grade Spetzler-Martin lesions compared to Grade I lesions [146]. Hartmann et al. reported 4% out of 116 patients with residual AVMs after the combined endovascular and surgical treatment where one of the patient experienced haemorrhage within 3 months of surgery resulting in mild neurological deficit [111]. Further, 11% from 201 patients died or had a permanent neurological deficit as a result of embolisation with a follow-up period

of 11 years [147]. Overall morbidity and mortality rates for embolisation vary from 6 to 28% and 1 to 8% respectively [148, 149].

1.7.3 Limitation of stereotactic radiosurgery

Although radiosurgery is a good therapeutic option, it is not effective for AVMs greater than 25 mm in diameter [150]. Another limitation of standard radiosurgery is long latency periods until complete obliteration is achieved, with some cases reported to have no closure even after 5 – 8 years [151-154]. Friedmann et al. reported a latency period of 2 or 3 years to achieve complete obliteration [155] and the risk of haemorrhage is not reduced until complete obliteration is achieved [131]. Therefore, a dose response curve was constructed in a study and reported 50% obliteration at 15 Gy and 80% at 22 Gy [156]. Still it has been open to question whether and to what extent the risk is reduced during this period as compared to the risk before radiosurgery [157-160]. This was clearly demonstrated in a study where 42 of 500 patients had haemorrhage before radiosurgery, 23 of 458 patients experienced haemorrhage during the latency period, while 6 of 250 patients experienced haemorrhage after obliteration [133].

Apart from a long latency period, haemorrhagic risk, and low obliteration rates, radiosurgery also has limitation with respect to the off-target effects. Kihlstrom et al. reported late radiation effects as abnormalities after AVM radiosurgery [161]. This may be due to the off-target effects resulting in brain necrosis which depend on target doses and treatment volume [75, 150, 162, 163]. The risk of complications in normal tissues increases with volume radiated [164, 165]. Therefore, it is important to use in-field obliteration as a final predictor for analysing significant radiobiological result which depend mainly on minimum target dose but does not seem to vary much with volume or maximum dose [166]. Complications after radiosurgery treatment mainly depend on the lesion location and dose [167].

Advances in standard radiosurgical techniques are unlikely to improve accuracy and off-target effects at high doses. Although treatment with fractionated doses is an option for some larger AVMs that are untreatable by other methods, rates of occlusion are greater with higher single doses [75, 150, 166]. However, higher dose carries a high risk of late radiation effects. At the same time, lowering the prescribed marginal dose is also associated with reduced obliteration rate [168]. Hence, the marginal dose used clinically is 15 – 25 Gy with no decrease in the obliteration observed above 25 Gy [169]. In some cases, AVMs stay unresponsive even after 3 years which may be due to various factors such as radiobiological resistance, lesion size, location, venous drainage, and patient age [151].

1.8 Other potential treatments

Although the cause of AVMs and its progression are still unclear, it is well known that AVMs are also associated with some angiogenic markers due to venous hypertension as mentioned earlier. Recently, inhibition of angiogenesis has been used as a therapeutic goal in AVMs since cellular and molecular mechanisms of angiogenesis stay distinguishable in various tissues, as in cancer [170, 171]. In one study, 2 methoxyestradiol (2-ME) was used as an anti-angiogenic treatment for AVMs using an intracranial venous hypertension rat model and cultured human umbilical vein endothelial cells under anoxic conditions. They successfully reported the inhibition of hypoxia/anoxia-induced angiogenesis by 2-ME considering it as a potential choice as an adjunct therapy for AVMs [172]. Other anti-angiogenic drugs such as Sirolimus, vascular endothelial growth factor (VEGF) pathway inhibitors, interferon or matrix metalloproteinase (MMP) inhibitors were shown to prevent the growth of remaining AVM nidus after partial removal when used before or after treatment [173]. Sirolimus (Rapamycin) was first used in the treatment of metastatic renal cell carcinoma where it inhibits angiogenesis through altering the mammalian target of rapamycin (mTOR) intracellular signal pathway [174, 175]. MMPs play an important role in angiogenesis as they are required to break down extracellular matrix

to allow vessel growth and expansion, and high levels of MMP activity in AVM vessels results in progressive AVM growth and bleeding [176]. MMP inhibitor doxycycline was used prior to AVM resection where it resulted in decrease of MMP-9 in AVM tissues [177]. Bevacizumab (a VEGF inhibitor) is a humanised monoclonal antibody directed against human VEGF which has been approved by the Food and Drug Administration (FDA) in the USA and used as the first anti-angiogenic drug to increase the survivability of cancer patients [178, 179]. VEGF levels were observed to be increased in resected AVM specimens and Bevacizumab treatment for AVMs proved to reduce the vessel density and dysplastic vessels by abrogating VEGF signaling [180]. However, although Bevacizumab has been approved by FDA for cancer treatment, 3.1% of cancer patients suffered haemorrhage after receiving Bevacizumab, with three patients dying from severe pulmonary haemorrhage [181]. Although, only bleeding with no death reported in AVMs, Bevacizumab has been considered for very careful use for the treatment [182]. Complications associated with bleeding and rupture have also been noted for other anti-mitogenic agents such as Paclitaxel, Carboplatin and Bevacizumab [183-185].

1.9 Medial management and risk reduction in AVM treatment

There are obviously limitations to the current interventions used for AVM treatment as reviewed above. There has always been some argument that simple medical management of AVMs to address symptoms and reduce haemorrhage risk may be a better way, at least in previously unruptured AVMs, and whether it is possible to prevent the situation becoming more severe at the early stage by considering and managing various risk predictors. Haemodynamic aneurysms seem to be an acquired pathology and serve as an indicator for intracranial haemorrhage from AVM nidus [186]. The natural history of associated aneurysms after AVM obliteration remains unpredictable, since they may get worse over time, but may also stay unresponsive, grow or rupture [187-190]. The haemodynamic relationship between AVMs and aneurysms is considered more important when planning for treatment modalities

[191]. This is because the pressure decreases after AVM removal make the vessel more difficult to constrict compared to normal vessels, causing the feeding arteries to remain dilated for a longer period. Hence it is beneficial for patients to suggest aneurysm exclusion as an initial step or simultaneously with AVM treatment [192]. Apart from these, many authors insisted on careful selection of treatments and multimodality options to reduce further risk [182, 193-196], this is because treatment carries several risks including lack of cure, morbidity, and mortality depending on the anatomy and treatment modality [197]. Thereafter, controversies exist over unruptured brain AVMs since the true natural history for brain AVMs may have lower risk of haemorrhage than for AVMs treated with interventional therapy [198]. This was further supported by the evidence that unruptured brain AVMs had lower haemorrhagic risk of 1% per year compared to more than 5% per year for those who had already experienced initial haemorrhage [199, 200]. This has led to various questions among researchers whether to treat the unruptured brain AVMs [201-204].

1.10 Randomised trial for unruptured brain AVMs

More recently a randomised trial for unruptured brain arteriovenous malformations (ARUBA) compared conservative management for unruptured brain AVMs against morbidity associated with interventional modalities which include microsurgery, radiosurgery, and embolisation [205, 206]. ARUBA aimed to assess the balance between the natural history and risk of haemorrhage from unruptured brain AVMs against the complications arising from treatment modalities [207] with the hypothesis that in terms of medical management, post-treatment risk dominates the natural history of an unruptured lesion [208]. Trial groups were selected from adult patients with unruptured brain AVMs and assigned to medical management alone or to medical management with interventional therapy. Medical management refers to patients receiving pharmacological therapy for existing clinical presentations or any coexisting vascular risk factors. These findings reported significant results of 3-fold increase in the risk of stroke

and death with the initiation of interventional therapy in the ARUBA trial compared to medical management alone [209]. Other recent studies that show the high risk of stroke and disability for unruptured AVM patients using interventional has generated more discussion about the need for using these modalities in this cohort [210-212]. However, the ARUBA findings remain somewhat controversial given a limitation of these studies was the relatively short study (33 months) with the reported overall risk of spontaneous rupture in patients without interventions is 2.2% per year [213]. Also, the long-term risk of haemorrhage and associated death or disability may clearly be an overriding concern [214].

Other studies have reported the benefits of intervention. For example, Javadpour et al. examined the clinical outcome from microsurgical resection for selected group of patients with unruptured brain AVMs. Interestingly, no deaths or strokes were observed with low neurological complications (14.7%, at 6 months follow-up) concluding that ARUBA does not necessarily apply to all or majority of unruptured AVM patients and may depend on the treatment modality [215]. Hence surgery is considered as a good option for immediate AVM cure with both ruptured and unruptured low grade AVMs [216]. This was further supported by another study which investigated the outcome of stereotactic radiosurgery for 502 ARUBA-eligible patients with Spetzler- Martin Grade I to II (46% of cohort) and Grades III to IV (54% of cohort) and a mean marginal dose of 22 Gy with follow-up period of 46 months. Complete AVM obliteration was achieved in 75% of the patients with a post-treatment haemorrhagic rate of 0.9% per year during the latency period. Also, no long-term treatment-related neurological deficits were observed concluding that the treatment attained a lifelong protection from haemorrhagic risk. Similarly, no mortalities with major complication rates of 6 out of 35 patients were noted in ARUBA-eligible patients treated with embolisation [197].

1.11 The future for AVM treatment?

Despite achieving reduced case fatality in recent years using various interventional modalities, still AVM treatment is associated with the substantial risk of deaths or impairments irrespective of the treatment chosen. There is currently no biological approach used to achieve complete AVM cure, Hence, there is an urgent need for a new possible biological treatment that could save the young patients who suffer from a high risk of sudden death or disability and who currently have no effective treatment approach.

1.12 Vascular targeting – a possible approach

Vascular targeting (VT) can be generally described as selective delivery of bioactive molecules to the vascular environment [217]. This is an attractive approach that targets the endothelial cells of the vascular bed selectively by identifying differentiating markers (targets) on it and administering treatment-effective drugs that bind the recognised targets (Figure 1. 4). The interesting part is to exploit potentially inherent differences between normal and pathologically different endothelium to selectively deliver bioactive molecules to the area of interest. The concept was initially used to treat solid tumours where the goal is to cause rapid shutdown of the tumour vessels [218]. It is therefore important to understand the origins of vascular targeting in tumour vessel destruction before introducing the concept for AVM treatment.

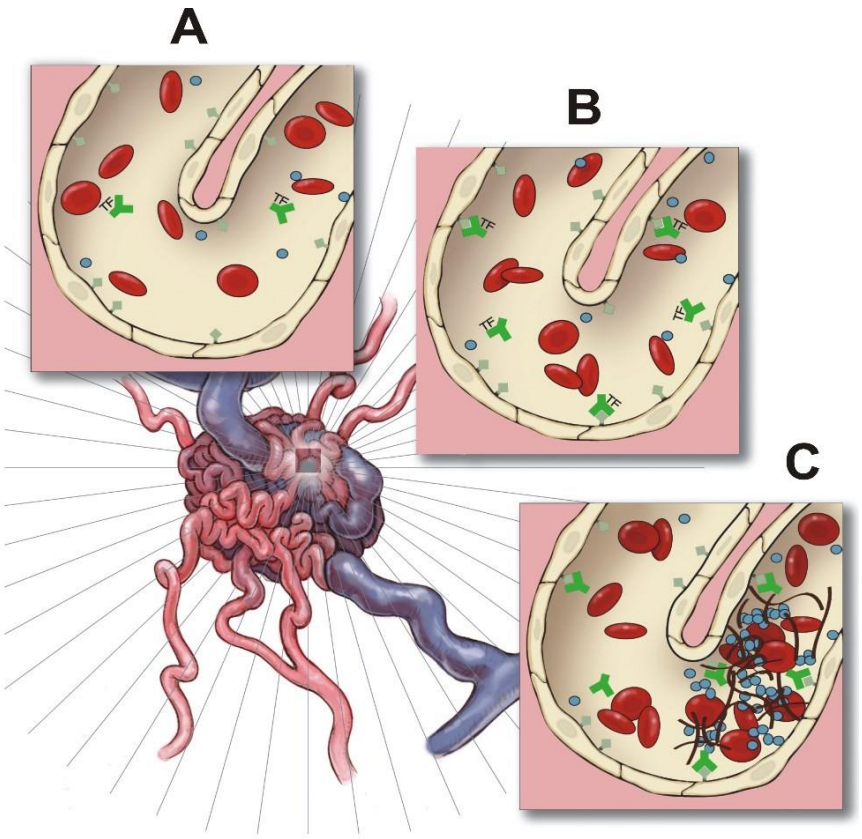

Figure 1. 4: Schematic representation of vascular targeting of AVMs. A) Upregulation of surface biomarkers on AVM endothelium in response to radiation. B) Targeted binding of ligand/antibody specific to the target molecule conjugated to pro-thrombotic molecule (pro-thrombotic conjugate). C) Selective thrombosis as a result of pro-thrombotic conjugate on irradiated AVM endothelium. Figure courtesy of Professor Marcus Stoodley.

1.12.1 VT in cancer

One of the major challenges in cancer treatment is selective targeting which involves good selectivity with high specificity. The previous concept of direct tumour targeting to tumour cells themselves using immunoconjugates and antibodies proved unsuccessful in achieving good selectivity and penetration due to various reasons such as physical barriers to macromolecular transport, densely packed epithelial tumour cells and high absorption rate of antibodies into perivascular regions [219-222]. Then, the concept of targeting the endothelial cells lining the tumour vasculature rather than tumour cells themselves was first proposed by Juliana Denekamp where the author found a 20-fold higher proliferation rate of tumour

endothelial cells compared to normal endothelial cells [223]. Following this, advantages of vascular targeting against tumour targeting were reported where vascular therapeutic agents can directly access endothelial cells without having the difficulties associated with crossing transport barriers into underlying tissues, and hypothesised that thrombotic agents could be delivered to the vasculature to cause occlusive vessel thrombosis through rapid shutdown of tumour nutrients and oxygen supply from the blood leading to eventual starvation and vessel destruction [218, 224]. Since then, various naturally occurring tumour endothelial cell markers such as CD105 [225, 226], CD44 [227], vascular cell adhesion molecule-1 (VCAM-1) [228] have been reported to overexpress in tumour endothelial cells compared to normal endothelium. In addition, several other markers of angiogenesis such as fibronectin-extra domain B [229-231], integrins $\alpha_v\beta_3$, integrins $\alpha_v\beta_5$, [232, 233] and VEGF [217] have been identified and characterised as potential targets for selective delivery of antibodies or peptides to the tumour vessels [217]. Other studies have used mRNA-based serial analysis of gene expression and microarrays to identify differentially expressed genes restricted to tumour endothelium [234]. Overall, there are inherent and significant differences between tumour endothelium and the normal endothelium that provide a source of valid discriminatory targets, which makes vascular targeting a good approach in cancer therapy.

In addition to identification of a good quality target molecule, an appropriate target-binding ligand with high specificity and affinity towards an antigen or target molecule – that has favourable pharmacokinetic properties is considered essential for efficient targeting [235]. Vascular targeting agents (VTAs) can be classified into small-molecule VTAs and ligand-directed VTAs. Small-molecule VTAs do not constrain selectively to tumour vessels but utilise the pathophysiological differences between tumour and normal endothelium to achieve vessel occlusion [218]. Ligand-directed VTAs uses a targeting moiety that binds to marker selectively on expressed tumour endothelium to administer an effector molecule specifically to tumour

vessels. The targeting moieties can be antibodies, peptides, or ligands [236]. The chemotherapeutic effect of drug penetration in tumours has been shown to be improved by vascular targeting where antibody-drug conjugation proved selective delivery of cytotoxic drugs to tumour vessels. The human antibody F8, against an angiogenic marker (fibronectin-extracellular domain A) was conjugated with a cytotoxic drug (cemadotin) which showed improved efficacy of targeting the tumour neovasculature offering strong anti-tumour activity in mice [237]. Also, vascular targeting was achieved by coupling TNF-α with CNGRC, a peptide that targets tumour vasculature. This resulted in an 8 – 10-fold increase in the uptake of chemotherapeutic drugs (doxorubicin and melphalan) with no evidence of toxicity [234].

Vascular targeting agents can also be well functionalised with various effector molecules that can range from toxins to cytokines or pro-coagulant factors [236]. One effector molecule, IL-2 (a cytokine) was fused to a human antibody fragment L19 (ScFv), directed against ED-B domain of fibronectin on tumour endothelium which showed increased anti-tumour activity due to the improved therapeutic index of this vascular targeting agent [238]. This selective delivery of antibody-cytokine conjugate to tumour neovasculature showed promising results with dramatic increase in lymphocyte infiltration and interferon-γ (IFN-γ) which inhibited the growth of tumour cells [239].

Apart from cytokines, a thrombotic molecule was also used as an effector molecule where the aim is to cause selective vessel thrombosis in the tumour environment. ‘Coaguloligand’ was developed by covalently linking an antibody targeting VCAM-1 with tissue factor (TF), a major initiator of blood coagulation to target selectively to the VCAM-1 expressing tumour endothelium causing thrombosis that is enough to occlude the blood vessels that feed tumour cells [228]. Several antibody/ligand-coagulant protein conjugates such as RGD/tTF, ScFv (L19)-TF, and tTF-NGR were developed to induce thrombosis and to achieve tumour cure [240-242].

1.12.2 Vascular targeting in AVMs

Achieving selective thrombosis in AVM vessels would be a great approach for complete AVM cure since AVMs are abnormal pathological vessels that simply cause arteriovenous shunting of the blood without feeding the brain. Hence, these can be blocked or occluded completely without causing ischemia in brain tissue. Therefore, the idea of thrombotically occluding vessels would be perfect for treating AVMs.

Thrombosis in tumour vasculature was achieved by using VTAs that include conjugates that contain fusion proteins of antibody (or ligand) with procoagulant factors or coagulant proteins (as an effector) to cause acute shutdown resulting in tumour necrosis [218]. This depends on constitutive molecular differences between tumour and normal vessels so that the coagulant protein attached to specific antibody binds selectively to the target protein in the tumour vessel without affecting normal tissues. Storer et al. reported the first study of thrombotic event using radiosurgery vascular targeting combination therapy which was a non-ligand based strategy to induce thrombosis in a rat AVM model using lipopolysaccharide and soluble tissue factor [243]. The concept of using a similar technique to induce thrombosis selectively in AVM vessels seems very attractive. However, it is necessary to understand the difference between AVM and normal vessels to achieve selective vessel thrombosis.

1.13 AVM endothelium

Several studies recognised phenotypic and functional differences between AVM and normal endothelial cell using primary cell culture [52], animal models, and surgically resected AVM specimens [244, 245]. In particular, there has been association with a high proliferative and angiogenic index and strong expression of various integrins with many reports of elevated VEGF and its receptors [54, 55]. Gene expression studies have found that more than 300 genes are up-regulated and 560 genes down-regulated with overall 900 genes differentially expressed

in AVMs where these genes encode cell adhesion, growth factors, extracellular matrix factors and inflammatory factors [246, 247]. Regulation of genes in transforming growth factor-ß (TGF-ß) pathways are common in non-sporadic AVMs (HHT1, HHT2) due to their mutations in ENG and ALK1 which have roles in regulating this pathway [248, 249]. Molecular studies in AVM specimens have shown moderate level expression of inflammatory molecules such as vascular cell adhesion moelucle-1 (VCAM-1) and intercellular cell adhesion molecule-1 (ICAM-1) in the AVM endothelium [250]. Despite identification of differences in AVM endothelium in the studies, to date, no molecules have been found on AVM endothelial surface that have been considered sufficiently discriminatory from normal endothelium for use in selective targeting in AVMs.

1.14 Radiosurgery as a priming mechanism for molecular changes in AVMs

Radiosurgery has been used to manage patients with AVMs for more than 3 decades [123] where it is considered as a promising treatment for patients who are considered inappropriate for surgical resection [251]. The main aim of standard radiosurgery in AVMs is to achieve complete obliteration by inducing a type of wound-healing, pro-inflammatory and pro-fibrotic reaction that leads to vessel wall remodeling and eventual closure. However, utilising both molecular and cellular responses of AVMs to radiation as potential targets could potentially improve the treatment in achieving complete obliteration with reduced latency period and dose limitations [129]. Therefore, radiosurgery has been suggested as a priming tool in combination with vascular targeting to enhance molecular changes in AVM endothelium [128, 243, 250, 252-256] that would be attractive in discriminating AVM vessels from normal vasculature.

Hence it is important to review the effects that radiation has on cells and tissues, particularly those of the vasculature.

1.15 Effect of radiation on the endothelium

Vascular endothelium lines the circulatory system and acts as a barrier between blood and tissue spaces thereby performing various biological functions. Different organs and vascular beds appear to have their own peculiar adaptation of endothelial structure to functional requirements, such as the unique properties exerted by the endothelium that forms the blood-brain barrier [257]. Endothelial cells are typically 'quiescent' in the sense that they are not actively proliferating but are metabolically active and perform control of cell movement, vascular permeability and immunity. They also regulate balance between thrombosis and thrombolysis, perform platelet adherence, and leukocyte interactions with the vessel wall [258, 259]. Endothelial injury or any events can contribute to disruption of endothelial integrity, permeability, and haemostasis properties thereby leading to endothelial cell damage and dysfunction. Most commonly free radical-induced reactions causes injury since endothelium is highly susceptible to oxidative stress that generates free radicals causing endothelial cell damage or injury [260].

Cell irradiation induces DNA damage through double-stranded breaks or production of reactive oxygen species via generation of free radicals [261, 262]. These radicals attack structural and functional molecules causing genetic mutation and cytotoxicity [263, 264]. Among all tissues in the body, damage to the blood vessel wall has been reported in many studies due to its sensitivity and prominent changes in response to radiation [265-267]. Irradiation alters endothelial cell proliferation rate as well as cell survival or can induce cell growth arrest (cell senescence) [256, 268]. The outcome of radiation exposure depends on the severity of radiation dose as well as the sensitivity or activity of inherent DNA damage response pathways, which can vary depending on cell type [269].

Radiation induced alterations were reported in epithelial, stromal, and vascular lesions. Necrosis occurs in many epithelial and parenchymal cells during severe radiation injury and fibrosis is the most common delayed presentation to occur in almost all tissues and organs depending on the site of injury [270-273]. Vascular lesions are well-known morphologically and highly significant in the context of pathogenesis of delayed radiation injury [274, 275]. Morphological studies reported the similarity of the irradiated endothelial cells to that of senescent cells with thickening of basement membrane and microvessel disintegration where cells with senescent-like phenotype [276]. The biological effects of radiation depend on various factors where two important things to consider are high dose and low dose over short period of time producing severe or short-term side-effects. High dose tends to kill the cells whereas low dose causes damage or alterations in cell phenotype [277, 278].

Radiation causes an early inflammatory response characterised by leukocyte-endothelial cell rolling, activation, adhesion, and migration [279] stimulated by up-regulation of pro-inflammatory transcription factors such as NF kappa B (NFκB), cytokines such as TNF-α, and IL-1 which are known to induce the expression of cell adhesion molecules. E-selectin expression was reported to be independent of these cytokines but requires the activation of transcription factor NFκB [280]. The role of cell adhesion molecules was well studied in the pathogenesis of radiation-induced inflammation where increased expression of E-selectin and ICAM-1 expression was reported [281].

Apart from an inflammatory response, endothelial cells also regulate thrombotic responses to radiation. The endothelium normally plays a crucial role in masking the signals that cause platelet activation, thereby preventing thrombosis [282], as well as producing other molecules such as thrombomodulin (TM), that convert thrombin to an anticoagulant molecule rather than pro-coagulant via active protein C [254]. In contrast, endothelial cells can rapidly change from an anti-coagulant to pro-coagulant state when exposed to stress or injury that causes endothelial

denudation and exposure to the subendothelium (that is rich in collagen and tissue factor) resulting in thrombosis via release of tissue factor, or platelet activating factor or plasminogen activating inhibitor [283]. This was supported by evidence that showed decreased expression of thrombomodulin, tissue factor pathway inhibitor (TFPI) which in turn increased the cellular procoagulant activity [283]. Hence, radiation induced endothelial cell necrosis or apoptosis exposes the raw thrombogenic components of the subendothelium that contain collagen, tissue factor, microfibrils, von Willebrand Factor (vWF), and fibronectin leading to platelet adhesion and thrombosis.

Given the significant changes induced by radiation in endothelial cells as described above, some of these molecular markers that act within these altered inflammatory and thrombotic pathways may serve as potential candidates for vascular targeting in achieving selective vessel occlusion. Looking for targets at the cell surface would be appropriate rather than intracellular molecules given the need for easy accessibility in reaching targeting moieties with efficient delivery and rapid accumulation of VTAs in AVM vasculature. Earlier studies reported possible radiation induced targets such as ICAM-1, VCAM-1 on endothelial cell surface [284]. Recent studies investigated post-irradiation ICAM-1 and VCAM-1 as endothelial targets in model AVMs however found that high basal expression and lack of significant *in vivo* induction in response to radiation precluded them from further investigation as vascular targets [284]. Another radiation induced surface molecule that has been identified is phosphatidylserine which will be described in greater detail.

1.16 Phosphatidylserine as a radiation-stimulated endothelial target

Phosphatidylserine (PS) is a negatively charged phospholipid present in the plasma membrane of all prokaryotic and eukaryotic cells where it is highly enriched in the inner leaflet. It accounts for 3 – 15% of phospholipids distributed asymmetrically in the plasma membrane [285, 286]. Though PS is usually present in the inner side of the plasma membrane, certain conditions cause translocation of PS to the outer leaflet where it plays a role in phagocytosis and activation of the coagulation system [287-292]. Disruption of lipid asymmetry with the translocation of PS to the outer membrane leaflet is a hallmark of cells undergoing apoptosis thereby it is considered as an early apoptotic marker [293, 294]. PS exposure on apoptotic cells is necessary for macrophage clearance through phagocytosis where PS-dependent phagocytosis of apoptotic cells not only acts to remove dead cells from tissues but also acts to enhance macrophage production of anti-inflammatory, pro-fibrotic cytokines such as TGF-ß1 and further inhibits the production of TNF-α and other pro-inflammatory cytokines [295]. PS exposure has also been found in solid tumour endothelium caused by various factors such as hypoxia, acidity, inflammatory cytokines, and thrombin which either have role individually or mutually to induce PS exposure [296, 297]. It has been assumed that cancer cells expose elevated levels of PS due to their high rate of division and apoptosis but it still remains unclear how and why cancer cells expose PS to the outer membrane [298]. PS-positive tumour endothelium was reported to be viable without displaying markers for apoptosis where it remained metabolically active [296]. PS exposure has also been observed in several types of viable cells such as ovarian carcinoma cell line, viable B cells, and a mouse brain endothelial cell line [299-301].

Radiation-induced PS exposure has been well documented recently to understand the radiation induced molecular response of brain endothelial cells and its potential to serve as a molecular

target for vascular targeting in AVMs. PS exposure on brain microvascular endothelial cells was observed after radiation at 15 Gy and 25 Gy dose by *in vitro* live cell imaging using a fluorescently labelled annexin V ligand [256]. Annexin V is a calcium dependent phospholipid binding protein with high affinity to PS where it has been used in assay for detecting apoptosis via its binding to apoptotic cells [302, 303]. Another study demonstrated PS translocation after radiosurgery using an AVM rat model created by end-to-side anastomosis of left external jugular to the left common carotid artery in six-week-old male Sprague Dawley rats [255]. The elevated levels of PS exposure over time were observed in irradiated AVM rats at 15 Gy compared to non-irradiated controls [284]. These initial studies show that PS could potentially be an ideal target for vascular targeting in AVM treatment.

1.17 Other potential radiation-induced targets

While PS appears a viable radiation-stimulated molecule for targeting in irradiated AVMs, there may be other markers that may be suitable. Recent studies have used surface protein biotin-labelling and proteomic analysis to identify radiation induced proteins on the endothelial surface in a rat model of AVM and *in vitro* using cultured brain endothelial cells [304]. Investigation of these and other markers may provide highly novel and discriminatory radiation-stimulated targets and will be discussed later in this thesis.

1.18 Vascular targeting in AVMs

VT combined with radiation priming could be a valid method for AVM treatment. To date, several radiation-stimulated potential targets have been identified, including PS. The next step is to develop a pro-thrombotic conjugate using these targets by combining ligand or antibody specific to the target with an effector molecule (coagulant protein) to induce selective vessel thrombosis. Testing these conjugates using animal models would be expensive and time consuming. Hence, the aim of this study was to develop an *in vitro* flow system to test the

efficacy of these conjugates for endothelial cell binding and thrombosis prior to animal studies. This will be of ethical benefit in reducing the amount of testing of various combinations of target moieties, doses, and concentrations using an animal model. The type of system that could enhance pre-testing of conjugate under pulsatile flow conditions would be the parallel-plate flow chamber.

1.19 Parallel-plate flow chamber

A parallel-plate flow chamber is an *in vitro* flow system that maintains a controlled environment where the cells are exposed to a mechanical force thereby creating a pressure gradient along the chamber (Figure 1.5) [305]. A recent study demonstrated the design and use of a parallel-plate flow system to stimulate bone cells and their response to a mechanical environment [306]. The cells are placed between the parallel-plates in a sealed chamber where the fluid flows through the chamber at controlled rates enforced by a syringe pump [307, 308]. The design of the flow system can include both open and closed systems. The closed loop configuration maintains constant pressure throughout the flow in contrast to an open system where the pressure changes with respect to the flow resistance created through the chamber during inlet and outlet flow. Open systems can cause leakage due to formation of sudden pressure gradients across the chamber resulting in cell deformation [306]. A variety of *invitro* flow chamber designs have been used recently to assess the shear stress stimulated response of cells under flow where the response includes changes in cell morphology, number, cell adhesion and metabolism [308-310]. These changes are usually influenced by haemodynamic conditions, but there are only limited studies involving effect of pulsatile flow on cell behaviour, since most of them involve steady-state flow conditions [311-313].

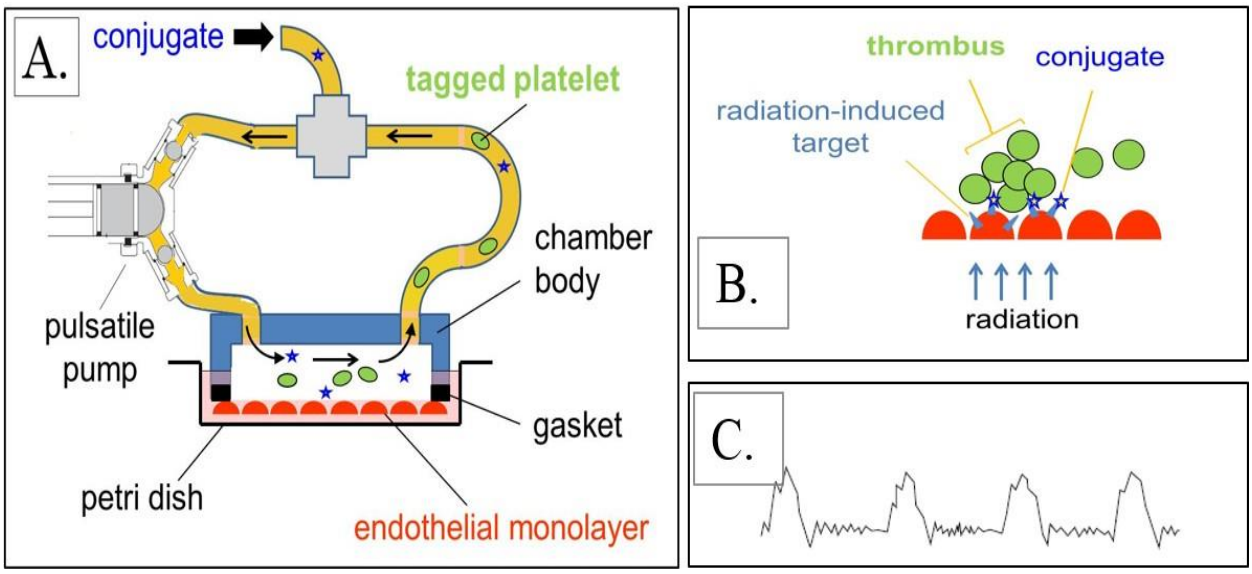

Figure 1.5: Schematic representation of the parallel-plate flow chamber system. A) Enclosed circulation system containing inlet, outlet, syringe pump connected to the petri dich containing irradiated/non-irradiated endothelial cells. B) Formation of thrombosis due to binding of pro-thrombotic conjugate on irradiated endothelial cells. C) Pulsatile profile of the flow system. Figure courtesy of Dr Zhenjun Zhao and Professor Georges Grau.

To date, the majority of perfusion chambers have used the parallel-plate concept to investigate the mechanisms of platelet adhesion and aggregation at different shear conditions using whole blood [314-316]. Measuring platelet adhesion under flow is more physiological than assessment in a static cellular system, as flow plays a significant role in platelet binding as well as subsequent thrombus formation and thrombus stability [317]. A recent study on cardiovascular disease involved development of an *in vitro* perfusion chamber model to understand the shear-mediated role of platelets by using endothelial cells and whole blood [318]. Van Kruchten et al. demonstrated the practical use of parallel-plate flow chamber with microscopic imaging techniques to enhance better understanding of *in vitro* thrombus formation under flow and its quantification using z stacks of confocal microscopy [319].

Although blood generates high shear stress in human arteries (2 – 20 dynes/cm^2 varying to 3 – 300 dynes/cm^2 in arterial branches) compared to the custom-made parallel-plate flow systems [320], it would be ideal to assess thrombus formation under low pre-defined shear conditions

since the formed thrombus could be detached or embolised at high shear rate. Moreover, introducing human whole blood in the flow system helps to monitor clot formation at near-physiological conditions with complex blood rheology that is essential for thrombus growth [321]. Hence, a parallel-plate flow chamber with human whole blood could be a good model to study the effect of pro-thrombotic conjugates in stimulating thrombosis under controlled shear stress conditions using irradiated endothelial cells.

1.20 Pro-thrombotic effectors and the coagulation cascade

Knowledge of the basic processes involved in stable thrombus formation is important to choose appropriate pro-thrombotic effectors for VT conjugates and assessing their effectiveness in the whole blood parallel-plate flow systems, in addition to determining what type of analysis may be required to assess stages of thrombus formation in the systems. Previously, thrombin and TF have been investigated as effector molecules in VTAs developed for cancer and in animal studies on targeting in AVMs [218, 243]. Under normal conditions, the coagulation system is balanced in favour of blood anticoagulation. The coagulation system triggered in response to rupture of the endothelium exposes circulating blood platelets to extravascular tissue that occludes the vascular lesion completely by forming a blood clot [322]. Blood coagulation and inflammation is considered a significant defence system to maintain health in normal and pathological conditions. Initiation of the coagulation cascade leads to inflammatory pathways and vice versa, providing strict control and balance between the systems [323]. In case of injury, blood starts to form a thrombus or clot immediately, where the approximate time it takes for the skin to stop bleeding is 2 to 5 minutes if the coagulation system works properly [324]. The coagulation system consists of various proteins, enzymes, mediators and cofactors to trigger thrombosis and to control fibrinolysis, the ability to break down a clot [325].

It is well known that platelets play a key role in thrombosis. Platelet aggregation at a site of vascular injury is a necessary step for the formation of a primary haemostatic plug thereby contributing to bleeding arrest [326]. On the endothelium, von Willebrand Factor (vWF) initiates platelet adhesion during vessel wall injury forming a complex with membrane glycoprotein GPIbα which is initially required for platelet recruitment. Platelet aggregation requires a second adhesive interaction of vWF-integrin aIIbb3 [327]. An *in vitro* flow-based platelet aggregation assay reported continuous tethering, translocation, and detachment of platelets from developed thrombus at both arterial and venous shear rates where platelet-vWF played an important role. Ruggeri et al. proved that platelets tends to aggregate irrespective of initial platelet activation under physiological flow conditions when the shear rate exceeds 400 dynes/cm^2 [327]. In this situation, the formed platelet aggregates were not stable and started to detach from the surface until the shear rate was reduced [328]. Hence platelet aggregation is considered a necessary step for platelet-platelet contacts and thrombus formation.

Thrombus formation is the final step in the cascade following platelet aggregation that maintains the integrity of the closed circulatory system after vessel wall damage. Thrombus formation is determined and quantified based on the amount of fibrin deposited on the surface [329]. Thrombotic pathways can be activated either by intrinsic or extrinsic stimuli but the pathways coverage on common elements that finally cause conversion of fibrinogen to fibrin and fibrin polymerisation to produce a clot [330].

Tissue factor (TF) initiates the extrinsic pathway by participating as a cofactor in the activation of factor VII to its active form (factor VIIa). Factor VIIa-tissue factor complex acts on factor X and IX in the presence of calcium ions (Ca^{2+}), to produce activated factor Xa and IXa responsible for conversion of pro-thrombin to thrombin. Thrombin is the enzyme which converts soluble fibrinogen in the blood to insoluble fibrin resulting in thrombosis [325, 331].

The intrinsic pathway involves exposure of circulating blood platelets to factors such as factor XII, and high molecular weight kininogen that leads to initiation of coagulation by converting factor XII to XIIa where inactivated prothrombin gets converted to activated thrombin [332, 333]. Thrombin can directly activate factor XI to promote fibrin cross-linking and polymerisation, where platelets provide surface for activation of factor XI by thrombin under physiologic conditions [334]. This converts soluble fibrinogen to insoluble fibrin resulting in thrombosis [323].

The intrinsic pathway is significant for studying *in vitro* blood clotting mechanism since platelets provide the surface that enhance activation of factor XI by thrombin without any addition of non-physiological cofactors [335]. Baglia et al. studied the physiological importance of thrombin as an initiator of intrinsic blood coagulation where activated platelets were compared with dextran sulfate, as a surface for thrombin-induced factor XI activation. As a result, addition of prothrombin in the presence of $CaCl_2$ showed thrombin-stimulated activation of platelets and factor XI independent of any proteins, factor XII, and high molecular weight kininogen [336].

In contrast, TF-mediated coagulation in the extrinsic pathway requires activation of various cofactors and signaling proteins where exposure of vascular injury with plasma factor VIIa activates X and IX resulting in generation of a small amount of thrombin [337]. Thrombin, in turn, primes the intrinsic pathway, resulting in more generation of thrombin which cleaves fibrinogen to form a fibrin clot. Therefore, thrombin is the key effector enzyme that triggers blood coagulation more easily with many biologically important functions such as activation of platelets, conversion of fibrinogen to fibrin, and feedback amplification of coagulation where accurate and balanced generation of thrombin at the site of injury provides proper blood clot formation [338, 339]. Thrombin therefore may provide a more suitable and active effector for vascular targeting studies.

1.21 Summary

The overall goal of this project is to develop a vascular targeting treatment for brain AVMs. The hypothesis is that by developing pro-thrombotic conjugates based on previously identified/validated molecular targets on irradiated AVM endothelium and by linking the ligand/antibody specific to the target with a pro-thrombotic agent (thrombin) that selective thrombosis can be induced. The specific project goal was to develop these pro-thrombotic conjugates and test their efficacy in stimulating thrombosis on irradiated human cerebral microvascular endothelial cells using an *in vitro* parallel-plate flow chamber system. The optimisation of flow system, development of conjugate and testing its effect under flow will be explained in the following chapters.

1.22 Hypothesis

Overall hypothesis for this body of work: Radiation-induced biomarkers can be selectively targeted after AVM radiosurgery with a ligand-directed vascular targeting agent to achieve localised thrombosis and rapid occlusion of pathological AVM vessels.

Specific hypothesis for the current study: Ligand-directed vascular targeting agents can be rapidly assessed for endothelial binding and pro-thrombotic activity using an *in vitro* parallel-plate flow chamber system with circulating human whole blood.

1.23 Aims

The overall aim of this project is to develop and test novel pro-thrombotic conjugates targeting radiation-stimulated endothelial surface molecules using an *in vitro* parallel-plate flow chamber. The specific aims addressed in the following chapters are:

Aim 1: To establish and optimise an *in vitro* parallel-plate flow chamber using irradiated endothelial cells and human whole blood (chapter 2).

Aim 2: To develop pro-thrombotic conjugates targeting radiation-externalised phosphatidylserine and assess endothelial binding and thrombosis in the parallel-plate flow system at various conjugate and radiation doses (chapter 3).

Aim 3: To validate novel radiation-stimulated marker expression in human brain endothelial cells and develop and test novel conjugates to these targets (chapter 4).

Chapter 2

2. Development of parallel-plate flow chamber and optimisation of flow conditions

2.1 Introduction

The main aim of this study is to develop and test the efficacy of novel pro-thrombotic conjugates in inducing thrombosis on irradiated endothelial cells. *In vivo*, this can be a highly time consuming and expensive series of experiments when testing multiple targets and thrombotic conjugates. The use of *in vitro* systems that mimic blood flow provides more efficient way to pre-test the ligand and thrombotic components of conjugates and derive information on their ability to target and bind endothelial cells after irradiation, and to induce stable thrombus formation on these cells. Parallel-plate flow chambers have previously been used to examine thrombosis *in vitro* using free platelets and whole blood [314, 319, 340]. The purpose of developing this parallel-plate flow chamber was to simulate the *in vivo* haemodynamic conditions and the forces that act upon thrombus formation and stability. This is not something that can be achieved in static cell culture.

Before progressing to testing under flow, it is necessary to develop an *in vitro* flow system and optimise various parameters to achieve stable conditions for cell survivability and response. Hence, the specific aim of this work was to develop a parallel-plate flow chamber using human cerebral microvascular endothelial cells and fresh human whole blood by optimising various conditions. This chapter outlines the various steps in developing the parallel-plate flow chamber system to enable efficient and economical testing of various pro-thrombotic conjugates under *in vitro* flow conditions.

2.2 Standard methods

2.2.1 Tissue culture experiments

2.2.1.1 Cell culture

An immortalised human cerebral microvascular endothelial cell line, hCMEC/D3 (CELLutions Biosystems Inc) was cultured in Endothelial Basal Medium-2 (EBM-2) (Lonza) supplemented with 5% fetal bovine serum, 1% penicillin/streptomycin, 10 mM HEPES (Life Technologies), and 1 ng/mL human basic fibroblast growth factor (Sigma-Aldrich) at 37˚C in 5% carbon dioxide, controlled oxygen level between 1% to 20% and passaged at 90% confluence with trypsin-EDTA (Life Technologies). Cells were seeded at 1 x 10^4 cells/mL onto collagen coated 35 mm glass bottom petri dishes (MatTek Corporation) containing 1.5 mL EBM-2 medium and allowed to grow for 2 days to achieve 100% confluency. The hCMEC/D3 cells were kindly provided by Professor Georges Grau (The university of Sydney) and tested free of any infection by HIV-1, -2, HTLV-1, HBV, HVC and controlled free from mycoplasma contamination by the commercial Mycoplasma Detection Assay MycoAlert, (Lonza, #LT07-118).

2.2.1.2 Collagen coating

All culture vessels were pre-coated with 100 µg/mL rat tail collagen (In Vitro Technologies) and incubated at 37˚C in 5% carbon dioxide for at least 1 hour to set. This was followed by washing three times with phosphate buffered saline (PBS) to be ready for the cell culture.

2.2.1.3 Cell irradiation

Cells were irradiated by a linear accelerator (LINAC) (Elekta Synergy, Crawley, UK) at Macquarie University Hospital (MUH). The cells were irradiated at three different doses (5, 15 or 25 Gy) when they reached 100% confluence.

Each petri dish containing cells was refreshed with 1.5 mL EBM-2 growth medium prior to radiation. Then, the dishes were transported to MUH at room temperature and placed on a solid water phantom on the treatment couch and set at the isocenter for dose delivery. All the cell

irradiation work was performed by Genesis Care radiation physicists (Mr. Vaughan Moutrie and Mr. Estavam Daniel Santos). The non-irradiated cells (sham controls) were kept at room temperature for an equal length of time without exposing them to the radiation field. All cells were returned to the 37˚C incubators after sham or radiation treatment and harvested for the flow system at defined time points post-irradiation.

2.2.2 Whole blood experiments in the flow system

2.2.2.1 Human ethics

All experimental procedures using human blood were approved by the Macquarie University Human Ethics Committee (approval number HREC: 5201300883) and were carried out following the Australian Code of Practice for the Care and use of Human Tissues for Scientific Purposes (Version 4) with consent.

2.2.2.2 Collecting anticoagulated blood and recalcification

A volume of 20 mL of human whole blood was collected at each sitting from 83 healthy volunteers age 25 – 55 free from medication known to affect platelet function. The blood was drawn using standard venepuncture protocols into 4.5 mL anti-coagulation tubes containing 3.2% buffered sodium citrate solution (BD Bioscience). The first 3 – 5 mL of collected blood was discarded to prevent activation of platelets. The tubes were then kept at room temperature until use. The protocol for recalcification of citrated blood was optimised by testing different concentrations of calcium chloride/magnesium chloride ($CaCl_2$/$MgCl_2$) (75 mM/37.5 mM, 20 mM/10 mM, 5 mM/10 mM) with a final volume of 1:10 dilution to the blood and checking the effect at each concentration using blood under flow conditions. 75 mM/37.5 mM was initially used that caused rapid activation of blood coagulation causing systemic thrombosis within 3 mins after introducing it into the flow system. Using another concentration of 20 mM/10 mM $CaCl_2$/$MgCl_2$ caused blood clot in the system within 10 mins while 5 mM/10 mM $CaCl_2$/$MgCl_2$ caused no activation of blood coagulation. Therefore, the final recalcification concentration of

5 mM/10 mM $CaCl_2$/$MgCl_2$ in the whole blood was used in the flow system in all the experiments.

2.3 Results

2.3.1 Parallel-plate flow chamber assembly and setting

The flow apparatus used here is the parallel-plate flow chamber (Harvard Pulsatile blood pump model 1407) with an enclosed microcirculation system consisting of: - 1) flow deck with inlet and outlet tubes connected to syringe pump; 2) silicone rubber gasket (Glycotech) with a flow width of 1 cm and a thickness of 0.010 cm fitted beneath the deck; 3) a 35-mm glass petri dish in which cells are cultured (Figure 2.1). The pump used in this study is pulsatile in nature and maintained physiological flow conditions throughout. This allowed a controlled environment to study the cell adhesion and behaviour under well-defined shear conditions where it delivered uniform pulsatile shear conditions to an adherent cell population [305, 307].

All system parts were thoroughly cleaned with milliQ water before assembly and before using in the flow experiments. For initial optimisation experiments, the flow system was run with circulating EBM-2 medium assembled with the petri dish containing 100% confluent hCMEC/D3 cells.

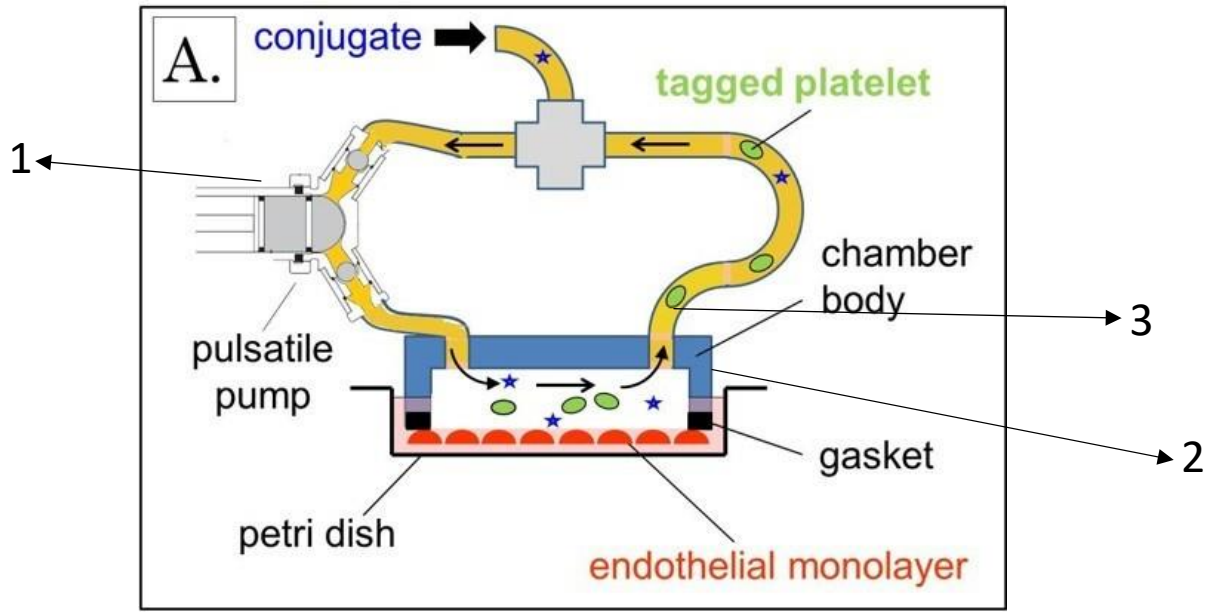

Figure 2.1: Schematic representation of *in vitro* parallel-plate flow chamber system. 1) Initiation of flow by pulsatile syringe pump across the inlet and outlet tubing by forward and reverse pulsing. 2) Petri dish with endothelial monolayer below the chamber with inlet and outlet tube forming enclosed circulation loop. 3) Flow field for endothelial cells to contact with human whole blood/EBM-2 medium. Figure courtesy of Dr Zhenjun Zhao and Professor Georges Grau.

Figure 2.2: The assembly of the parallel-plate flow chamber device with petri dish connected to inlet, outlet and vacuum port. Original Image.

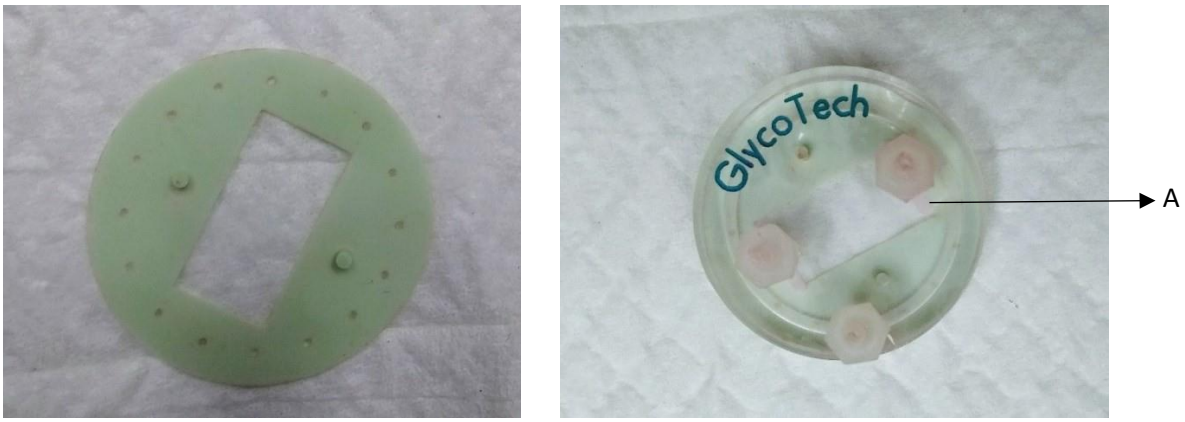

Figure 2.3: The assembly of flow deck with a silicon rubber gasket. A) flow field in which cells contact with the whole blood/EBM-2 medium. Original image.

2.3.2 Optimisation of flow conditions

In this study, the parallel-plate apparatus was designed in such as a way to minimise the entry length and pressure variations across the width of the flow field (Figure 2.1). This was achieved by reducing the tubing size (inner diameter of 1.5 mm) and adjusting strokes/min, stroke volume and flow time. The volume of EBM-2 used in the system was approximately 12 mL. Flow conditions were optimised to ensure proper cell adherence to the collagen-coated monolayer without uplifting till the end of the experiment. Figure 2.5 shows the effect of changes on strokes/min, stroke volume and flow time observed on cell confluency in this flow system. It was established that to maintain cell confluence throughout each flow run, that the stroke rate was optimised at 38 strokes/min and the flow volume and flow time were analysed to be optimal at 2.4 mL/min and 15 min respectively (Figure 2.5). Increasing any of these parameters led to decreased cell confluency. The shear stress profile further confirmed the pulsatile flow of the system simulating the *in vivo* environment (Section 2.3.3).

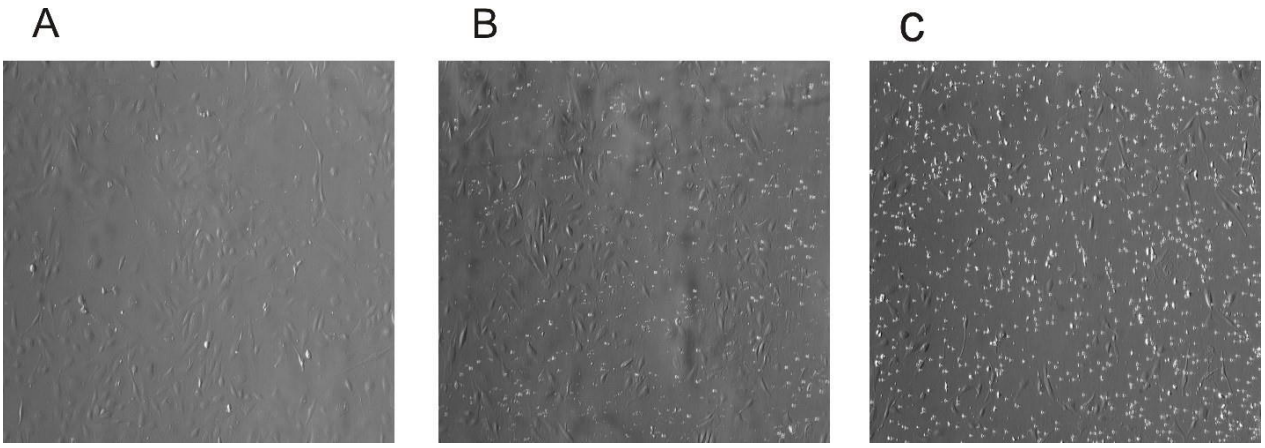

Figure 2.4: Endothelial cells under brightfield microscopy after the flow with EBM-2 medium at varying conditions. Cells A) without flow B) at 28 strokes/min at 15 mins C) at 28 strokes/min at 20 mins.

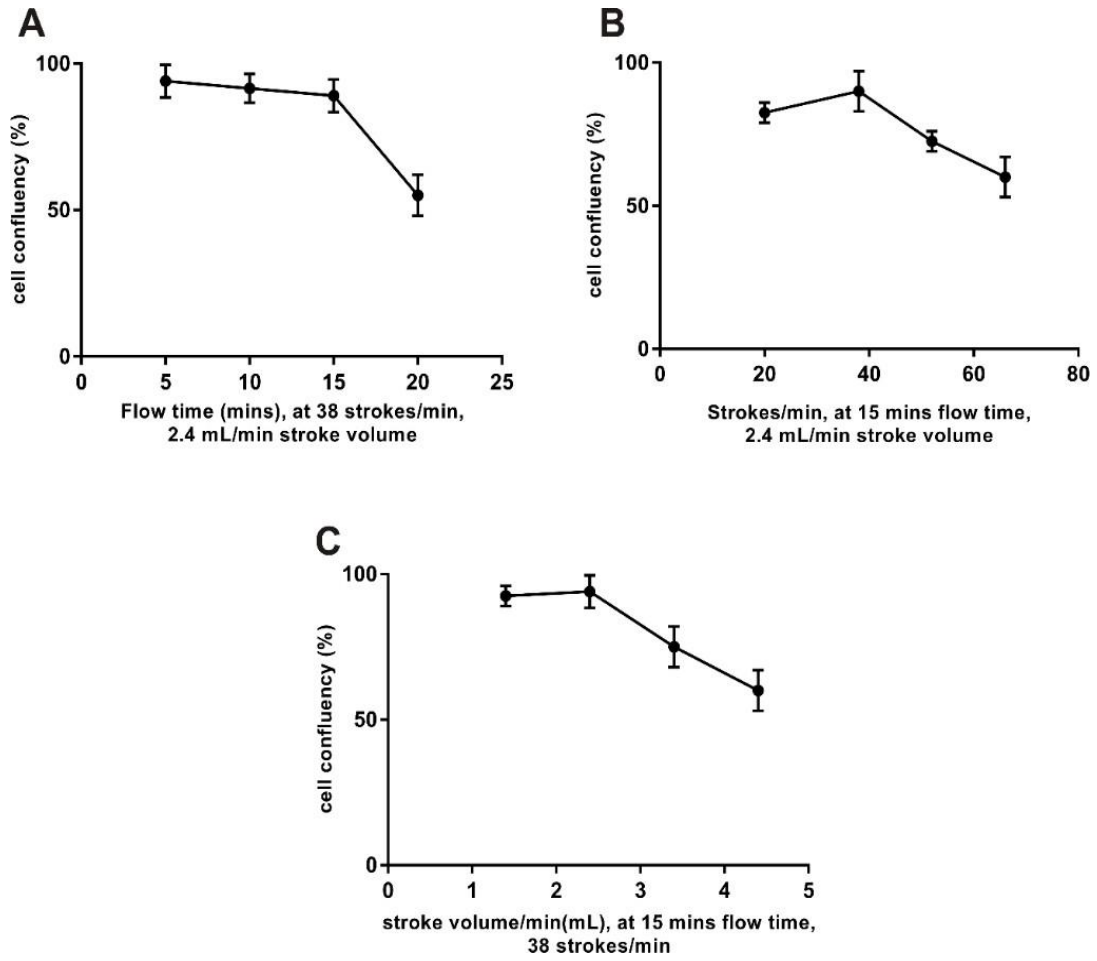

Figure 2.5: Optimisation of flow conditions using the parallel-plate flow chamber. Cell confluency was observed after the flow by optimising flow time at 38 strokes/min, 2.4 mL/min (A); strokes/min at 15 min flow time, 2.4 mL/min (B); stroke volume/min at 15 min flow time, 38 strokes/min (C). Data are shown as mean ± SD using 3 independent experiments.

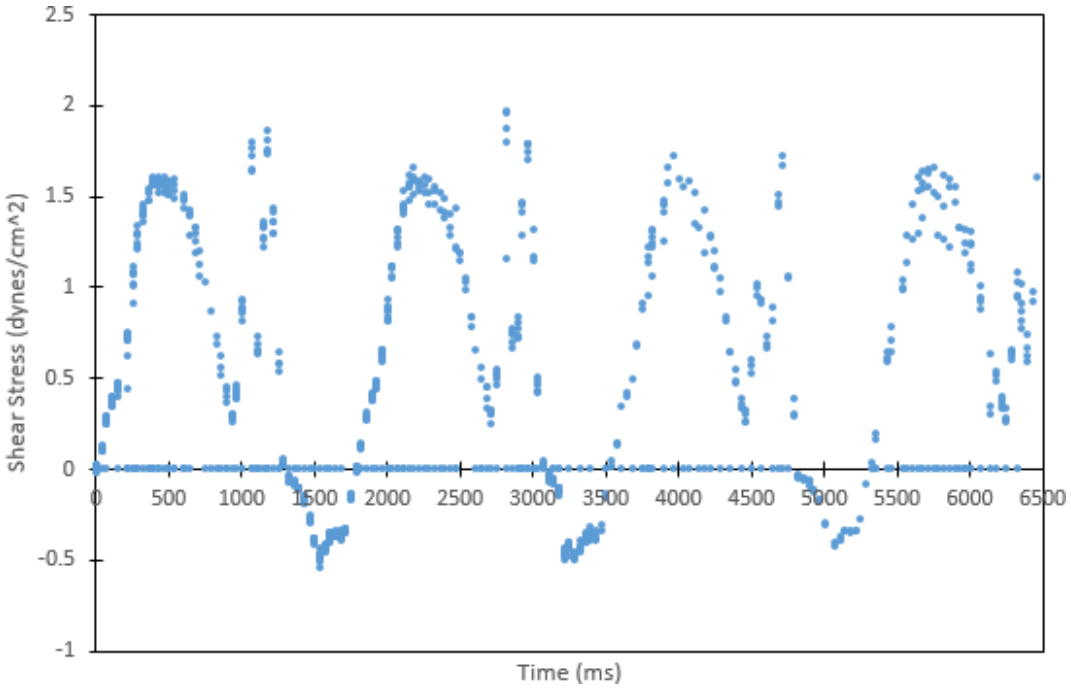

Figure 2.6: The measurement of shear stress using pulsatile flow pattern.

2.3.3 Shear stress measurement

Vascular endothelial cells lining the inner surface of blood vessels are constantly exposed to both biochemical and biomechanical forces during physiological blood flow conditions. Shear stress is the biomechanical forces created by the flowing blood along the vessel wall [341]. It is generally determined by blood flow, vessel geometry and blood viscosity. Pressure acts perpendicular to the vessel wall and shear stress acts parallel to the wall creating a frictional shear force on the surface of the endothelium [342, 343].

Shear stress is usually measured using the formula $\tau = v.dv/dx$, where v is the fluid viscosity, dv is shearing velocity, and dx is the distance between the wall and initial shearing velocity point [344]. In a previous study, *in vitro* measurement of wall shear stress (WSS) in an anastomotic graft design model was demonstrated by Kabinejadian and co-workers using particle image velocimetry under pulsatile flow where hollow glass spheres with mean diameter of 10 µm and density of 1.1 g/cm^3 were used as tracer particles in working fluid.

WSS was calculated based on the movement of these particles by using the formula WSS = μ.dv/dn, where μ is the fluid viscosity, dv is the velocity of tracer particles and dn is the distance moved by tracer particles in the direction perpendicular to the wall [345].

In this study, the average wall shear stress within the flow chamber was determined by introducing 6 μm fluorescent beads (FluoroSpheres sulphate microspheres, Molecular Probes, Ore, USA) in a non-cellularised circulatory system at a volume of 20 μL (500× dilution) and images were captured at 100 ms frame intervals with 10 ms exposure time where the peak speed of the beads in the centrer line of the flow chamber was determined over the duration of the pump cycle. The wall shear stress (WSS, in dynes/cm^2) can be related to the peak (centre line) velocity (V_{Peak} in m/s) by: WSS = 10 × ($4\mu V_{Peak}/t$), where μ is viscosity of water (8.90×10^{-4}) in Pascal seconds (Pa.s) which is 10 times less compared to blood viscosity, and t is the chamber thickness in metres. The WSS was determined to be 3.1 dynes/cm^2.

2.3.4 Cell adherence post-irradiation in the flow system and determination of assay time points

After optimisation of the flow conditions in the parallel-plate flow system, the best time points post-irradiation to assay thrombus formation were established. This was considered as time points where cells continued to maintain a confluent layer without uplifting, that did not expose the collagen base that may itself promote platelet adhesion and potentially thrombus formation. The irradiated cells (5, 15 or 25 Gy) were assembled in the system either 1, 3, or 5 days after radiation and operated initially with EBM-2 medium, not blood, using the flow system under optimised flow conditions. Sham irradiated cells were used as controls. The cells were washed two times with PBS after flow and fixed with 50% ethanol for 15 mins at room temperature. The cells were then stained with 100 μg/mL Hoechst 33342 solution (Thermo Fisher Scientific), washed, and mounted for confocal microscopic analysis. The cell confluency was analysed after each radiation dose and at each time point.

No significant changes in cell confluency was observed at day 1 or day 3 compared to the sham controls with all radiation doses (Figure 2.7). At day 5, decreases in population numbers and cellular hypertrophy were noticed. Differences in cell morphology were observed compared to sham controls with cell enlargement consistent with induction of a radiation-stimulated senescent phenotype [268]. While cell numbers were reduced, the enlarged, senescent-like cells spread to cover the collagen-coated dish, but still some reduction in confluence was observed at day 5.

A quantitative study of radiation effects on cell numbers was performed using an automated cell counter (Countess II, Thermo Fisher Scientific) to measure the number of live cells after each radiation dosage (5, 15, or 25 Gy) and at the designated time points (day1, day 3 and day 5). Cells on collagen-coated 6 well plates were irradiated at the above-mentioned dosages as per the previous procedure with sham-irradiated cells used as control. Cells were washed, trypsinised, and resuspended in equal volumes of PBS before addition of Trypan blue to the cells in a 1:1 dilution. After a few minutes uptake, the number of live cells (unstained, white) per mL were counted. Radiation at all doses appeared to inhibit proliferation relative to the sham controls. Figure 2.8 showed no progression in cell growth at day 5 after radiation at all doses compared to sham control. In relation with previous findings to cell adherence under flow, in further experiments, flow analysis was performed and optimised at day 1 and day 3, not day 5, to ensure a consistent monolayer was always present.

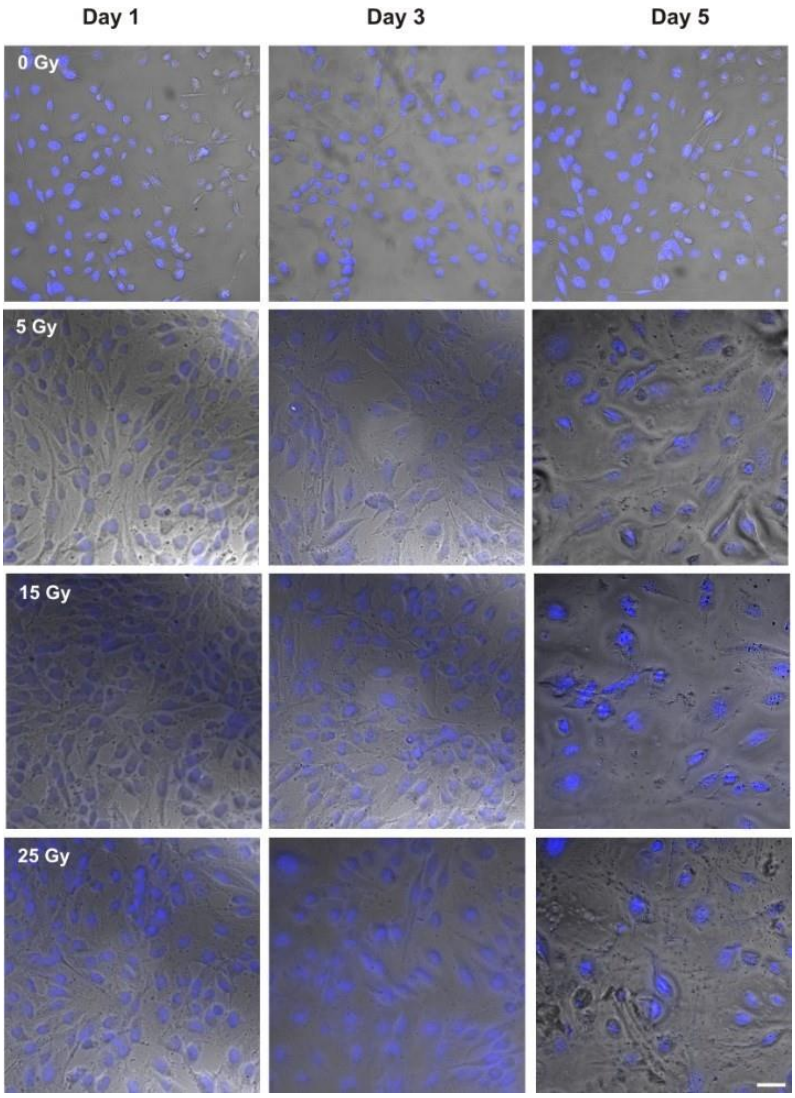

Figure 2.7: Cell confluency after radiation using the parallel-plate flow chamber. Cells were exposed to optimised flow conditions at 1, 3 or 5 days after irradiation and analysed by qualitatively observing cell confluency. Representative brightfield images show hCMEC/D3 cells on the parallel-plate flow system after 15 min of flow. Cell nuclei were stained with Hoechst 3342 (blue) and viewed under 200× magnification. Scale bar = 50 µm.

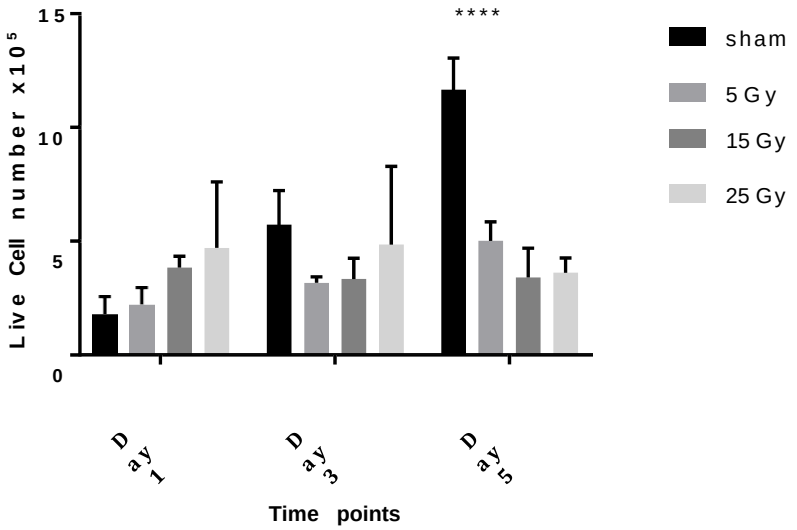

Figure 2.8: Live cell number after irradiation at all doses (5, 15 or 25 Gy) and time-points (day 1, 3 or 5). Data are shown as mean ± SD (3 independent experiments) and were analysed using two-way ANOVA with Tukey's post-hoc analysis. ****p<0.0001 comparison relative to sham-irradiated control.

2.3.5 Introduction of whole blood into the flow system

To assess pro-thrombotic activity of conjugates, it is necessary to use whole blood in the flow system. Whole blood was used in this flow system with endothelial cells to simulate an *in vivo* vascular environment. Previous studies have used whole blood to study thrombosis of heart attack, stroke, and vascular injury [314, 346]. The use of whole blood in these systems can be difficult because of the high viscosity of blood. Thepulsatile syringe in the pump was initially checked to start with pushing mode (forward pulse) instead of pulling mode to avoid backward negative pressure and air bubbles. Air bubbles in the *in vitro* flow system was common especially when using whole blood due to its high viscosity which was further prevented by maintaining constant flow rate with controlled pressure limit.

The anti-coagulated blood was recalcified before introducing it into the flow system by adding 5 mM $CaCl_2$/10 mM $MgCl_2$ (10x dilution) into whole blood as described. The anticoagulant works by chelating the calcium present in the blood to prevent coagulation, whereas 5 mM/10 mM $CaCl_2$/$MgCl_2$ achieved proper restoration of calcium in the blood to restore its ability to coagulate.

2.3.6 Labelling platelets in whole blood

To allow the downstream analysis of platelet binding, it was desirable to label platelets fluorescently before addition to the system. A series of preliminary studies assessed optimal conditions for platelet labelling. Blood was collected from a healthy volunteer and different concentrations (1 µg/mL, 3 µg/mL, or 10 µg/mL) of rhodamine 6 G (R6G) (Sigma-Aldrich) were tested by adding it to the blood followed by 5 min incubation at room temperature. R6G binds platelet mitochondria and exhibits fluorescent spectra of wavelength 480 nm /524 nm (em/ex). The stained blood smears were spread onto glass slides for microscopic analysis. Figure 2.9 shows the fluorescently labelled platelets (red) in whole blood, where 3 µg/mL showed the clearest image of platelets compared to the other concentrations prepared. This concentration was used in all further flow experiments.

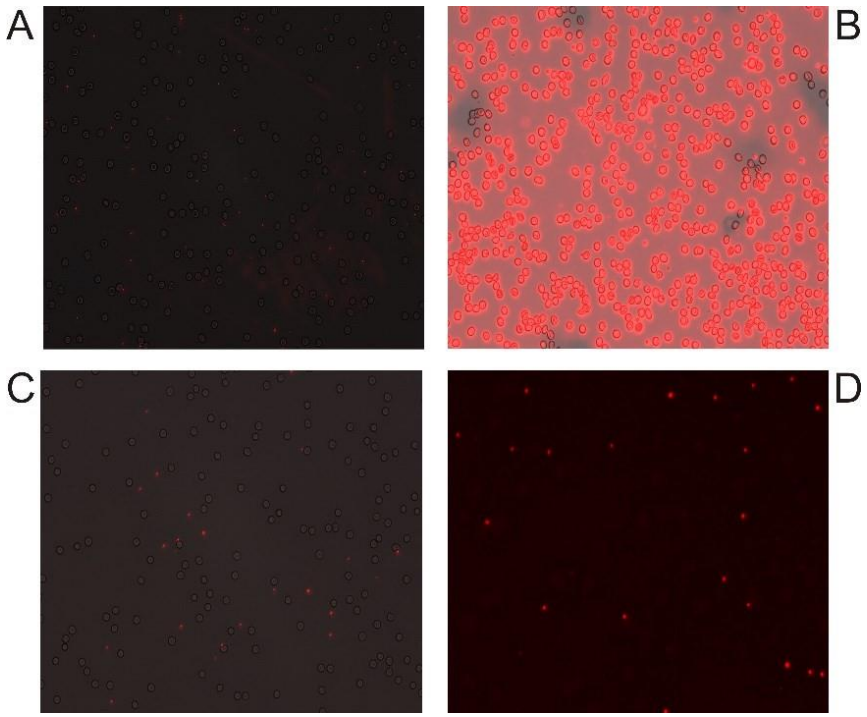

Figure 2.9: Representative fluorescent images of platelets in blood smear. Different concentrations of R6G were added to whole blood to stain platelets (red); A) 1 µg/mL B) 10 µg/mL C) 3µg/mL with red blood cells D) 3µg/mL without red blood cells.

2.3.7 Validation of platelet adhesion by TNF-α activation of endothelial cells

Initial testing for fluorescently-labelled platelet adhesion to endothelial cells in the flow system using whole blood was performed using endothelial cells treated with tumour necrosis alpha (TNF- α). Chronic inflammatory diseases are also associated with thrombotic events and the release of cytokines such as interleukin-2 (IL-2), TNF-α during inflammatory conditions causes endothelial cell activation which can increase thrombosis due to increases in pro-coagulant effects. TNF-α was initially useful to validate the thrombotic system by observing platelet adhesion and aggregation under flow.

TNF-α (1 ng/mL) or vehicle (PBS) was added to the culture medium of cells in the 35 mm petri dish and incubated for 6 hours at 37˚C in 5% carbon dioxide. The cells were then assembled in the flow system with whole blood containing fluorescently labelled platelets (3 µg/mL) under

the previously optimised flow conditions. The cells were fixed and stained with Hoechst nuclear stain, as per previous methods, for microscopic observation. The platelet aggregation was observed under confocal microscopy. Images in Figure 2.10 show that TNF-α stimulated endothelial cells and formed platelets aggregates on their surface under flow compared to the vehicle control. The platelets were clearly visible and hence able to be recorded and assessed quantitatively per field of view.

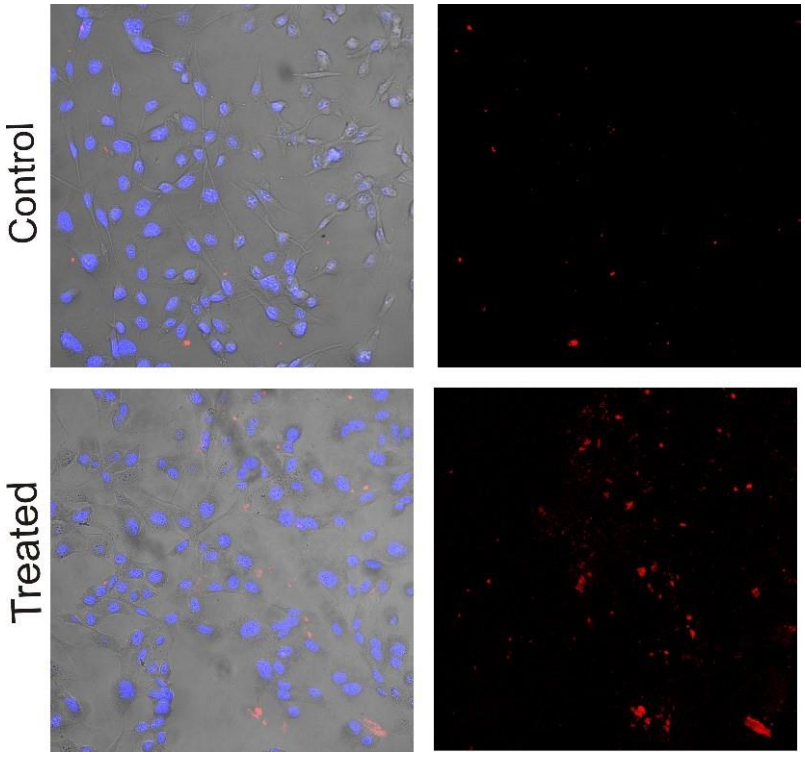

Figure 2.10: Representative confocal images of platelet aggregation on non-irradiated endothelial cells in the presence of TNF-α under flow. The platelets (red) were pre-stained with R6G in human whole blood and cell nuclei (blue) of endothelial cells with Hoechst 33342. Platelet aggregation in TNF-α treated cells was observed with no aggregation in control.

2.4 Discussion

In this study, a parallel-plate flow chamber was developed successfully using fresh human whole blood and irradiated endothelial cells under controlled shear flow conditions based on the cell behavior and adhesion. More recently, parallel-plate flow chamber systems have gained wide popularity due to their accurate specifications of the applied shear stress and absolute laminar flow regime between the parallel-plates [305, 306, 309]. This study demonstrated the

shear-mediated platelet thrombi formation under flow using the optimised flow conditions. There has been significant progress in assessing whole blood thrombus formation using *in vitro* flow systems via platelet binding and accumulation [317, 319, 321, 347]. Methodologically, thrombus growth has frequently been determined by platelet adhesion and aggregation where it usually occurs by: 1) initial deposition of platelets to the thrombogenic surface; and 2) rapid phase of platelet-to-platelet recruitment promoting large thrombosis and occlusion [314, 348]. Though current results demonstrated the aggregation of platelet on blood smear and TNF-treated cells compared to control, still some non-specific labelling of R6G could be noticed on the cell surface. However, it was unlikely that leukocytes would be non-specifically labelled with R6G due to the morphological differences the platelets and leukocytes [438]. This could be improved further in this study by labelling fibrin for more specific analysis and that will be discussed in Chapter 3.

Therefore, in this study, platelets were fluorescently labelled in whole blood before introduction into the flow system where the platelet thrombi on endothelial cells showed the efficiency of the designed parallel-plate flow chamber in achieving effective thrombus stimulation.

The flow system experienced uniform shear stress of 3.1 dynes/cm^2 and thereby maintained a uniform flow pattern throughout the experiment. In general, the flow of blood generates shear stress on the luminal vessel wall and endothelial surface where the estimated average shear stress in major human arteries has previously been determined to range between 2 – 20 dynes/cm^2 which increases to 30 – 100 dynes/cm^2 near arterial branches [320]. Further, arterial thrombus formation is directly associated with the mechanical shear experienced by platelets within the flow [349]. Shear stress varies from the normal range in many pathophysiological conditions due to stiffness of the arteries that changes the blood pressure and flow conditions [344, 350-352]. However, this is not the case in AVMs where there is evidence that the AVM

vessels alter their inner diameter for long-term changes to blood flow such that a constant level of shear stress is maintained throughout the wall [353]. This would be an important point to note in this study as the developed flow system maintains constant shear flow conditions thereby experiencing near *in vivo* AVM haemodynamic conditions. Initially, optimization of flow system was done using EBM medium to adjust the stroke volume, rate and time which was useful ethically in reducing the blood usage but unlikely to be continued throughout the experiment due to changes in the viscosity of blood and medium. The experiment was then continued and validated using whole blood with same parameters to check its effect on cells under flow where no major differences were noted.

However, this study is limited with respect to achieving a complete physiological condition which requires high shear flow and strokes/min. Shear stress (3.1 dynes/cm^2) and pulse rate (38 strokes/min) comes within or near the normal range of human arteries (2 – 200 dynes/cm^2) and pulse rate (40 – 100 beats/mins). Hence, perfusion of whole blood into the parallel-plate flow system with endothelial cells was well operated to mimic *in vivo* physiological conditions with the pulsatile blood pump. In addition, the flow apparatus maintained an enclosed circulation loop with a single flow entry where it was quite challenging to use whole blood due to its high viscosity, formation of air bubbles, and activation of coagulation cascade [319].

Anticoagulant of blood samples is necessary to maintain proper blood rheology without any biological effects [354]. Use of heparin for this purpose was reported to be associated with potential systemic anti-coagulation and bleeding disorders whereas trisodium citrate proved safe to use as an anti-coagulant by chelating ionised calcium in blood [355, 356]. The proper balance in the blood flow was well maintained in this study by using the trisodium citrate buffer with a concentration of $CaCl_2$/$MgCl_2$ (for recalcification) where no change in blood viscosity was noticed.

Maintaining a proper vascular environment was well achieved in this study not only by using

whole blood but also with human cerebral microvascular endothelial cell (hCMEC/D3). The cells maintained a heathy cell population with the benefits of media supplements for optimal growth and function [357]. Further, functional integrity was well maintained as numerous studies demonstrated the use of hCMEC/D3 *in vitro* as a blood brain barrier (BBB) model thereby considered the cell line as a best option to mimic human brain endothelial cells [358-361]. However, use of primary endothelial cells would be more appropriate though practically difficult to culture due to more contamination and requirement of unique media to maintain its survivability and growth. Further, the outcome from primary cells would difer from the current results. Cellular maintenance under flow in this work was supported by having endothelial cells growing on a collagen substratum, which is known to improve cell adherence where collagen-coated dishes sustained cell growth and retention under shear stress for longer periods compared to cells grown without a collagen coating [362, 363]. This was well proven in this study where the shear-mediated cells under flow maintained good confluency even after the flow without loss or uplifting of cells. Apart from acting as an attachment factor, collagen is normally present in the subendothelial basement membrane as an extracellular matrix component which gets exposed during tissue injury to platelets causing activation and aggregation [364, 365]. Endothelial cells over pre-coated collagen in this study therefore simulated a complete and more physiological brain endothelial cell model where the possibility for collagen to cause initial platelet adhesion was limited by using 100% confluent cells in the flow.

The effect of radiation on hCMEC/D3 was also well investigated in this initial study by using various doses and time-points post irradiation for analysis. Cells of the endothelium are highly vulnerable to radiation causing vascular injury [268, 366]. Zhao et al reported the changes in endothelial cell cycle stage after irradiation at different doses where 15 Gy and 25 Gy caused significant cell cycle arrest with more cells accumulating in the G2 phase [256], while a dose of 5 Gy caused primarily moderate changes in cell morphology, though not significant

compared to the non-irradiated control. Radiation-induced cellular arrest in the current study was also associated with changes in cell shape especially at 15 and 25 Gy with cellular hypertrophy observed as cell swelling with multinucleated cells compared to non-irradiated control. This could be due to cell senescence, which is a state of permanent cell cycle arrest most commonly associated with aging or stress leading to tissue malfunction and inflammation, and often associated with cellular hypertrophy as a marker [367]. Radiation-induced cell senescence has been demonstrated in many studies due to cellular stress as a result of radiation-induced DNA damage [368-371]. McRobb et al recently reported stress-induced senescence after radiation (20 Gy) in brain microvascular endothelial cells with the evidence of hypertrophy and other senescence-associated markers such as increased senescence-associated beta-galactosidase activity [268]. The current results showed changes in irradiated cell morphology at day 1, day 3 and day 5 with more cells uplifted at day 5 after flow compared to other doses and sham control. This could be due to the combined effect of both radiation and shear flow conditions at the later time-point (day 5) since the irradiated cells usually undergo oxidative stress, DNA damage, inflammation, and potentially cell arrest and apoptosis [270, 271, 372] where the chances that these factors would have contributed to the loss of cell integrity and population was high. This might not be the case from the clinical aspect to treat AVMs at day 5 considering the point that *in vitro* condition would be different from *in vivo.* Using these results, analyses of the irradiated cells under flow were limited to day 1 and day 3 and not day 5. Overall, this study has successfully demonstrated the platelet-thrombi formation on irradiated endothelial cells under optimised flow conditions.

2.4 Summary and Conclusion

The aim of this chapter was to develop a parallel-plate flow chamber that was well established with proper control of flow conditions using irradiated endothelial cells and fresh human whole blood. The benefits of a parallel-plate flow device are its reliable way of observing fluid flow,

simple to use, and more easily reproducible with relatively high throughout and potential cost benefits for development of targeting agents [308]. This study demonstrated the successful development of a parallel-plate flow chamber system designed to test the effect of pro-thrombotic conjugates in achieving thrombosis on irradiated cells under optimised flow conditions. Preparation and testing of pro-thrombotic conjugate using the flow system will be continued in Chapter 3.

Chapter 3

3. Development and testing of a selective phosphatidylserine- targeting pro-thrombotic conjugate on irradiated human microvascular endothelial cells under *in vitro* pulsatile flow

3.1 Introduction

The overall goal of this project is to develop a vascular targeting treatment for brain arteriovenous malformations that causes complete AVM vessel occlusion. Radiation causes upregulation of surface biomarkers on AVM endothelium that makes it different from normal endothelium serving as a potential target for a vascular targeting approach. The purpose of this work was to develop a novel pro-thrombotic conjugate using these targets by linking a ligand/antibody specific to the target protein with effector moiety (coagulant protein), and then to test its efficacy in stimulating thrombosis on irradiated endothelial cells using the parallel-plate flow chamber as developed in Chapter 2. Recent studies demonstrated significant externalisation of endothelial phosphatidylserine upon radiation both *in vitro,* using brain microvascular endothelial cells, and *in vivo* using a rat AVM model [255, 256].

The specific aims of the work were: 1) to develop a pro-thrombotic conjugate using annexin V (a ligand that targets phosphatidylserine) with thrombin (effector molecule); 2) to test the efficacy of the conjugate in stimulating thrombosis on irradiated microvascular endothelial cells under flow; and 3) to test the effect of different combinations of conjugate and radiation doses in inducing stable thrombosis under flow.

3.2 Standard methods

3.2.1 Cell culture, collagen coating and irradiation

hCMEC/D3 cells were cultured in a 75 cm^2 flask or 35 mm glass bottom petri dish pre-coated with collagen and irradiated at 0, 5, 15 or 25 Gy by using the protocol described in Chapter 2.

3.2.2 Conjugate preparation

Thrombin (Jomar Life Research) was conjugated with annexin V (Jomar Life Research) using a Lys-Lys protein-protein conjugation kit (Click Chemistry Tools Bioconjugate Technology Company) according to the manufacturer's instructions. Briefly, 300 µL thrombin (2 mg/mL) in BupH buffer (pH 7.5) was labelled using 12-fold molar excess tetrazine (Tz) reagent, and 300 µL annexin V (1 mg/mL) in BupH buffer was labelled using 12-fold molar excess trans-cyclooctene (TCO) reagent. Annexin-TCO and thrombin-Tz were mixed together (ratio 1:2) and the conjugation reaction analysed by sodium dodecyl sulfate polyacrylamide gel electrophoresis (SDS-PAGE) (Figure 3. 1). Image J (Version 1.5, rasband, W.S., Image J, National Institute of Health, USA) was used to determine efficiency of conjugation as 40%. Thrombin activity was also measured before and after conjugation using a commercially available thrombin activity assay kit (Ana Spec, CA, USA). This conjugation involved catalyst-free ligation in mild buffered media which included long-term stability of TCO and T_z functional groups on modified protein thereby enhancing the efficiency of conjugate.

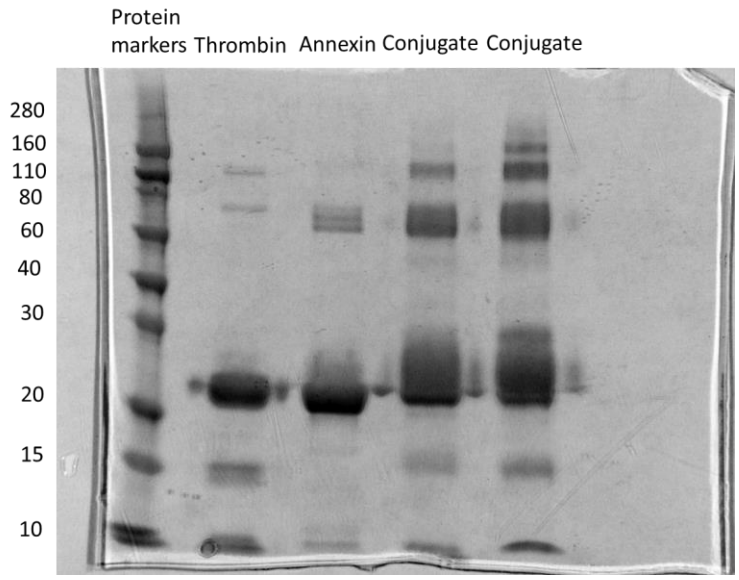

Figure 3. 1: SDS analysis for annexin V-thrombin conjugate. Thrombin (37 kDa) was linked to annexin V (36 kDa) to get annexin V-thrombin conjugate (69 kDa). The two conjugate lanes were the duplicates.

3.2.3 Fibrinogen-FITC conjugate

Fibrinogen from human plasma (Sigma-Aldrich) was purchased and conjugated to fluorescein isothiocyanate (FITC) using the FluoroTag^{TM} FITC Conjugation kit (Sigma-Aldrich) according to the manufacturer's instructions.

3.2.4 Thrombosis under flow

Approximately 17 – 20 mL of human blood was collected from healthy volunteers (as described in Chapter 2). Then, 3 µg/mL of rhodamine 6G (Sigma-Aldrich) and 0.13 mg/mL of fibrinogen-FITC was added to the whole blood. The blood was recalcified and separated into 2 tubes which was sufficient to run two experiments (treated and control). The parallel-plate flow chamber was assembled with human whole blood and sham or irradiated endothelial cells as per the protocol described in Chapter 2. At time zero, different concentrations of conjugate were injected into the system to achieve final concentrations of 1.25 µg/mL, 2.5 µg/mL or, 5 µg/mL. The pump was operated under optimised flow conditions as determined in Chapter 2.

After 15 min of flow, the pump was disassembled followed by cell nuclear staining and mounting for confocal microscopic analysis (as described in Chapter 2). After each run, the pump was washed, and control experiments were done using whole blood and non-irradiated endothelial cells with the same conjugate concentrations (1.25 µg/mL, 2.5 µg/mL or 5 µg/mL). Experiments were also carried out with saline, free unconjugated 1.5 µg/mL thrombin, and free unconjugated 0.9 µg/mL annexin V as controls, where percent loss of thrombin activity (5%) was taken into consideration. An equivalent volume of saline injected into the system was used as a non-conjugate control.

3.2.5 Microscopy and image analysis

Cells were viewed under bright-field and using ex358nm/em461nm channels for Hoechst. Platelets and fibrin were viewed at ex550nm/em570nm and ex 495/em519nm, respectively. Z stacks were taken, and 3D image reconstruction was done using Bitplane (IMARIS software version 8) for measuring thrombus volume. First, the image was selected by adding its surface into the analysis toolbar and absolute intensity was applied after selecting the source channel. Threshold was applied and adjusted manually until the image distribution over the surface was observed with all deposited fibrin. The volume was obtained by unifying whole fibrin volume in a field of view. 2D analysis of platelet area was obtained with the same software tool settings. Five fields of view from each experiment were selected and the average measurements were considered for analysis. Data analysis was performed using Prism 6.01 (Graphpad software Inc., La Jolla CA). Values are given as mean ± standard deviation (SD) of 3 independent experiments. Multiple comparisons were performed using two-way ANOVA with Tukey's post-hoc analysis and the level of significance was set at $p<0.05$.

3.2.6 Analysis of fibrin degradation product (FDP)

As a further measure of thrombotic activity in the flow system, whole blood was analysed after flow for the presence of fibrin degradation product (FDP). Whole blood was collected after each flow experiment, centrifuged at 1000 x g for 10 min to separate plasma, which was stored at -80˚C until analysis using a fibrin degradation product (FDP) enzyme-linked immunosorbent assay (ELISA) kit (Jomar Life Research) according to the manufacturer's instructions.

3.3 Results

3.3.1 Annexin V-thrombin conjugate enhances platelet binding and aggregation on irradiated endothelial cells under flow

Evidence for thrombus formation was estimated by measuring platelet and fibrin aggregation and accumulation by confocal microscopy (Figure 3.2). The platelet adhesion and aggregation were first determined on the endothelial surface, one of the first steps in thrombus formation. The average size of the platelet aggregates as well as the total area of platelet deposition per field of view was measured. Overall, increased platelet binding and aggregation was observed with increasing doses of both conjugate and radiation (Figure 3.2A – D). The average size of platelet aggregates (Figure 3.2A, B) increased significantly (2.1-fold, $p<0.0001$) at the higher doses of 15 and 25 Gy using 2.5 µg/mL conjugate dose at both day 1 and day 3. No major differences were observed between day 1 and day 3 values. Total platelet area (per field of view) increased modestly with each radiation dose in the absence of conjugate (up to 1.5 – 2-fold), though this was not statistically significant (Figure 3.2C, D). However, in the presence of conjugate, significant increases in total platelet area were observed relative to the non-irradiated, saline control at all radiation doses (3 – 4-fold; Figure 3.2C, D).

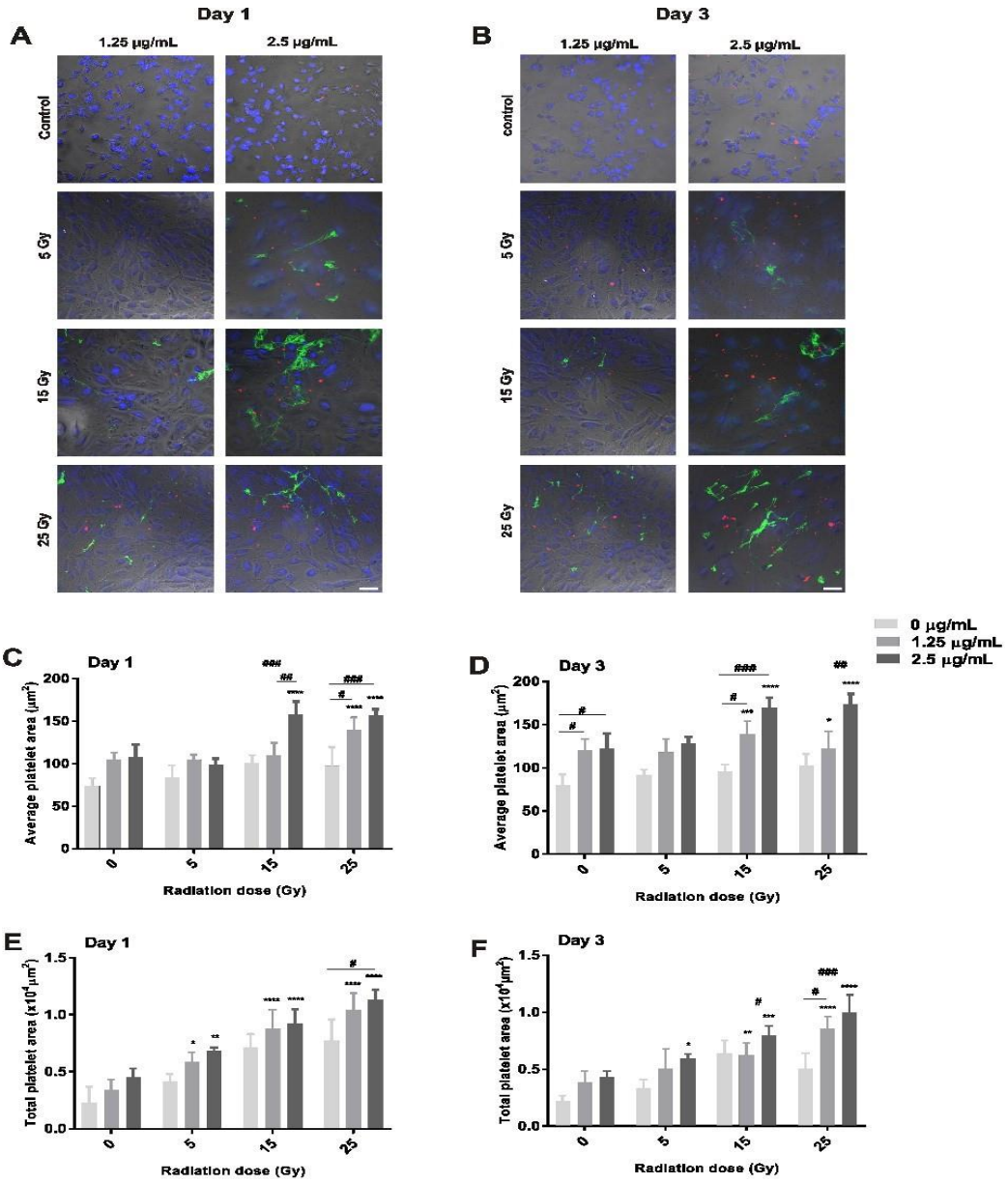

Figure 3.2: Platelet aggregation and fibrin formation on irradiated endothelial cells. Representative confocal images of platelet aggregation and fibrin formation on irradiated endothelial cells in the parallel-plate flow system at day 1 (A), or day 3 (B); post-irradiation or sham. Platelets were pre-stained in whole blood with R6G (red) and FITC-labelled fibrinogen (green) prior to circulation. Cell nuclei were stained post-flow with Hoechst 33342 (blue). Bar = 50 µm; magnification = 200x. Average size of platelet aggregates (μm^2) at day 1 (C) and day 3 (D) post-irradiation. Total platelet area per field of view at day 1 (E) and day 3 (F). Data are shown as mean ± SD (3 independent experiments) and were analysed using two-way ANOVA with Tukey's post-hoc analysis. ****p<0.0001, ***p<0.001, **p<0.01, *p<0.5 comparisons relative to saline, non-irradiated control. ####p<0.0001, #p<0.5, comparisons within radiation dose group.

3.3.2 Annexin V-thrombin conjugate enhances fibrin deposition on irradiated endothelial cells under flow

Incorporation of fluorescently labelled fibrinogen was used as a measure of stable thrombus formation (Figure 3.2 and Figure 3.3A – G). 3D reconstruction using z stacks of confocal microscopy was used (Figure 3.3A, B, C) to determine the average volume of individual fibrin thrombi (Figure 3.3D, E) as well as the total fibrin volume per field of view (Figure 3.3F, G) at day 1 and 3. At both post-irradiated time points, no fibrin deposition was observed on non-irradiated controls with or without conjugate addition (Figure 3.2 and Figure 3.3D – G). No fibrin deposition was observed at any radiation dose in the absence of conjugate. A dose of 1.25 µg/mL conjugate showed significant fibrin development at 15 Gy and 25 Gy with minimal to no fibrin deposition at 5 Gy on both day 1 and day 3 (Figure 3.3D – G). A dose of 2.5 µg/mL initiated fibrin formation at 5 Gy, followed by formation of a more interlinked fibrin network at 15 and 25 Gy. At both 15 Gy and 25 Gy using 2.5 µg/mL conjugate, average fibrin volume increased 32 – 64-fold ($P<0.0001$) compared to non-irradiated saline control and respective irradiated saline control (at same radiation dose) (Figure 3.3D, E). No major differences were noted between day 1 and day 3 except significant differences between the two conjugate doses were more apparent at day 1 ($P<0.0001$). Values of total fibrin volume (Figure 3.3F, G) showed a similar trend to average volume (Figure 3.3D, E).

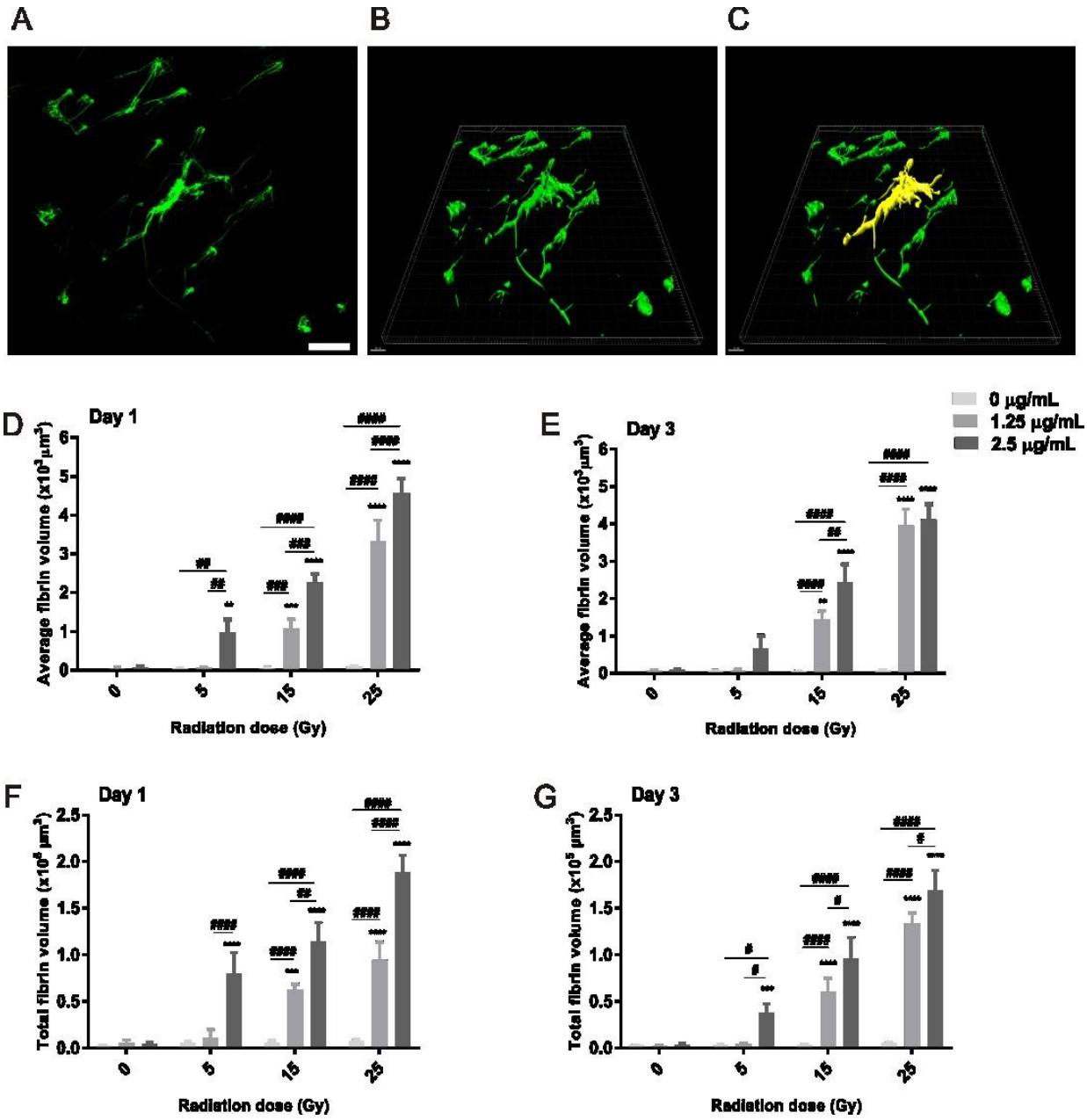

Figure 3.3: Fibrin thrombus formation on irradiated endothelial cells. (A) Representative confocal image of cross-linked fibrin fibers in 2D (green); (B) 3D reconstruction of Z stacks showing deposited fibrin on the surface. (C) Individual 3D fibrin thrombi (yellow) could be measured independently to give average fibrin volume (D, E) or summed to give total fibrin volume (μm^3) per field of view (F, G) at day 1 (D, F) or day 3 (E, G). Data are shown as mean ± SD (3 independent experiments) and were analysed using two-way ANOVA with Tukey's post-hoc analysis. ***p<0.001, **p<0.01, comparisons relative to non-irradiated control. ####p<0.0001, ##p<0.01, #p<0.5, comparisons with saline control within radiation dose group. Scale bar = 30 µm. Magnification = 200×.

3.3.3 Free thrombin or annexin V induces low level activation of blood coagulation

Thrombosis was examined in the presence of free, non-targeted thrombin and free annexin V at activity levels/doses equivalent to that of the conjugate. Base levels of platelet binding and aggregation were observed at all radiation doses using saline, free thrombin and free annexin under flow at both time points (Figure 3.4). Average platelet area was not generally affected by free thrombin or annexin V at any radiation dose at either time point (Figure 3.4A, B). Total platelet area increased 2 – 3-fold in response to free thrombin in non-irradiated controls and at all radiation doses in the range relative to the non-irradiated saline control (Figure 3.4C, D). Similarly, annexin V increased total platelet area at the higher radiation doses relative to the non-irradiated saline control, however was not significantly different to the respective saline control at the equivalent radiation dose.

Average fibrin volume and total fibrin volume increased from 4 – 5-fold in response to thrombin alone relative to the non-irradiated saline control at both days, however, minimal significant difference was seen relative to the respective irradiated saline controls (at same dose) (Figure 3.4E – H). However, when compared to levels of fibrin deposition in response to conjugate, maximal levels of total fibrin deposited in response to free thrombin and free annexin V were in the range $0.05 – 0.1 \times 10^5$ μm^3, while the conjugate resulted in volumes in the range of $1 – 2 \times 10^5$ μm^3, a 10 – 20-fold increase.

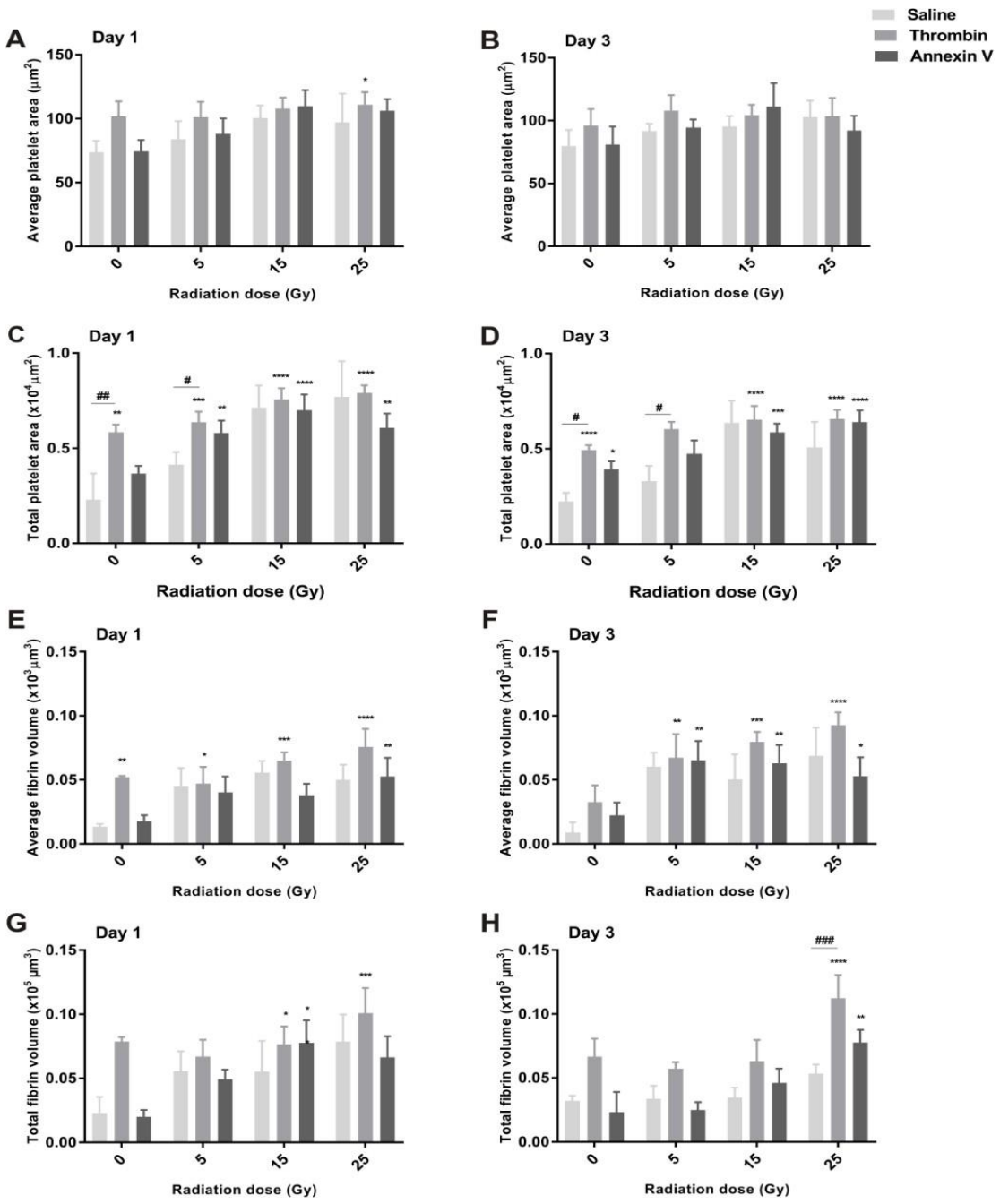

Figure 3.4: Platelet and fibrin deposition in response to free annexin and free thrombin. Average platelet area (A, B), total platelet area (C, D), average fibrin volume (E, F), and total fibrin volume (G, H) in response to saline control, free thrombin and free annexin at each radiation dosage on both day 1 (A, C, E, G) and day 3 (B, D, F, H). Data are shown as mean ± SD (3 independent experiments) and were analysed using two-way ANOVA with Tukey's post-hoc analysis. ****p<0.0001, ***p<0.001, **p<0.01, *p<0.5, Comparisons relative to sham-irradiated control. ####p<0.0001, ###p<0.001, ##p<0.01, #p<0.5, comparisons relative to saline control within radiation dose group.

3.3.4 Plasma FDP level

The FDP concentration was measured in plasma from whole blood after flow in blood treated with 2.5 µg/mL conjugate at the day 1-time point (Figure 3.5). Significant increases were observed at both 5 Gy (28-fold, $p<0.01$) and 25 Gy (68-fold, $p<0.0001$). FDP levels increased 9-fold in response to 15 Gy however this did not reach statistical significance with the 3 replicate samples.

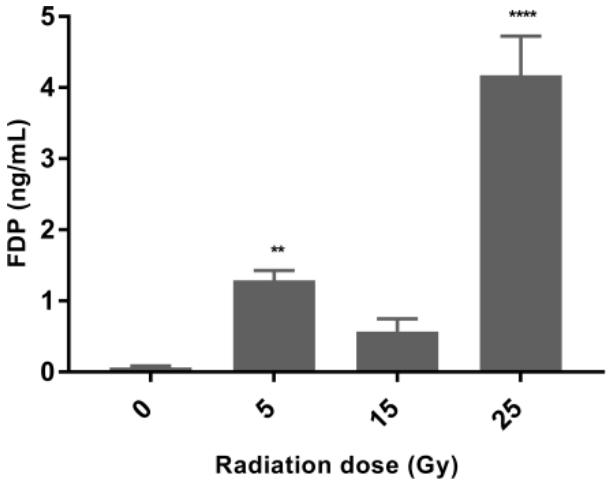

Figure 3.5: Plasma FDP concentration after flow. Presence of FDP analysed in plasma treated with 2.5 µg/mL conjugate at day 1 post-irradiation with controls under flow. Data are shown as mean ± SD (3 independent experiments). Statistical differences were analysed using one-way ANOVA Tukey's post-hoc analysis. ****$p<0.0001$, comparisons relative to sham-irradiated, saline control.

3.4 Discussion

In this study, annexin V-thrombin conjugate was investigated for its efficacy to bind selectively to irradiated endothelial cells and induce thrombosis under flow using an *in vitro* parallel-plate flow chamber. This demonstrated the successful development and testing of pro-thrombotic conjugate under flow in stimulating platelet aggregation and fibrin formation. The use of fresh human whole blood with irradiated endothelial cells to demonstrate *in vitro* shear-dependent thrombosis in the presence of a PS-targeting pro-thrombotic conjugate showed the synergistic

effect of radiation and conjugate in inducing stable thrombosis under optimised shear flow conditions. The current study demonstrates that durable platelet adherence to HCMEC and stable fibrin thrombi formation is possible by priming the endothelial cells with radiosurgery and using the developed pro-thrombotic vascular targeting agent under flow conditions.

Irradiation causes cellular changes that tend to up-regulate various cell adhesion, pro-inflammatory, and pro-thrombotic molecules on the endothelial surface [250, 253, 373, 374], and this includes the externalisation of PS [296]. Earlier studies reported the post-irradiation PS externalisation on microvascular endothelial cells *in vitro,* using live cell imaging, and *in vivo,* using near-infrared fluorescent optical imaging in a rat AVM model [255, 256]. Thus, PS appears a valid target for a vascular targeting approach to AVM treatment and therefore a PS-targeting, annexin V-thrombin conjugate was developed in this study for testing its effect under flow. In agreement with earlier studies, this study successfully demonstrated that this conjugate can bind effectively on irradiated endothelial cells, and further, that this occurs under high flow and initiates platelet aggregation and fibrin clots in the presence of whole blood. Not unexpectedly, higher radiation doses (15 and 25 Gy) caused significantly greater thrombus formation when compared to the lowest dose (5 Gy) and when in combination with a conjugate dose of 2.5 µg/mL.

Overall, the data suggest that there was a significant synergistic interaction between the effects of radiation dose and conjugate dose, and that low radiation dose could still induce endothelial PS exposure and thrombosis when used in combination with the higher conjugate concentration. This is considered noteworthy for future applications to AVM treatment in the clinic. Treatment of large AVMs by stereotactic radiosurgery alone is often limited by the high dose requirement to achieve complete obliteration (>15 Gy) [375]. Larger AVM volumes receiving higher doses have greater risk of complications and this is often not achievable in large lesions without significant off-target and late necrosis effects to the surrounding brain

[167, 376]. The potential ability to use a lower dose of radiation when combined with a vascular targeting agent would potentially decrease the latency period associated with current standard radiosurgery approaches and increase the number of patients considered treatable.

It was important in this study to examine not just thrombus formation but also thrombus stability in the presence of the developed conjugate. Formation of fibrin polymers occurs later in the coagulation cascade to attain a mature, stable clot. Fluorescently labelling fibrinogen with FITC gave evidence of terminal thrombotic events. This technique of labelling thrombus through fibrinogen has been used previously as an advanced method of studying platelet activation in whole blood [377, 378]. This is in contrast with the binding and aggregation of platelets which occurs early in the clotting cascade but does not necessarily indicate that a stable thrombus will be formed [379].

Confocal microscopy and digital image reconstruction allowed reconstruction of a 3D image of fibrin deposition to give more detailed information on whole thrombus volume using fibrin structure. Similar analysis approaches were suggested by other authors previously [319]. It was possible to observe the initiation of fibrin and branched fibrin network on activated platelets in response to increases in radiation and conjugate dose. Measuring thrombosis using the deposited fibrin was far superior to assessing platelet binding and aggregation. However, by examining both platelet and fibrin deposition in this study, we could see that though free thrombin caused platelet activation with more platelet aggregates under flow, the level of activation was still well below the baseline activation of combined conjugate and radiation dose groups. In addition, there was no significant fibrin formation observed in response to thrombin alone, in comparison to that induced by conjugate. Radiation alone (in the absence of conjugate), caused a dose-dependent increase in platelet adhesion and aggregation, however did not significantly increase fibrin deposition. Similarly, conjugate had a dose-dependent effect on platelet aggregation but not fibrin deposition in the absence of radiation. Thus, in

alignment with the literature [130, 253], radiation appears to induce a pro-thrombotic, platelet-binding surface on the endothelium but does not necessarily induce rapid formation of more stable thrombi and this clearly explained the differences in platelet activation between controls (free thrombin, saline, annexin V) and annexin V-thrombin conjugate. Further, these findings showed that delivery of PS-targeted thrombin to the irradiated cells was far superior to adding free thrombin in the blood. This suggests that systemic thrombosis would be unlikely to occur in the presence of conjugate on non-irradiated vessels without the initial pro-thrombotic radiation stimulus.

In addition, FDP analysis was used in this study using unconditioned (post-flow) plasma to assess thrombus stability since a fine balance between clot formation and fibrinolysis determines the thrombus maturity [380-382]. The determination of FDP in plasma or serum has been used previously and considered as an effective indicator of a patient's coagulative-fibrinolytic state in thrombosis, acute myocardial infarction, or sepsis [383-386]. The findings clearly indicate the presence of increasing levels of FDP in response to radiation at the 2.5 µg/mL conjugate dose which confirmed the fibrin deposition data and formation of highly stable thrombus under flow conditions. This suggests the possibility of achieving fully developed thrombosis even at low radiation doses.

The development of this parallel-flow system has significant advantages over prior studies. The inclusion of 3 different methods for analysis of thrombus formation was important to fully determine the effects of combined conjugate and radiation doses and for their comparison to the effects of thrombin alone. The parallel-plate flow system provided a simpler and cost-effective way to test the conjugate under flow since it is not feasible to test various doses of radiation and conjugate using more animals. Moreover, achieving this vascular targeting approach under physiologic flow conditions rather than steady flow added advantage to this study by simulating the *in vivo* haemodynamic condition using the pre-defined shear stress with

pulsatile flow pattern. However, the system is limited with respect to achieving a complete physiological flow rate and shear stress level of normal human arteries and veins, as described in the preceding chapter and associated with limited ability of the endothelial cells to adhere to the artificial collagen substratum. The ability to culture human AVM endothelial cells isolated from surgically excised human AVMs would also be more physiologically relevant but considered not necessary in this study since this is the early development and pre-testing of conjugate once a valid target is identified.

3.5 Summary and Conclusion

The aim of this chapter was to develop a pro-thrombotic conjugate using annexin V that has high affinity towards the identified target, phosphatidylserine, and thrombin as the effector molecule, and testing the efficacy of the developed conjugate in stimulating thrombosis using the parallel-plate flow chamber under optimised flow conditions. Further, various conjugate concentrations and radiation doses were used to determine the best synergistic dose effect of radiation and conjugate in enhancing fibrin thrombus formation under flow. Finally, a FDP assay was used to validate the advanced stage of mature and stable thrombosis.

Hence, the study demonstrated the successful development and testing of this pro-thrombotic conjugate on irradiated endothelial cells using the established parallel-plate flow chamber. The parallel-plate flow system proved to be a simple and effective way to develop the vascular targeting approach. There was good reproducibility between each experimental run considering the use of different patient samples.

Chapter 4

4. Validation of new molecular targets on irradiated endothelial cells: development and testing of an anti-CRYAB antibody-thrombin conjugate under flow

4.1 Introduction

The main aim of the work in this chapter was to validate other radiation-stimulated targets from a previous proteomic analysis using immunostaining with irradiated hCMEC/D3 cells and then to develop and test a pro-thrombotic conjugate based on the identified target in inducing thrombosis using the established *in vitro* parallel-plate flow chamber. Although the current study has reported a thrombotic response using the PS-targeting annexinV-thrombin conjugate (as described in Chapter 3), it is important to identify and validate various other targets to select the best target to advance for further animal trials and before progressing to clinical trials for treating human patients.

Previous studies have reported the radiation-induced molecular changes on the endothelial surface that could potentially be selectively targeted for vascular targeting therapy [128, 243, 250, 254-256, 284]. Recently, studies using *in vivo* biotin labelling of surface accessible protein in an AVM animal model and comparative proteomics identified 56 proteins with increased levels of expression after irradiation of a rat AVM model [304]. Further, proteomic studies (unpublished, L. McRobb) extended these findings to radiation-induced markers that were expressed for periods up to 3 weeks after irradiation. Using these identified proteins, 7 molecular targets were further assessed in this study for validation of expression on irradiated hCMEC/D3 cells using immunostaining analysis. These proteins were: ectonucleotide pyrophosphatase/pyrophosphodiesterase (ENPP3); ras-related protein Rab1A (RAB1A); protein disulphide-isomerase A6 (PDIA6); clusterin (CLU); activated leukocyte cell adhesion molecule (ALCAM or CD166); septin 2 (SEPT2); and α-crystallin B chain (CRYAB).

The purpose of this specific work was to identify from this group a novel protein target on the endothelial surface that could render the possibility for further investigating their vascular targeting potential and development and testing of an appropriate pro-thrombotic conjugate to induce rapid vessel thrombosis using the established parallel-plate flow chamber under optimised flow conditions.

4.2 Standard methods

4.2.1 Immunostaining

4.2.1.1 Cell culture, collagen coating and irradiation

These procedures were as described in Chapter 2, however for immunostaining the hCMEC/D3 cells were cultured and 1x 10^4 cells/mL were selected in pre-coated 8 well chamber slides (Nunc Lab-Tek II, Sigma) in a final volume per well of 500 µL. The cells were irradiated at 25 Gy with the radiation protocol followed as described in Chapter 2. Non-irradiated cells underwent the same procedure in separate chamber slides without radiation exposure.

4.2.1.2 Cell fixation and blocking

At 24 h post-irradiation, cells were washed briefly with cold 1X PBS and fixed at room temperature with either 50% ethanol (in PBS) for 20 min (permeabilised cell fixation protocol) or 2% phosphate-buffered paraformaldehyde (PFA) for 5 min (non-permeabilised fixation protocol). Cells were then washed three times for 10 min each in 1X PBS. Then, 200 µL of blocking buffer (containing 1X PBS, 5% donkey serum (Sigma-Aldrich) and 1% BSA (Sigma-Aldrich) was added to each chamber and incubated for 1 h at room temperature. Non-irradiated cells were used as a control.

4.2.1.3 Primary antibody labelling

The primary antibodies were diluted (1:100) with antibody dilution buffer (1% BSA in PBS) and 150 µL added to each appropriate well. The chambers were left for overnight incubation

at 4˚C. The primary antibodies used were anti-ectonucleotide pyrophosphatase/pyrophosphodiesterase (anti-ENPP3, bs-156-R, rabbit polyclonal, Bios/Sapphire Biosciences), anti-ras-related protein Rab1A (anti-RAB1A, ARP56561_P050, rabbit polyclonal, Sapphire Biosciences), anti-protein disulphide-isomerase A6 (anti-PDIA6, ARP52102_P050, rabbit polyclonal, Sapphire Biosciences), anti-clusterin (anti-CLU, LS-c331486, rabbit polyclonal, Sapphire Biosciences), anti-activated leukocyte cell adhesion molecule (anti-CD166/ALCAM, mouse monoclonal IgG1, Abcam), anti-septin 2 (anti-SEPT2, STJ25475, rabbit polyclonal, St James/Sapphire Biosciences), anti-αß-crystallin (anti-CRYAB, ab 13496, mouse monoclonal IgG, Abcam). Control primary antibodies included a mouse IgG control isotype (ab13496, Abcam) and rabbit IgG control antibody (ab171870, Abcam) at equivalent concentrations.

4.2.1.4 Secondary antibody labelling

Prior to labelling with secondary antibody, the wells were washed 2 times for 10 min each with PBS at room temperature. Appropriate secondary antibodies were diluted in antibody dilution buffer (1:500). The secondary antibodies used were donkey anti-rabbit-IgG conjugated to Alexa Fluor 647 (A-31373, Thermofisher Scientific) or donkey anti-mouse-IgG conjugated to Alexa Fluor 647 (A-31571, Thermofisher Scientific). Alexa Fluor 488-tagged wheat germ agglutinin (WGA, Life Technologies, W11261) was added to the same dilution buffer at a dilution of 1:1000 and used as a surface marker. The secondary antibody and WGA dilutions were added at 150 µL per well. The cells were incubated at room temperature in the dark for 1 h. Wells were washed once with PBS before removal of the well formers and cells in the slides were washed a further two times with PBS for 5 min. Then, the cells were stained with DAPI (200 µg/mL) to stain nuclei and incubated for 2 min at room temperature followed by PBS washing and mounting (DAKO aqueous mounting medium) for microscopic observation.

4.2.2 Parallel-plate flow experiments

4.2.2.1 Cell culture, collagen coating and irradiation

The cells were cultured in a 75 cm^2 flask or 35 mm glass bottom petri dish pre-coated with collagen and irradiated at 0, 5, 15 or 25 Gy by using the protocol described in Chapter 2.

4.2.2.2 Conjugate preparation

Thrombin (Jomar Life Research) was conjugated with anti-CRYAB (ab13496, Abcam) using a Lys-Lys protein-protein conjugation kit (Click Chemistry Tools Bioconjugate Technology Company) according to the manufacturer's instructions. Briefly, 130 µL thrombin (3.31 mg/mL) was labelled using 20-fold molar excess tetrazine (Tz) reagent, and 100 µL anti-CRYAB (1 mg/mL) in BUPH buffer (pH 7.5) was labelled using 20-fold molar excess trans-cyclooctene (TCO) reagent. Anti-CRYAB-TCO and thrombin-Tz were mixed together (ratio 1:3). The conjugation reaction was analysed by SDS-PAGE (Figure 4.1). Image J (Version 1.5, rasband, W.S., Image J, National Institute of Health, USA) was used to determine the efficiency of labelling anti-CRYAB-thrombin as 70%. Similarly, IgG-thrombin conjugate was developed by labelling with the same 20-fold molar excess of TCO and tetrazine and IgG-thrombin was developed with the same 1:3 ratio of IgG-TCO and thrombin-Tz. Thrombin activity was also measured before and after conjugation using a commercially available thrombin activityassay (AnaSpec, CA, USA).

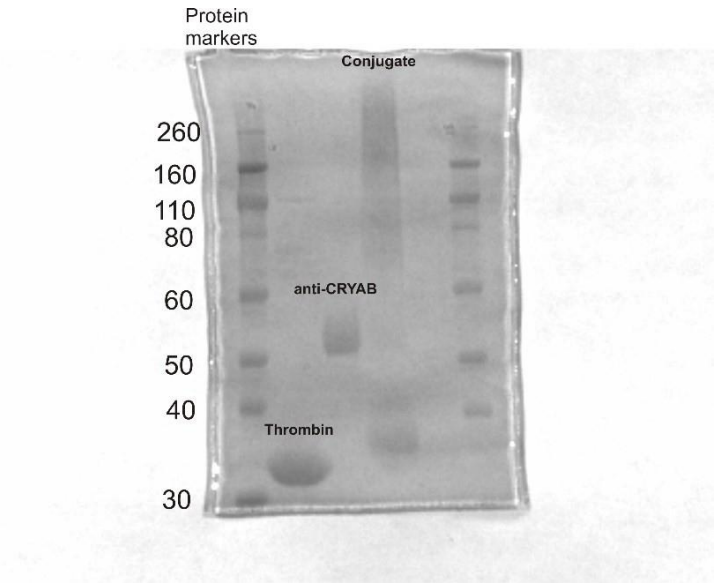

Figure 4.1: SDS-PAGE analysis of the anti-CRYAB-thrombin conjugate. Thrombin (37 kDa) was linked to anti-CRYAB (50 kDa heavy chain shown under reducing conditions) to develop an anti-CRYAB-thrombin conjugate (90 kDa+).

4.2.2.3 Fibrinogen-FITC conjugate

Fibrinogen from human plasma (Sigma-Aldrich) was purchased and conjugated to FITC using the FluoroTag^{TM} FITC conjugate kit (Sigma-Aldrich) according to the manufacturer's instructions. As described in Chapter 2, this was incorporated in whole blood to assess fibrinogen deposition as a measure of thrombus formation.

4.2.2.4 Thrombus under flow

The blood collection, labelling and flow system using whole blood and irradiated cells was assembled and operated based on the protocol described in Chapter 3. Different radiation doses (5, 15, or 25 Gy) and concentration of conjugate (1.25 µg/mL or 2.5 µg/mL) were used in the flow system under optimised flow conditions (described in Chapter 2) with both sham-radiation and saline controls. IgG-thrombin conjugate was used in the flow system as a non-targeting control.

4.2.2.5 Microscopy and image analysis

Cells were viewed under confocal microscopy and analysed for platelet area and fibrin volume using z stacks in the IMARIS software tool as described in Chapter 3.

4.2.2.6 Analysis of fibrin degradation product (FDP)

The whole blood was analysed after flow for the presence of fibrin degradation product (FDP) in plasma as described in Chapter 3.

4.2.3 Fluorescent labelling of anti-CRYAB antibody for immunostaining under flow

To independently assess antibody binding to the irradiated cells without thrombus formation, a near infrared fluorophore was conjugated to the same anti-CRYAB antibody used in the conjugate as well as the control non-specific IgG, and run in the flow system.

The antibody-dye probe was prepared by conjugating Xenolight CF^{TM} near-infrared CF750 (Caliper Life Sciences, Inc.) to the CRYAB and non-specific IgG antibodies according to the manufacturer's instructions (Figure 4.2). Briefly, 200 µg of each antibody was labelled by mixing with 0.04 nmol of dye in dimethylsulfoxide for 1 h at room temperature in the dark. After extensive washing through a Nanosep filter and resuspension in PBS, the absorbance was measured at A750 nm and A280 nm to determine the final concentration and degree of labelling (DOL). DOL was calculated as 0.4 for both CRYAB and IgG antibody-dye probes under these conditions. The CF750-conjugated mouse IgG and anti-CRYAB at 1 µg/mL were used in the flow system with EBM-2 medium where the flow was operated as established in Chapters 2 and 3. The cells after flow were washed, fixed, nuclei stained, and mounted for microscopic observation as described in Chapter 2.

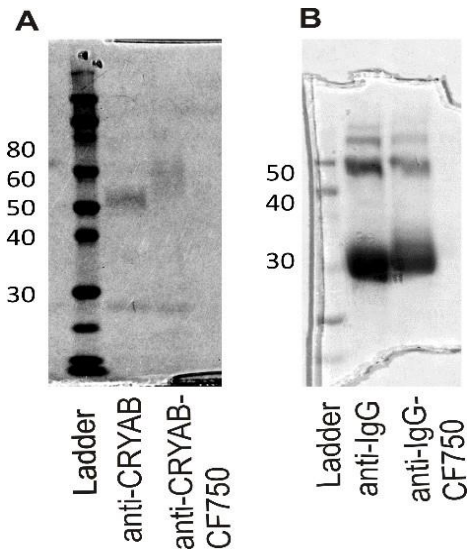

Figure 4.2: SDS-PAGE analysis of the anti-CRYAB-CF750 and anti-IgG-CF750 conjugates. (A) Anti-CRYAB (25 and 50 kDa, light and heavy chains shown under reducing conditions) was conjugated to CF-750 to develop anti-CRYAB-CF750 conjugate (60 kDa band). (B) Anti-IgG (25 and 50 kDa, light and heavy chains shown) was conjugated to CF750 to develop anti-IgG-CF750 (60 kDa).

4.3 Results

4.3.1 Molecular expression of novel protein targets on irradiated endothelial cells

The human microvascular endothelial cells were fixed with either ethanol, to allow permeabilisation of antibodies, or with PFA for a short period, to fix cells without allowing substantial membrane permeation. As many of the target proteins are typically intracellular proteins, the ethanol fixation method which allows antibody penetration was used for preliminary testing of the antibodies where it was hypothesised that the proteins may be more highly expressed and there was more chance of obtaining a positive signal. PFA fixation without a permeabilisation step allows examination of surface-specific expression. The ideal target would be a protein that is expressed on the surface of the endothelial cells only after radiation treatment. For these studies, immunostaining was performed at day 1 and day 3 after irradiation but only on cells irradiated at a dose of 25 Gy.

Some cell loss and cellular hypertrophy were observed, as described earlier, that was reminiscent of stress-induced cellular senescence.

In ethanol permeabilised cells (Figure 4.3), a positive signal was observed for all antibodies to all proteins however with variable patterns of staining in control and irradiated cells. Increased protein expression was observed for ENPP3 and RAB1A on day 1 compared to non-irradiated controls, whereas at day 3, in contrast, non-irradiated cells showed high basal levels of expression for both ENPP3 and RAB1A. SEPT2, PDIA6 and CLU showed high basal levels of AF647 signal in non-irradiated cells at both day 1 and day 3 with variable levels of expression in response to radiation. CD166 showed expression at only day 1 in control cells. Minimal staining was observed for CRYAB. As the purpose of this study with ethanol fixation was simply to test for protein presence, despite the erratic staining patterns, this was performed only once, and studies using light PFA fixation without permeabilisation were used to establish the pattern of surface expression.

In PFA fixed cells (Figure 4.4), the pattern of expression was quite different. These experiments were repeated three times. No molecular expression was observed for ENPP3, CLU, and CD166 in both radiated and control cells at both time points. RAB1A showed AF647 fluorescent signal only in sham controls at day 1 followed by protein expression at both control and 25 Gy on day 3. Increased expression was noted in PDIA6 at 25 Gy compared to control on day 1, whereas expression was noted at both 25 Gy and control on day 3. CRYAB was the most consistently expressed, with no expression in non-irradiated controls at both day 1 and day 3 with increased expression levels after 25 Gy irradiation at both time points.

Hence, CRYAB showed the most promising result of high-level expression at 25 Gy compared to control (Figure 4.4, 4.5). This protein was therefore taken forward as a target for further study to develop and test a CRYAB-targeting conjugate under flow.

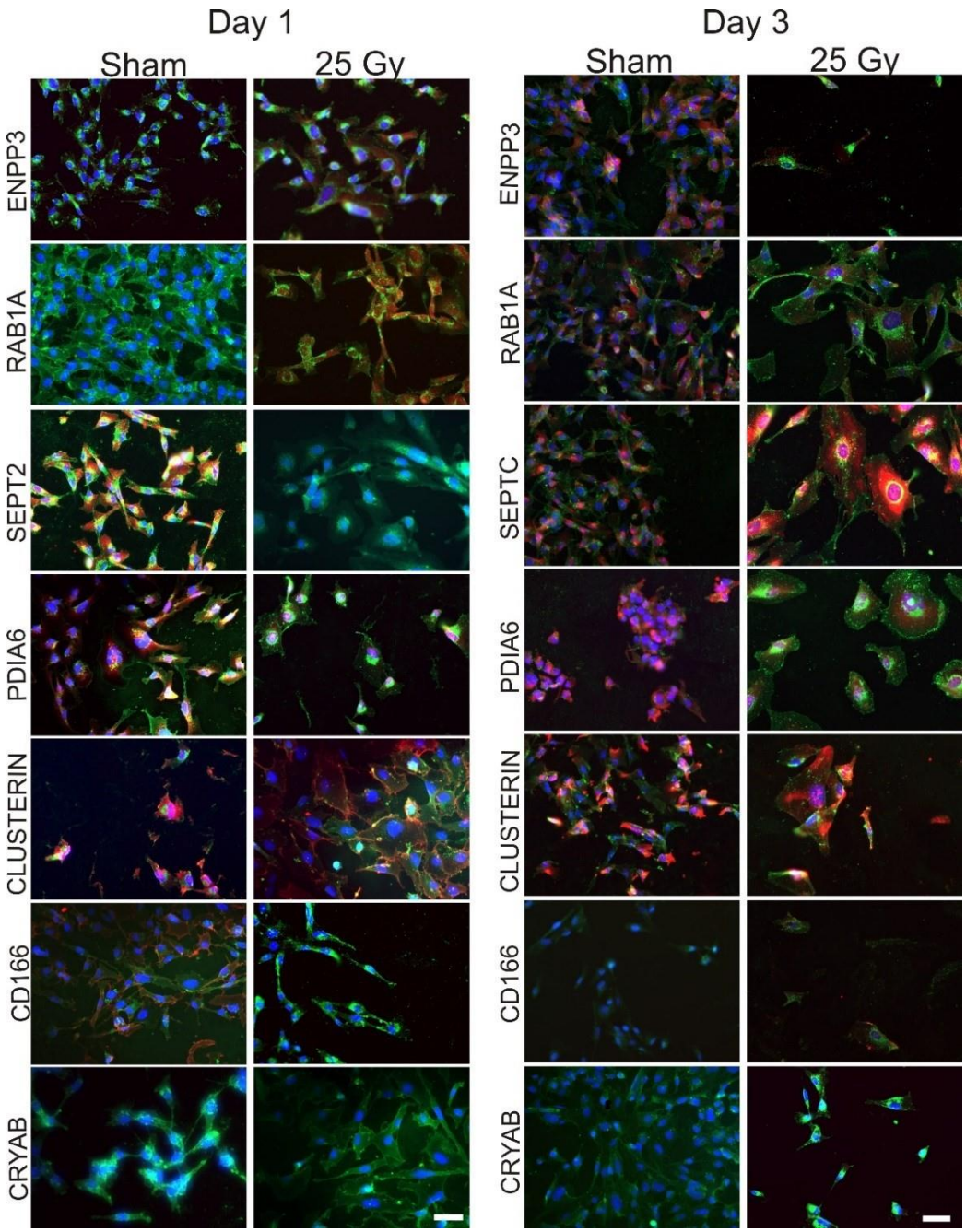

Figure 4.3: Immunostaining analysis of protein expression on irradiated endothelial cells fixed and permeabilised with 50% ethanol. Immunostaining was performed on day 1 and day 3 on irradiated endothelial cells using the designated primary antibody and secondary antibodies labelled with AF647 (red). The cell nuclei were stained with DAPI (blue) and the cell surface with wheat germ agglutinin-AF488 (green). Representative images show the biomarker expressions on irradiated HCMEC/D3 cells under fluorescent microscopy. Only one independent experiment was performed with this fixation method. Scale bar = 50 µm; magnification = 200×.

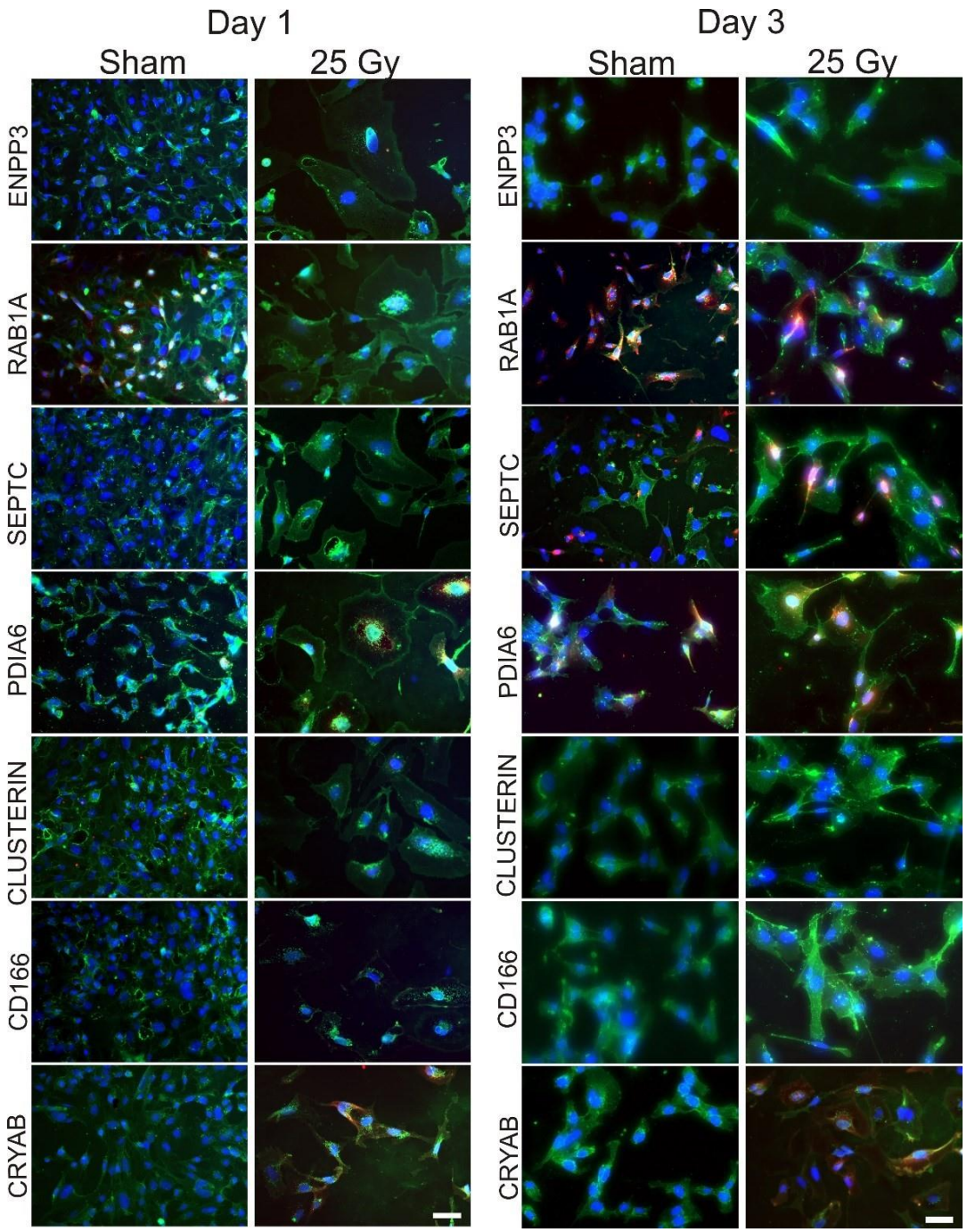

Figure 4.4: Immunostaining analysis of protein expression on irradiated endothelial cells fixed with 2% PFA (non-permeabilised). Immunostaining was performed on day 1 and day 3 on irradiated endothelial cells using the designated primary antibody and secondary antibodies labelled with Alexa Fluor 647 (red). The cell nuclei were stained with DAPI (blue) and the cell surface with wheat germ agglutinin-AF 488 (green) respectively. Three independent experiments were performed. Representative images show the biomarkers on irradiated hCMEC/D3 cells under fluorescent microscopy. Scale bar = 50 µm; magnification = 200×.

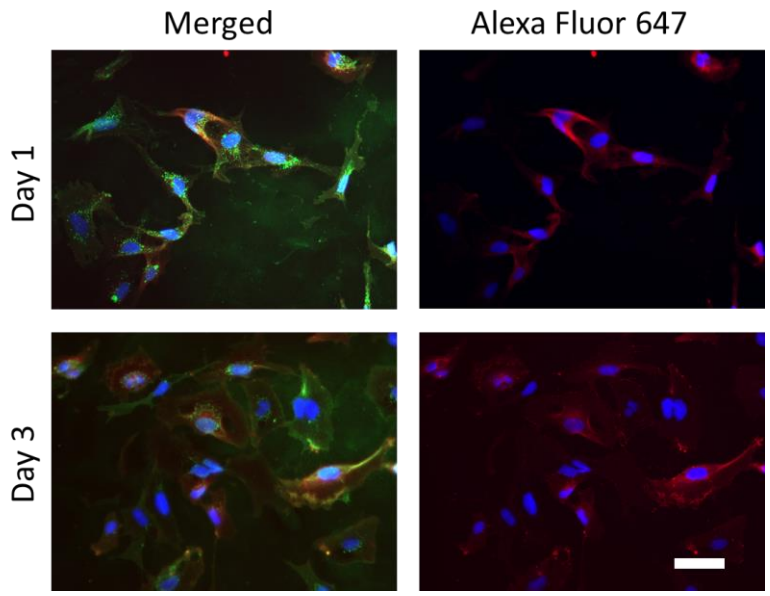

Figure 4.5: Immunostaining analysis of CRYAB expression on irradiated endothelial cells with 2% PFA. Immunostaining was performed on day 1 and day 3 on irradiated cells using anti-CRYAB antibody and secondary antibody labelled with Alexa Fluor 647 (red). The cell nuclei were stained with DAPI (blue) and the cell surface with wheat germ agglutinin-AF 488 (green) respectively. Three independent experiments were performed. Representative images show CRYAB on irradiated hCMEC/D3 cells under fluorescent microscopy. Scale bar = 50 µm; magnification = 200×.

4.3.2 Anti-CRYAB-thrombin conjugate induces platelet aggregation on irradiated cells under flow

From the immunostaining studies, CRYAB appeared the most promising target with no expression present in the absence of radiation and significant up-regulation at the surface in response to radiation at 25 Gy, hence a conjugate was produced between anti-CRYAB antibody and thrombin for testing in the parallel-plate flow system. This would further validate surface exposure of CRYAB after radiation and the ability of the CRYAB antibody carrying thrombin to bind to the upregulated CRYAB under flow, thereby generating significant thrombin levels for thrombus formation. Evidence for thrombus formation was observed by measuring platelet aggregation and fibrin deposition by confocal microscopy (Figure 4.6) as described in the previous Chapter.

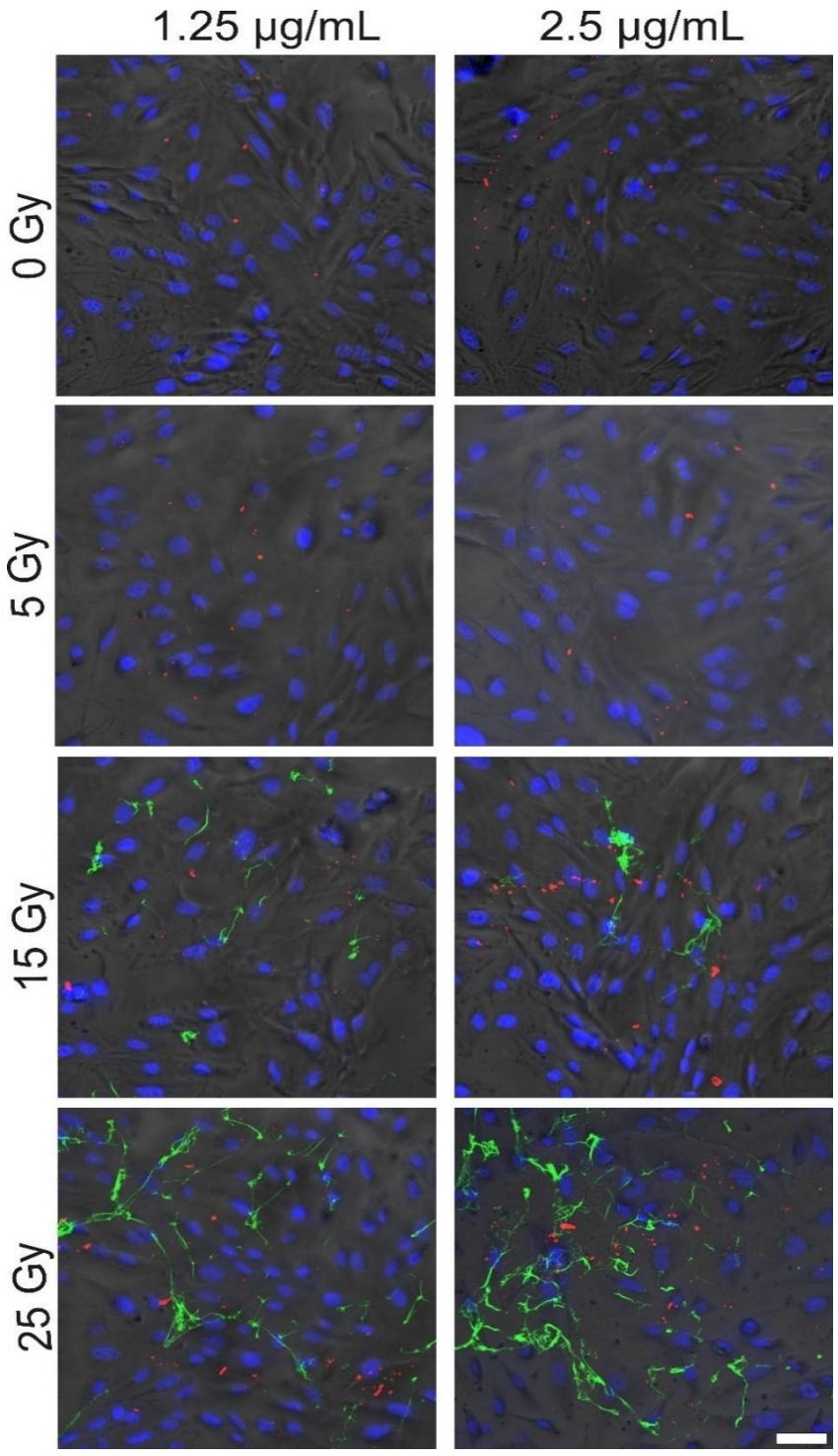

Figure 4.6: Platelet aggregation and fibrin formation on irradiated endothelial cells in the presence of anti-CRYAB-thrombin conjugate. Representative confocal images of platelet aggregation and fibrin formation on irradiated endothelial cells (0, 5, 15, or 25 Gy) in the parallel-plate flow system at day 1; post-irradiation or sham. Platelets were pre-stained in whole blood with R6G (red) and FITC- labelled fibrinogen (green) prior to circulation. Cell nuclei were stained post-flow with Hoechst 33342 (blue). Bar = 50 µm; magnification = 200×.

The average size of platelet aggregates (that is, average platelet area) and total area per field of view was measured first via platelet adhesion to the endothelial surface (Figure 4.6). Overall, a dose response was well observed where increased doses of radiation and conjugate resulted in increased platelet accumulation and aggregation on irradiated endothelial cells under flow (Figure 4.6 and Figure 4.7A, B). There was a statistically significant increase in average platelet area at 25 Gy (2-fold, $p<0.001$) using both conjugate doses (1.25 µg/mL, 2.5 µg/mL) compared to non-irradiated saline control (Figure 4.7A). Further, significant differences were also observed using low and high conjugate doses at 25 Gy (1.5-fold) compared to the irradiated saline control group. No such differences within conjugate doses were observed in total platelet area measurement (Figure 4.7B). However, a significant increase in total platelet area was noticed at 25 Gy using both conjugate concentrations (3.6 – 4.2-fold) compared to non-irradiated saline control.

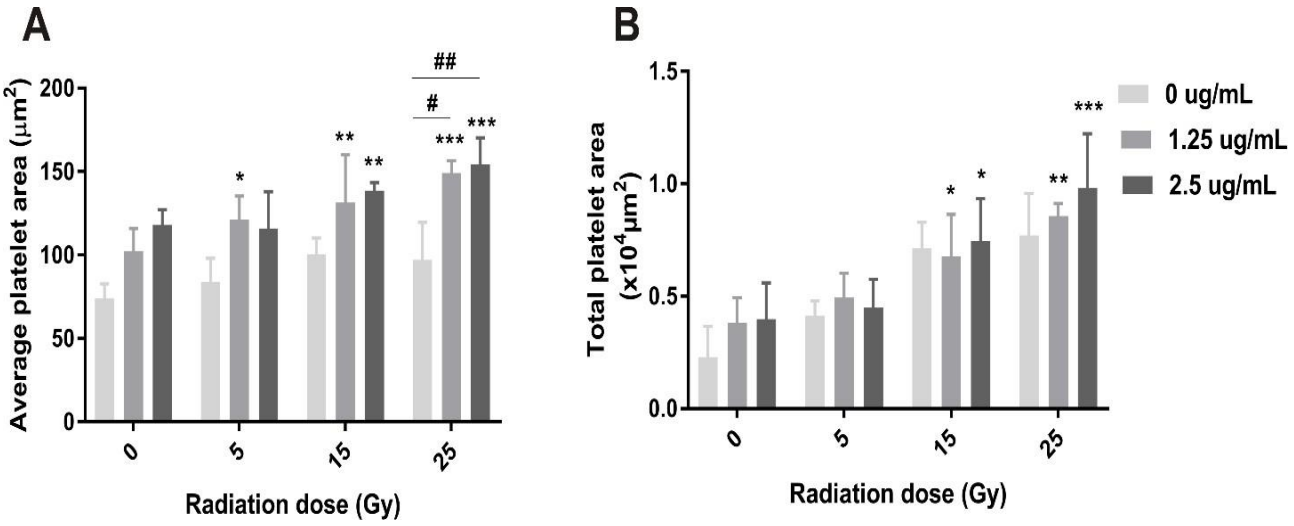

Figure 4.7: Platelet binding and aggregation with anti-CRYAB-thrombin conjugate under flow. Average size of platelet aggregates (A). Total platelet area per field of view (B). Data are shown as mean ± SD (3 independent experiments) and were analysed using two-way ANOVA with Tukey's post-hoc analysis. ***$p<0.001$, **$p<0.01$, *$p<0.5$ comparisons relative to saline, non-irradiated control. ##$p<0.01$, #$p<0.5$.

4.3.3 Anti-CRYAB-thrombin conjugate enhances fibrin deposition on irradiated endothelial cells under flow

No fibrin deposition was observed on non-irradiated controls with or without conjugate addition (Figure 4.6 and Figure 4.8A, B). No fibrin deposition was observed at any radiation dose in the saline controls. A dose of 1.25 µg/mL and 2.5 µg/mL conjugate showed significant fibrin development at 15 Gy and 25 Gy with no substantial fibrin deposition at 5 Gy (Figure 4.8A, B). Increases in average fibrin volume and total fibrin volume followed similar trends in response to radiation and conjugate doses. Average fibrin volume increased significantly ($p<0.0001$) at both 15 Gy and 25 Gy using the high dose of 2.5 µg/mL compared to both non-irradiated saline and relative radiated non-conjugate control (Figure 4.8A). Values of total fibrin volume showed a significant difference at both 15 Gy (24-fold, $p<0.001$) and 25 Gy (53-fold, $p<0.0001$) compared to non-irradiated saline controls (Figure 4.8B)

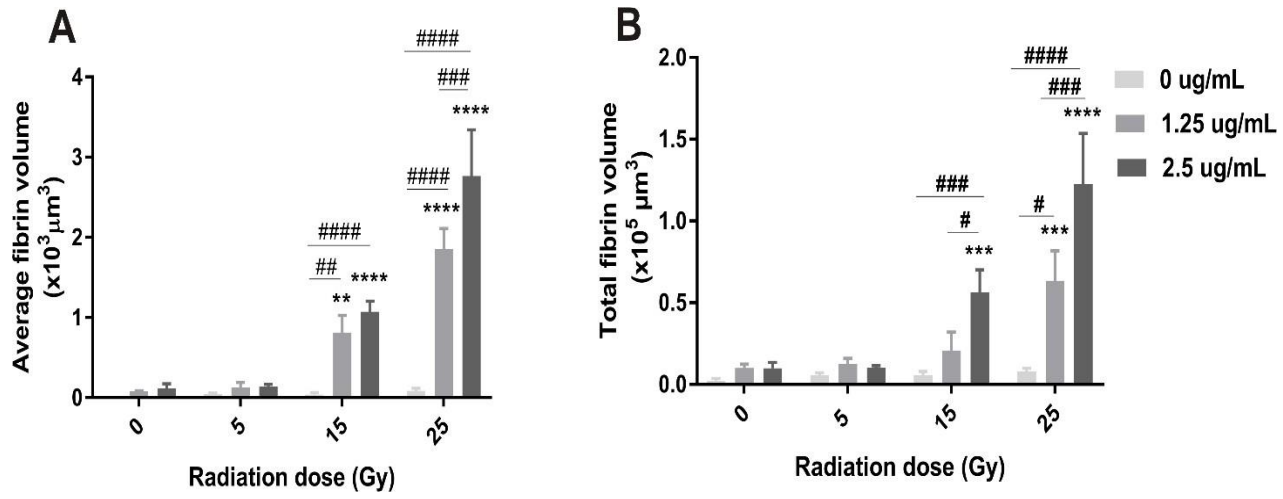

Figure 4.8: Fibrinogen deposition with anti-CRYAB-thrombin conjugate under flow. Average fibrin volume (A). Total fibrin volume (B). Data are shown as mean ± SD (3 independent experiments) and were analysed using two-way ANOVA with Tukey's post-hoc analysis. ****p<0.0001, ***p<0.001, **p<0.01 comparisons relative to saline, non-irradiated control. ####p<0.0001, ###p<0.001, ##p<0.01, #p<0.5 comparisons within radiation dose groups.

4.3.4 Non-targeting IgG-thrombin induces modest thrombus formation on irradiated endothelial cells under flow

Thrombus stimulation was also examined using non-targeting conjugate at activity levels /doses equivalent to that of the conjugate. These experiments were only performed at the highest radiation dose of 25 Gy. The result showed minimal stimulation of platelet and fibrin accumulation at both low and high conjugate doses in the absence of irradiation however some accumulation was evident after radiation at 25 Gy (Figure 4.9) compared to non-irradiated controls. Although platelet aggregation was observed under confocal microscopy, no significant increase was observed in average and total platelet area at both IgG-conjugate doses compared to non-irradiated control (Figure 4.10A, B). However, both average and total fibrin volume showed statistically significant increases ($p<0.0001$) at 2.5 µg/mL compared to non-irradiated controls (Figure 4.10C, D). Also, no significant differences were observed at low conjugate dose or between two conjugate doses (1.2 µg/mL, 2.5 µg/mL) with respect to both average and total platelet area (Figure 4.10A, B). In contrast, average fibrin volume showed 8 – 10-fold ($p<0.001 – 0.0001$) increase at both conjugate doses compared to the respective non-irradiated controls. Moderate differences were noted within each dose at 25 Gy (Figure 4.10C). A similar trend was observed with total fibrin volume analysis (Figure 4.10D).

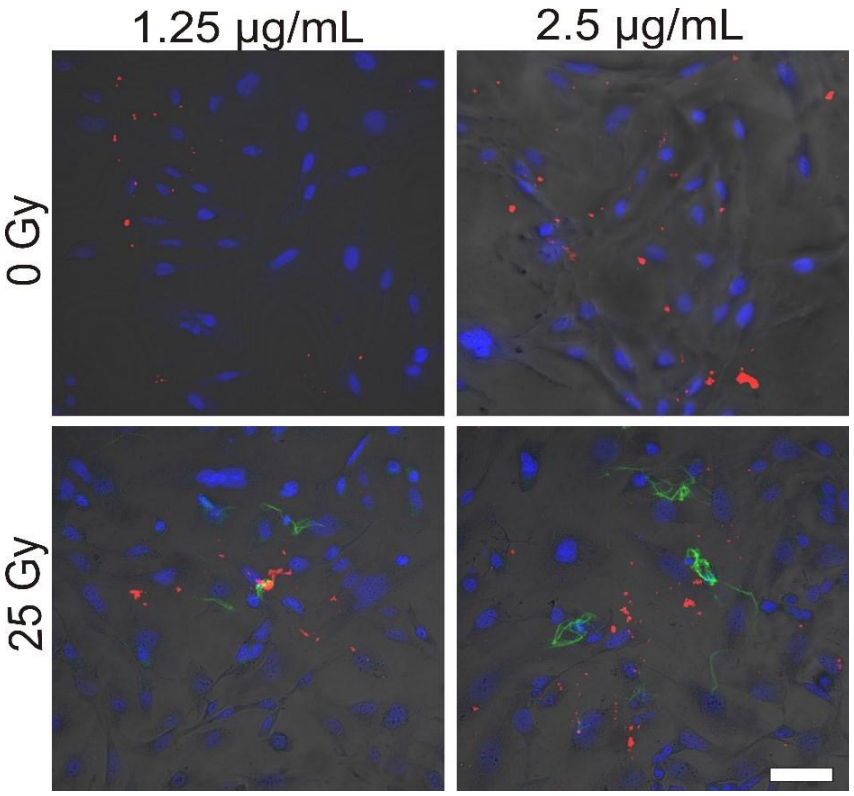

Figure 4.9: Platelet and fibrin deposition in response to non-targeted IgG-thrombin conjugate. Representative confocal images of platelet aggregation (red) and fibrin formation (green) on irradiated endothelial cells or sham control in the presence of IgG-thrombin conjugate under flow. Nuclei were stained with DAPI (blue). Scale bar = 50 µm; magnification = 200×.

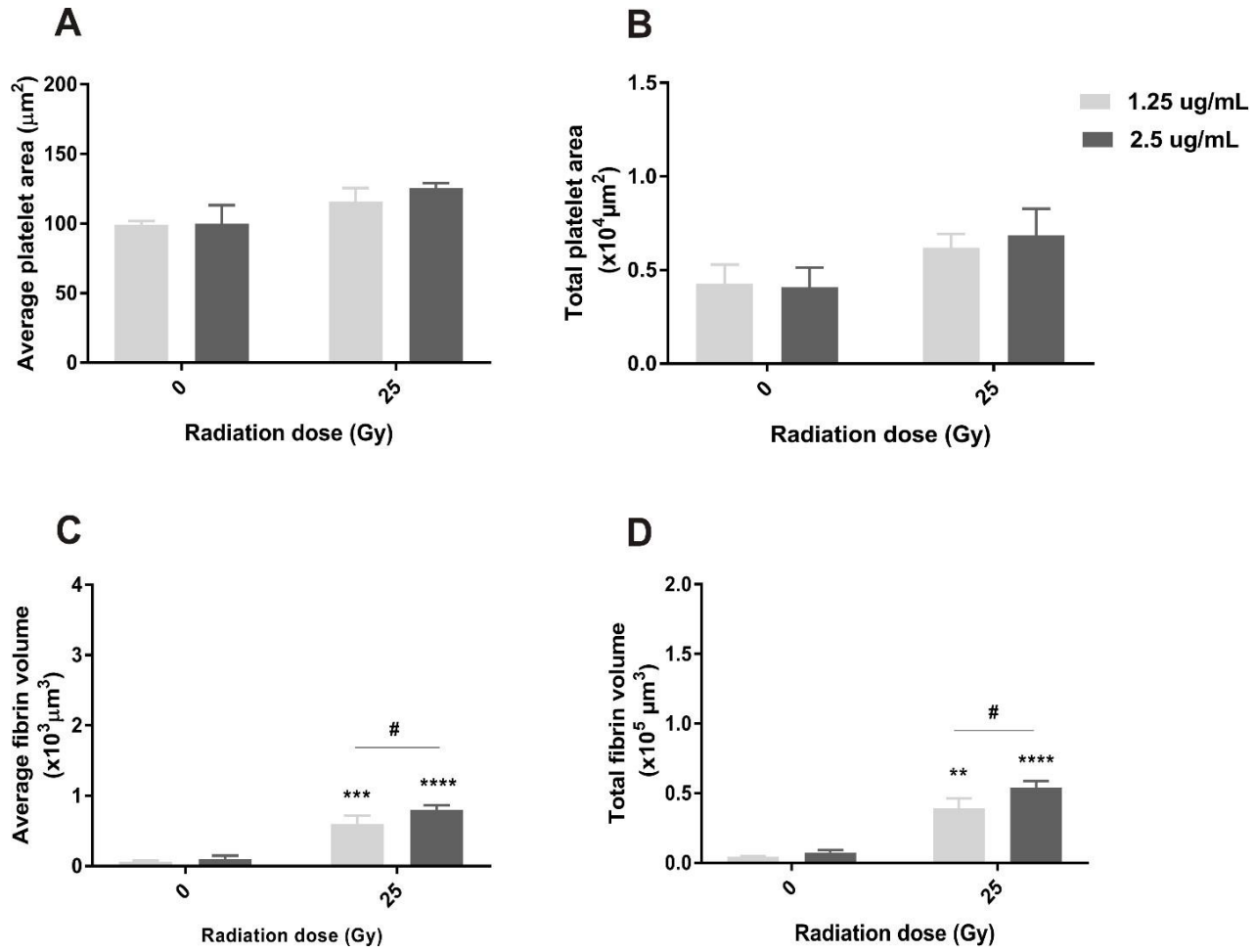

Figure 4.10: Platelet accumulation and fibrin deposition in the presence of IgG-thrombin conjugate on irradiated cells under flow. Average platelet area (A), total platelet area per field of view (B), average fibrin volume (C), total fibrin volume per field of view (D) at 25 Gy on both conjugate doses. Data are shown as mean ±SD (3 independent experiments) and were analysed using two-way ANOVA with Tukey's post-hoc analysis. ****$p<0.0001$, ***$p<0.001$, **$p<0.01$, comparisons relative to sham control. #$p<0.5$, comparisons relative to low conjugate dose within radiation dose group.

The results obtained with the IgG-thrombin were compared directly with anti-CRYAB-thrombin conjugate at 25 Gy using the low (1.25 µg/mL, Figure 4.11) and high (2.5 µg/mL, Figure 4.12) conjugate doses and further statistical analysis performed. In the presence of low conjugate dose (Figure 4.11), no significant increase in average (Figure 4.11A) or total platelet area (Figure 4.11B) was observed between IgG-thrombin conjugate compared to anti-CRYAB-thrombin conjugate. However, a statistically significant increase (3-fold, $p<0.0001$) in average fibrin volume was observed in anti-CRYAB-thrombin conjugate compared to IgG-thrombin

conjugate (Figure 4.11C). There was an increase in total fibrin volume with anti-CRYAB relative to IgG- thrombin however this did not reach statistical significance (Figure 4.11D). However, both average ($p<0.01$) and total fibrin ($p<0.5$) showed increases in irradiated IgG-thrombin treated groups compared to non-irradiated saline control groups.

In the presence of high conjugate dose (Figure 4.12), no significant differences were noted in average (Figure 4.12A) and total platelet area (Figure 4.12B) between IgG-thrombin and anti-CRYAB-thrombin conjugate. For fibrin deposition, a significant increase in average fibrin volume (3-fold, $p<0.001$) was observed in the presence of anti-CRYAB compared to IgG-thrombin (Figure 4.12C). Similarly, total fibrin volume showed a significant increase (2-fold, $p<0.01$) in the presence of anti-CRYAB to IgG-thrombin (Figure 4.12D). Significant increases ($p<0.01$) with respect to non-irradiated, saline control were observed for anti-CRYAB-thrombin relative to saline controls for both average and total fibrin volumes, but only for total fibrin volume for the IgG-thrombin control (Figure 4.12D).

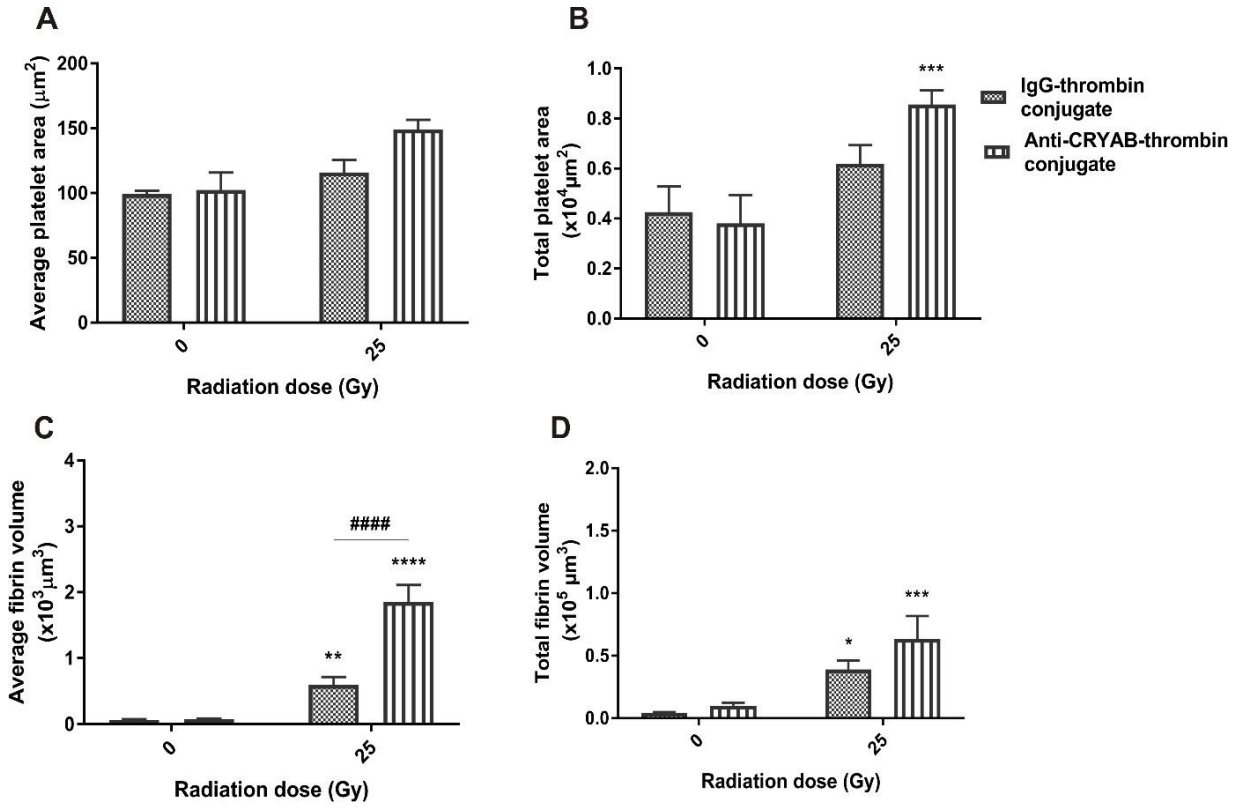

Figure 4.11: Comparison of non-targeted IgG-thrombin conjugate with targetedanti-CRYAB-thrombin conjugate on irradiated cells under flow (low dose). Average Platelet area (A), total platelet area per field of view (B), average fibrin volume (C), total fibrin volume per field of view (D) at 25 Gy using low conjugate dose (1.25 µg/mL). Data are shown as mean ± SD (3 independent experiments) and were analysed using two-way ANOVA with Tukey's post-hoc analysis. ****p<0.0001, ***p<0.001, **p<0.01, *p<0.5, comparison with non-irradiated control. ####p<0.0001, comparison within IgG-thrombin and anti-CRYAB-thrombin conjugate within the radiation dose group.

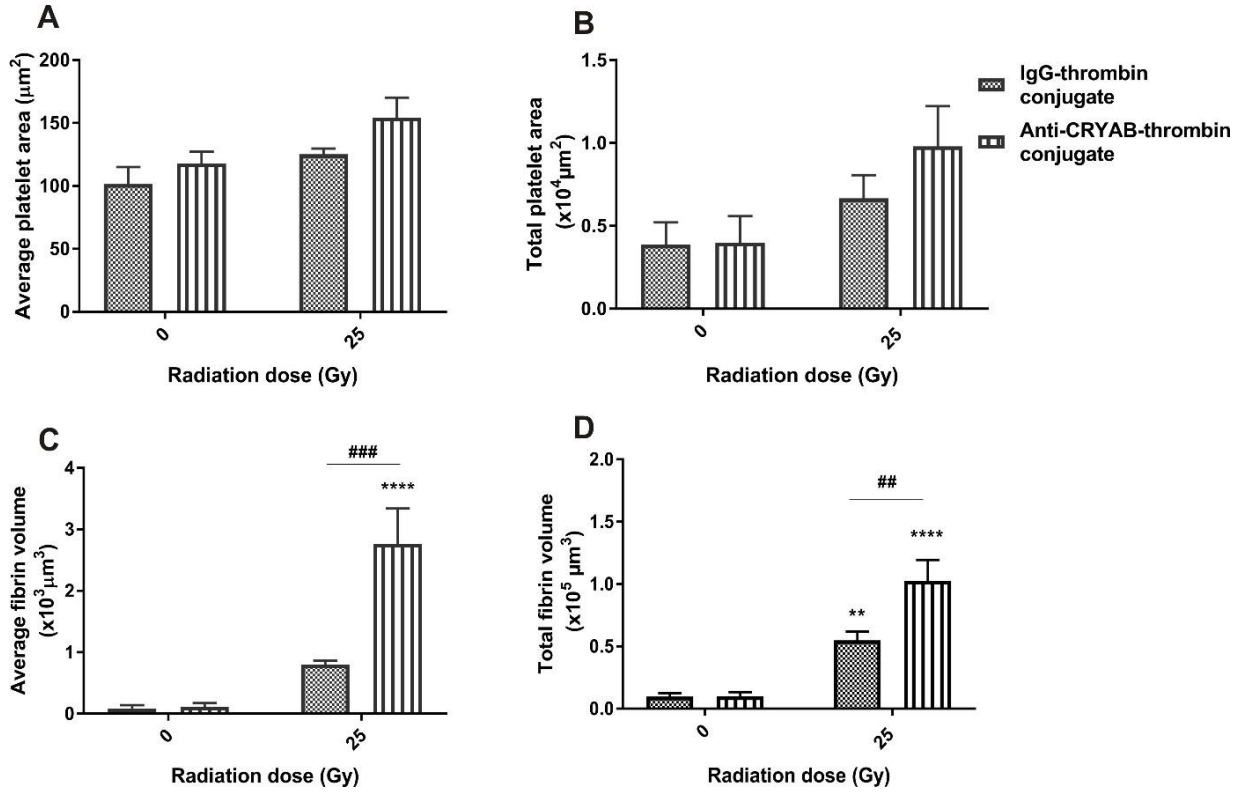

Figure 4.12: Comparison of non-targeted IgG-thrombin conjugate with targetedanti-CRYAB-thrombin conjugate on irradiated cells under flow (high dose). Average platelet area (A), total platelet area per field of view (B), average fibrin volume (C), total fibrin volume per field of view (D) at 25 Gy using high conjugate dose (2.5 µg/mL). Data are shown as mean ± SD (3 independent experiments) and were analysed using two-way ANOVA with Tukey's post-hoc analysis. ****p<0.0001, **p<0.01, comparison with non-irradiated control. ###p<0.001, ##p<0.01 comparisons between anti-CRYAB-thrombin and IgG-thrombin conjugate within the radiation dose group.

4.3.5 Plasma FDP measurements

The FDP concentration was measured in plasma from whole blood after flow in blood treated with both low (1.25 µg/mL) and high (2.5 µg/mL) CRYAB conjugate dose at the day 1-time point (Figure 4.13). Significant increases were observed at low conjugate dose (28-fold, p<0.001) and high conjugate dose (38-fold, p<0.0001) after 25 Gy irradiation. A significant difference was noted between these two doses at 25 Gy (p<0.01). FDP levels also increasedin response to the lower radiation dose of 15 Gy at both conjugate doses compared to non-irradiated control (16-22-fold, p<0.01) however no difference was observed between the two conjugate doses. No significant increase in FDP levels was noted at 5 Gy or with either

conjugate doses in line with the lack of fibrin deposition seen at these radiation dose groups. Interestingly, no increase in FDP levels were observed in the presence of IgG (Figure 4.13) despite the finding that a moderate increase in fibrin accumulation was observed under flow (Figure 4.9).

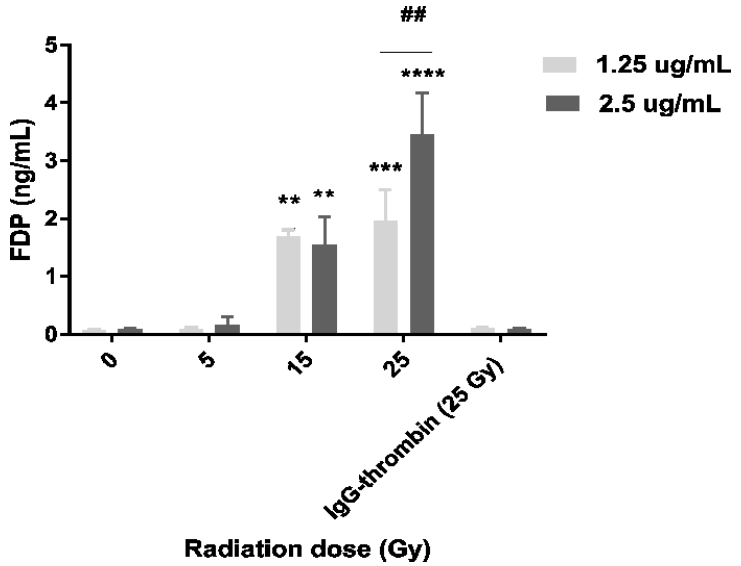

Figure 4.13: Plasma FDP concentration after flow in the presence of anti-CRYAB-thrombin conjugate. Presence of FDP analysed in plasma treated with 1.25 µg/mL and 2.5 µg/mL anti-CRYAB-thrombin conjugate at day 1 post-irradiation with controls under flow. Data are shown as mean ±SD (3 independent experiments). Statistical differences were analysed using one-way ANOVA with Tukey's post-hoc analysis. ****p<0.0001, ***p<0.001, **p<0.01 comparisons relative to non-irradiated control. ##p<0.01, comparison relative to low conjugate dose within radiation dose.

4.3.6 Binding specificity of CF^{TM}750-anti-CRYAB and CF^{TM}750-IgG to irradiated endothelial cells under flow

The accumulation of platelets and fibrinogen on irradiated cells in the previous studies confirmed the ability of the CRYAB antibody to bind irradiated cells under flow and allow significant accumulation of thrombin to induce thrombus formation. To further examine this binding and compare to non-specific IgG control, antibodies were labelled with fluorophores and introduced into the flow system in the presence of EBM-2 medium, not blood, and run under the same optimised flow conditions (as described in Chapter 2). The binding efficiency

of both targeted CF^{TM}750-anti-CRYAB and non-targeted CF^{TM}750-IgG on irradiated endothelial cells under flow was analysed by fluorescence microscopy. Expression was only analysed at a dose of 25 Gy in one experiment to confirm this binding. The results show that the CF^{TM}750 fluorescent signal was evident on the endothelial cells exposed to radiation at 25 Gy using the CF^{TM}750-anti-CRYAB construct compared to the CF^{TM}750-IgG control (Figure 4.14)

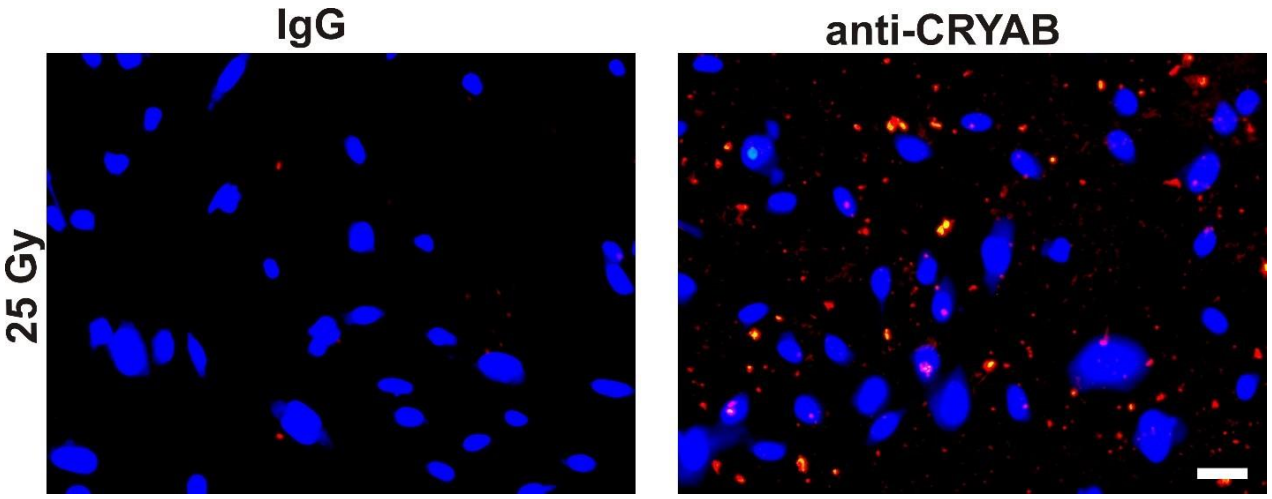

Figure 4.14: Binding of CF^{TM}750-anti-CRYAB to irradiated endothelial cells (25 Gy) under flow. Representative images of CF^{TM}750-IgG and CF^{TM}750-anti-CRYAB staining (red) of irradiated endothelial cells under flow. The cell nuclei were stained with DAPI (blue). Representative image shows specific targeting of CF^{TM}750-anti-CRYAB to the exposed CRYAB on irradiated cells under flow. The standard gain setting was used throughout the imaging. Scale bar = 50 µm; magnification = 200×.

4.4 Discussion

In this study, a new molecular target, CRYAB, was identified and validated using immunofluorescent staining and a pro-thrombotic conjugate was developed using a CRYAB specific antibody and thrombin and tested under flow for its efficacy to stimulate thrombosis on irradiated endothelial cells. The current study demonstrated the successful identification of CRYAB on irradiated endothelial cells followed by development and testing of anti-CRYAB-thrombin conjugate under flow where the result showed the formation of stable thrombosis via platelet aggregation and fibrin formation on irradiated endothelial cells.

Based on previous proteomic studies that searched for novel radiation induced markers (McRobb et al, unpublished), 7 molecular targets were selected and examined for molecular expression upon radiation of hCMEC/D3 cells. These targets (ENPP3, RAB1A, SEPT2, PDIA6, CLU, CD166, or CRYAB) showed increase in expression levels up to three weeks after irradiation with further work being performed to validate using immunocytochemistry and animal studies (McRobb et al, unpublished). Also, in the literature, differential expression and regulation with the possibility for translocation to the cell surface under certain conditions was observed in several studies, thereby potentially representing interesting targets under pathological conditions [387-396].

Among all those markers investigated, only CRYAB showed a promising result of increased surface expression on irradiated endothelial cells compared to non-irradiated controls. CRYAB is a multimeric heat shock protein that is present in the eye lens which is known to have chaperone-like activity to prevent enzyme aggregation [397, 398]. CRYAB is normally present in the brain in small amounts where it accumulates in reactive and neoplastic glial cells under pathological conditions where it is mainly localised to intracytoplasmic compartments [399-402]. High level CRYAB expression was noticed during oxidative stress or diseased conditions not only in the lens but also in the heart, skeletal muscles and kidney with low level expression in brain and spleen [403].

The lack of typical surface localisation of this protein but upregulated surface expression observed in this study in response to radiation suggested this protein could make an ideal target. Hence, CRYAB was selected as a promising target and, anti-CRYAB-thrombin conjugate was developed and tested on irradiated cells under flow. In this study, the CRYAB conjugate was tested at only the day 1 time-point since no major changes were noted between day 1 and day 3 on immunostaining analysis.

The immunostaining data in this work using 2% PFA fixative cells clearly demonstrated the surface expression of CRYAB on irradiated endothelial cells at both day 1 and day 3. Formaldehyde fixation generally enhances the detection of cell surface antigens since it does not interrupt the cell membrane thereby clearly showing the protein expression is present on the cell surface [404-406]. However, the initial studies using 50% ethanol showed no remarkable CRYAB expression on irradiated cells at both time points. Antibody binding to target epitopes can be affected by the fixation protocols, and it may be that ethanol fixation altered the 3D confirmation of the CRYAB epitope such that this particular antibody could not bind under these conditions, while PFA fixation maintained the epitope in a recognisable conformation [407]. The PFA fixation results suggested evidence of CRYAB expression on the cell surface though most studies reported its intracellular accumulation (mostly in cytoplasm and nucleus) under pathological conditions where it acts to bind misfolded or unfolded proteins to protect them from aggregation that may otherwise lead to cell toxicity and death [395, 396]. This confirms the identification of this protein as surface expressed and able to be bound by non-membrane permeable, modified biotin in earlier proteomic studies (McRobb et al, unpublished). It may be possible that the protein is expressed and secreted outside the membrane on the surface in response to radiation but how this may occur is unclear. The reason that the other identified targets showed no differences in expression levels on irradiated endothelial cells in contrast to the findings of the earlier proteomic studies, might be due to the use of human *in vitro* cell lines for this study in contrast to the original studies that were performed with irradiated AVM tissues in an animal model, and potential species-specific effects. Rather than completely rejecting these targets however at this stage, they could be further checked and validated in future perhaps using different antibodies as there were significant differences in staining between the ethanol-fixation and PFA-fixed expression levels.

Upon considering CRYAB for a vascular targeting, the developed anti-CRYAB-thrombin conjugate also proved successful in enhancing effective platelet binding followed by platelet aggregation and fibrin clot formation on irradiated hCMEC/D3 cells using the parallel-plate flow system under optimised flow conditions. Overall, the results show a significant synergistic interaction between the effects of radiation and conjugate dose where the higher doses (25 Gy and 2.5 µg/mL) induced more effective thrombosis. Although low radiation dose (5 Gy) with/without conjugate caused platelet stimulation and aggregation, no significant fibrin formation was observed.

In addition, thrombus stimulation was also examined using non-targeting conjugate on irradiated endothelial cells under flow. Anti-CRYAB is an IgG subtype, so it is important to check the non-specific binding of IgG-thrombin conjugate to irradiated cells. Antibodies can bind non-specifically via their Fc fragment, or constant domain, to Fc receptors on cells, which are often expressed during inflammatory conditions and may contribute to non-specific antibody binding [408, 409]. Surprisingly, IgG-thrombin conjugate at both low and high dose resulted in moderate thrombus formation on irradiated cells (25 Gy) under flow. The level of stimulation was however below the stimulation caused by the combined effect of anti-CRYAB-thrombin conjugate dose and radiation dose, especially at the higher conjugate dose, suggesting there was CRYAB specific binding occurring. Nevertheless, at least in part, this non-specific binding may have contributed to some of the platelet/fibrin accumulation observed with the anti-CRYAB conjugate. There was no binding on non-irradiated cells however, suggesting that specificity in the irradiated zone would still be valid. This was further examined by using CF^{TM}750- IgG and CF^{TM}750-antiCRYAB on irradiated cells under flow where the data clearly demonstrated the adhesion of anti-CRYAB to the upregulated CRYAB on irradiated hCMEC/D3 cells compared to IgG using the flow system. Both the results from CF^{TM} 750-IgG and CF^{TM} 750-anti-CRYAB clearly demonstrated the high binding capacity of anti-CRYAB

more specifically to the upregulated CRYAB thereby confirming their specificity in this study. There seemed a much greater difference between IgG and CRYAB binding in this context which may suggest that thrombin receptors as well as Fc receptors induced on the irradiated endothelial cells may also contribute to non-specific thrombin accumulation in some way. This might also be the reason for the fibrin deposition on irradiated cells using IgG-thrombin conjugate. From the data, it may be expected that there may be potential for off-target antibody binding in other inflammatory regions, therefore, it would be important to think about the radiation and conjugate doses to use in animals in order to avoid non-specific thrombus generation. Potentially, development of antibodies that lack the Fc regions may provide greater CRYAB-specific targeting, and the established *in vitro* flow system would be an ideal place to pre-test and compare such newly developed antibodies and test this hypothesis. Otherwise, CRYAB is considered a potential target to use for vascular targeting where the findings are well supported by the successful stimulation of thrombus in the presence of anti-CRYAB-thrombin conjugate on irradiated endothelial compared to non-irradiated and IgG control groups under flow.

On comparing the data with the previous annexin V-thrombin conjugate results (Chapter 3), the higher combined dose of radiation (25 Gy) and conjugate (2.5 µg/mL) caused significantly greater thrombus formation compared to the lower doses with both conjugates. However, unlike the findings with the annexin V-thrombin conjugate, anti-CRYAB-thrombin reported no low-level fibrin formation at 5 Gy with either conjugate dose. Although high dose requirement is considered a major limitation for treating large AVMs using radiosurgery [375], a dose range of 15 – 25 Gy has been used in the clinical setting as a marginal dose where complete AVM obliteration was achieved in lesions that are less than 3 cm in diameter [166, 410, 411]. The data still suggest the possibility of achieving selective vessel thrombosis by using anti-CRYAB conjugate at 15 and 25 Gy, but further studies will need to assess whether CRYAB or PS make the better targets. It must be remembered when comparing these findings

that although the same concentrations (1.25 µg/mL, 2.5 µg/mL) were used for each of the conjugates in the flow system, that these are not truly equivalent given the differences in sizes of annexin and the CRYAB antibody as well as the degree of labelling and final thrombotic activity that was achieved with each.

As with the annexin V-thrombin conjugate, further FDP analysis using post-flow plasma samples at all radiation doses (5, 15, or 25 Gy) with anti-CRYAB conjugate (1.25 µg/mL, 2.5 µg/mL) clearly indicated formation of highly stable thrombus at higher doses of radiation and conjugate suggesting the possibility of achieving fully developed mature thrombosis using anti-CRYAB-thrombin conjugate. The lack of FDP production at 5 Gy reflected the lack of fibrinogen deposition and accumulation observed at this radiation dose. On comparing these data with the findings of the annexin V-thrombin conjugate, significantly elevated FDP levels noted at 5 Gy with annexin V-thrombin were in line with the elevated fibrinogen deposition (as reported in Chapter 3), which again suggests that this conjugate may be a better treatment approach where lower radiation doses are required. However, surprisingly, IgG-thrombin showed no FDP levels at both low and high dose although moderate fibrin deposition was observed under flow. This could be an incorrect result due to some experimental error or it could be a genuine finding, that such a low-level platelet-fibrin activation which was not sufficient enough to release FDP thereby confirming that there was no stable thrombus formation occurred or a lack of induction of any fibrinolysis cascade. If this is the case, it proves that there is no high-level non-specific thrombus stimulation occurring in response to the IgG-thrombin non-specific control relative to the CRYAB-thrombin conjugate. This needs further examination and repeat experiments. The use of other assays in future apart from the FDP assay such as a D-dimer which measures more complex cross-linked cleavage products may analyse and predict the results more accurately. Otherwise, this suggests that the approach is methodologically sound, given the good correlation between the two methods of analysis.

The parallel-plate flow chamber provided an easy way to test and compare the effect of various molecular targets efficiently using the same combined radiation and conjugate doses as used for the previous annexin V-thrombin conjugate (Chapter 3). On using this flow system for testing these two conjugates, the most common thing noticed was the accurate or high-level measurement of fibrin deposition which clearly demonstrated the significant differences between various doses, and that this was far more significant compared to platelet measurements.

4.5 Summary and conclusion

The aim of this work was to validate some new molecular targets that were previously identified to show increased level of expression on the endothelial surface after radiation and further, develop and test the efficacy of novel pro-thrombotic conjugates to these target molecules to test their efficacy in inducing thrombosis on irradiated endothelial cells under flow. CRYAB was confirmed for its surface expression on irradiated endothelial cells compared to sham control using immunostaining analysis and anti-CRYAB-thrombin conjugate was developed and tested using the established parallel-plate flow chamber in inducing stable thrombosis on irradiated endothelial cells. Further, various combined radiation and conjugate doses were tested to examine the best synergistic dose effect that induces a more stable thrombus formation under flow. Finally, stability of thrombosis was further validated using an FDP assay.

The study demonstrated the successful validation and testing of a new molecular target, CRYAB, and its pro-thrombotic conjugate using the already developed parallel-plate flow chamber under optimised shear-flow conditions. The parallel-plate flow system seems reliable in showing clear evidence of the designed conjugate to bind to the specific target selectively under uniform shear flow conditions resulting in thrombosis and satisfies the hypothesis of this study that radiation-stimulated targets can be used for vascular targeting using these vascular targeting agents on irradiated cells in stimulating thrombosis under flow. The flow system also

proved reproducible in testing various other molecular targets and doses which would be highly useful in future for selecting the best targets and doses to take to further animal studies. Future animal studies will not only help to further analyse target expression *in vivo* but will also to validate the utility of this system for preliminary establishment of radiation and conjugate dose ranges.

Chapter 5

5. Overall discussion and future directions

Brain arteriovenous malformations are vascular abnormalities resulting in a high risk of haemorrhagic stroke in children and young adults [31, 93]. Although most small AVMs are curable, over one-third of large AVMs remains untreated using current treatment methods. The main goal of this project is to develop a new treatment for these young patients who suffer from a high risk of sudden death or disability. Vascular targeting was proposed as a biological technique to deliver bioactive molecules more selectively to a vascular environment that causes vessel thrombosis and occlusion. This concept was initially used in cancer therapy where the pathophysiological differences between tumour and normal vessels were exploited in achieving selective thrombosis by delivering a treatment-effective drug that carries an antibody specific to the unique biomarker on tumor endothelium and attaching a thrombotic agent [218, 236]. In the case of AVMs, no specific markers have been identified on the AVM endothelial surface that make it sufficiently discriminatory from normal endothelium to enable a vascular targeting approach. Hence, stereotactic radiosurgery has been used as an effective priming technique to induce molecular changes on AVM endothelium that can be selectively targeted using a pro-thrombotic conjugate that contains an antibody/ligand specific to the target molecule and coagulant protein (thrombin) to achieve AVM vessel occlusion [128, 129, 250, 253, 254, 374, 412].

5.1 PS as a vascular target in irradiated AVMs

Previous studies have reported changes in the molecular expression of AVM endothelium upon radiation compared to normal vessels and have identified various molecular targets on the AVM endothelial surface [129, 374]. More recently, translocation of PS from the inner membrane leaflet to outer membrane leaflet after irradiation was demonstrated both *in vitro* using live cell imaging and *in vivo* using a rat AVM model [255, 256, 284]. These initial studies confirmed that PS could be used as a potential target therefore PS was used in this study as a

valid target for the vascular targeting approach. In developing a conjugate, it is important to select a ligand that has high affinity towards PS. Annexin V is a calcium dependent phospholipid binding protein with high affinity to PS where it has been used in several assays for detecting apoptosis via its binding to apoptotic cells during PS translocation [302, 303]. In this study, annexin V was successfully conjugated with thrombin to develop the annexin V-thrombin conjugate to check its efficacy in inducing selective thrombosis. Stable fibrin thrombus formation was well achieved especially with the highest combined dose of radiation and conjugate (25 Gy, 2.5 µg/mL) suggesting PS as a good target molecule to translate to animal studies and potentially human trials, and the annexin V-thrombin conjugate may also make a suitable product to take to further pre-clinical studies. Nevertheless, it is important to note that while PS may be an ideal target, annexin V as a ligand, may not necessarily be the best choice when thinking about achieving more selective occlusion. There may be the possibility to achieve more effective thrombosis using other PS- targeting antibodies and *in vivo* pharmacokinetics will also play a role in determining ligand/conjugate efficacy. For example, a new generation of PS-targeting peptide/plasma protein (betabodies) such as peptide-peptoid hybrid (PPS1) or PS-specific antibody such as IN11-T [413] have been developed to target the exposed PS or associated proteins on the surface more selectively, these therefore may be able to achieve greater thrombus occlusion on irradiated endothelial cells with attached coagulant protein.

To this end, some preliminary experiments were performed using a PS-specific 'betabody' (provided by R. Brekken, UTSouthwestern, Texas, USA) conjugated to thrombin as a preliminary understanding of the future work. Testing at high conjugate dose (2.5 µg/mL) using the established parallel-plate flow chamber system with pre-stained whole blood showed platelet-fibrin formation on irradiated cells (15 Gy) without formation on non-irradiated cells (Figure 5.1). However, at this stage, the level of thrombin formation in this initial experiment

with the PS-targeting betabody did not appear to reach that achieved with annexin V as a ligand. Obviously more experiments are needed and this work will be further progressed in future by testing varying dose combinations *in vitro*. However, this result alone begins to demonstrate the utility of this flow system for rapidly and cost-efficiently assessing the relative ability of various ligands, targets and conjugates for their vascular targeting potential.

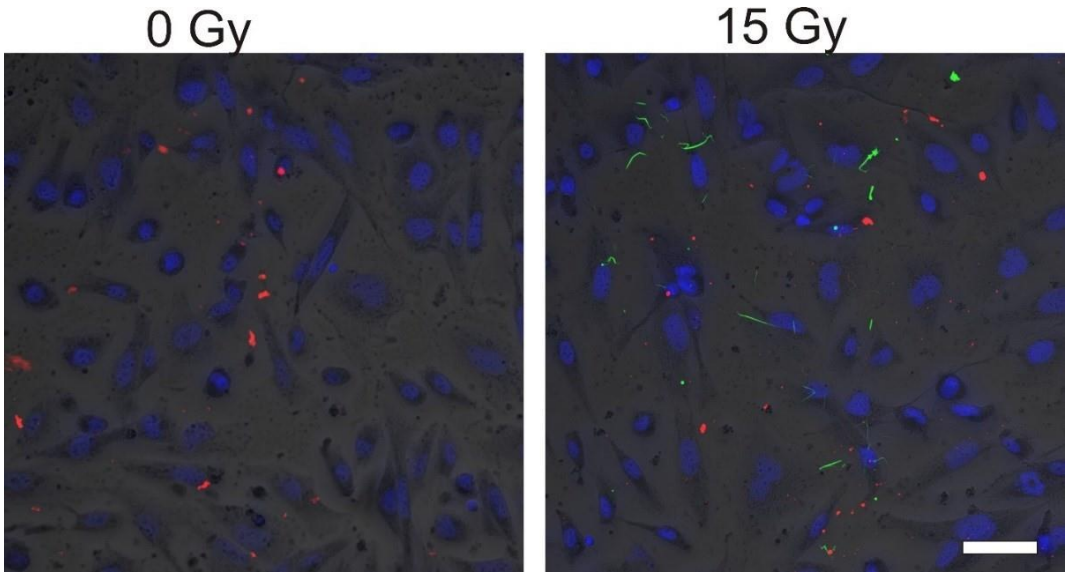

Figure 5.1: Platelet aggregation and fibrin formation on irradiated endothelial cells under flow in the presence of betabody-thrombin conjugate. Representative confocal images of platelet aggregation and fibrin formation on irradiated endothelial cells (15 Gy) in the parallel-plate flow chamber at day 1; post-irradiation or sham in presence of betabody (2.5 µg/mL). Platelets were pre-stained in whole blood with R6G (red) and FITC-labelled fibrinogen (green) prior to circulation. Cell nuclei were stained post-flow with Hoechst 33342 (blue). Bar = 50 µm; magnification = 200×.

5.2 CRYAB as a molecular target

This work was continued to search for other novel targets using previous proteomic data for the potential to enhance the thrombotic stimulation on irradiated endothelial cells under flow using the specific vascular targeting agents [304, 268, McRobb et al. unpublished]. CRYAB proved promising as a valid target with differential expression on irradiated cells compared to non-irradiated control. Using this result, anti-CRYAB-thrombin conjugate was successfully developed and tested under flow, where stable thrombus formation was achieved to a greater extent on irradiated endothelial cells compared to non-irradiated cells. Similar to the previous

conjugate, the same radiation and conjugate doses were used to study the comparison of the effect of both conjugates at the same dosage level though with consideration that there is a difference in the molecular weight between ligands that affects calculation of dose and their level of equivalence. Interestingly, the annexin V-thrombin conjugate caused moderate thrombosis under flow at 5 Gy compared to no fibrin thrombus formation using the anti-CRYAB-thrombin conjugate. This data would be highly useful in translating to clinical trial for human patients at low radiation dose to avoid late radiation necrosis and off-target effects in future. This suggests that perhaps the PS-targeting approach may be superior to targeting CRYAB. Further, non-targeting thrombosis was noticed using IgG- thrombin conjugate with moderate fibrin formation whereas no fibrin thrombus formation was observed using free thrombin and annexin under flow. This could be improved in future by the use of modified antibodies or single chain variable fragments (ScFv), that remove the IgG constant domains and eliminate non-specific Fc receptor binding, making the antibody more selective to recognise and bind to the target protein. Overall, on comparing the two conjugates, annexin V-thrombin conjugate proved more specific and effective in this context rather than the anti-CRYAB-thrombin and must be considered in translating to preclinical or clinical studies in treating patients. However, various other targets are yet to be validated to identify the best conjugate and doses that can be advanced to animal studies.

5.3 Thrombin as an effector molecule

Thrombin was used in this study as the pro-thrombotic effector molecule. Thrombin is an enzyme normally generated in the coagulation cascade by cleavage from pro-thrombin via the prothrombinase complex (Xa/Va) once platelets are activated. It is common to both intrinsic and extrinsic signaling pathways in the coagulation cascade. Thrombin is a key enzyme that converts soluble fibrinogen to insoluble fibrin resulting in formation of the blood clot [325, 331]. Thrombin also directly activates factor XIII to XIIIa inducing fibrin polymerisation [414]. Use of this pro-thrombotic molecule was highly effective in this context. However, it may also

be worth considering the significant safety issue when using an *in vivo* approach of having this molecule circulating in the blood stream. Of note, the addition of equivalent levels of free thrombin in this study had no evidence of effect on blood coagulation within the circulation of the flow system, and further did not bind at sufficient levels to induce localised thrombosis on the irradiated cells. This suggests that at least within the tested dose range, that targeted thrombin should be a relatively safe approach without induction of systemic thrombosis.

Another option however may be to examine whether tissue factor (TF) may provide an even safer thrombotic effector molecule. Other studies have used TF with vascular targeting peptides to selectively target and occlude tumour endothelium resulting in tumour infarction [241, 415, 416]. TF normally participates in the extrinsic pathway as a cofactor in the activation of factor VII to its active form (factor VIIa), where the TF-factor-VIIa complex activates factor X and IX in the presence of calcium ions to generate conversion of pro-thrombin to thrombin [332, 333]. Beiker et al. showed thrombotic occlusion of 90% of the tumour vessels in the presence of TF-NGR (TF linker with peptide) supporting the fact that there was reduction in tumour growth observed after binding of TF-NGR to the cell surface of tumour endothelium [241]. Shwoppe et al. used TF without its transmembrane domain (truncated TF) fused to peptides (TF-fusion protein) that has low coagulation inducing activity in circulation but recovers its activity after binding to the target molecule at the endothelial surface, and demonstrated reduction in tumour blood volume with fibrin formation in the tTF-fusion protein treated tumours [415]. Use of TF may therefore have greater benefits compare to thrombin in terms of safety, as TF requires multiple other factors for its activation of the coagulation cascade, including close interaction with the plasma membrane with exposed PS [417]. Thus, irradiated endothelial surfaces that expose PS would be susceptible to TF-stimulated coagulation if targeted, while normal unstimulated endothelial cells would not. Similarly, an even lower risk

of systemic thrombosis would also be hypothesised with use of this effector molecule. This may be of interest to test in the system and safe to achieve highly selective thrombosis without any non-specific activity of conjugate or blood coagulation. Although thrombin is basically a key effector enzyme to trigger blood clotting more effectively, it may be safer to use TF in combination with peptide/ligand/antibody in future to avoid non-specific thromboembolic events. Again, this developed flow system provides an easy and economical way to compare different effectors and these experiments can be performed in the future. Further animal experiments will also be better placed to investigate *in vivo* safety profiles.

5.4 Parallel-plate flow system: - advantages and limitations

It is not possible to extensively test multiple targets, conjugates, and doses using animal work due to the cost and in the interest of refinement of animal studies and associated ethics. Therefore, the parallel-plate flow system was developed to determine the binding specificity, dose-effect and selectivity of these designed conjugates in a more simple and cost-effective way before testing it with an animal AVM model.

The developed parallel-plate flow chamber was considered a simple and effective technique to test the effect of the developed conjugate and various combined doses of both radiation and conjugate using its flexible design and limited complexity. This flow system was successfully established with proper control of flow conditions where it has been designed to test the efficacy of annexin V-thrombin and betabody-thrombin conjugate on irradiated endothelial cells in stimulating thrombosis. The parallel-plate flow system proved reproducible in maintaining uniform shear stress conditions throughout where the measured shear stress of the flow system (3.1 dynes/cm^2) correlated well within the estimated range of average shear stress in major human arteries (2 – 100 dynes/cm^2) [320]. Use of human whole blood with pulsatile flow pattern in the flow system further supported the work in testing the vascular targeting agents under near physiological flow condition. Although the shear stress levels achieved were

at the lower range of that found physiologically, it remains superior to any studies that may be performed in a completely static system. This flow system remains an intermediate step and bridges the *in vitro* cell culture and animal models where it must be remembered that these studies are still relatively preliminary in nature, and further experiments in animals are required where more physiological conditions can be achieved.

The thrombus formation was well validated in the flow system in the presence of annexin V-thrombin conjugate via platelet aggregation and fibrin deposition. Further, 3D reconstruction was made to measure the fibrin volume where the 3D image was useful in analysing shape and structure of fibrin deposited on the surface [319]. From the result, it is very clear that fibrin volume is a more accurate measurement compared to measuring only platelet area since platelet stimulation is the initial phase of blood coagulation [322]. It should be noted in the current study, that labelled commercially available fibrinogen was added to the whole blood and that this per se does not show the actual level of cleaved fibrin after thrombin activation. However, the fact that the observed fluorescence demonstrated what appeared to be long polymerised strands is consistent with thrombin-induced fibrin cleavage and polymerisation and has been previously used both *in vitro* and *in vivo* as a surrogate measure of fibrin deposition and thrombin formation [418]. It would be interesting and informative in future flow studies to also tag the actual fibrin using cleaved fibrin-specific antibodies post-flow to absolutely confirm the conjugate effect in stimulating fibrin-thrombus formation. Apart from thrombus volume, it could be possible to further test the thrombus weight, fibrin structure or fibrin strength as an additional way of analysing thrombosis. Mardel et al. has measured the clot weight using an electronic balance and clot strength and quality by observing fibrin arrangement using scanning electron microscopy [419].

After measuring thrombus formation, the study was finally concluded by further examining the stability of the formed thrombus using FDP assay to assess fibrin degradation products which

clearly demonstrated the highly matured thrombosis achieved at 25 Gy (2.5 μg/mL) in both the conjugates compared to less FDP levels at other doses. Fibrinolysis is the general mechanism to balance between coagulation and anti-coagulation processes via breakdown of unwanted cross-linked fibrin to avoid systemic whole blood coagulation in the body [420]. This rapid digestion of the cross-linked fibrin results in the release of fibrin fragments into the blood which can be easily detected using FDP assay in plasma sample [421]. However, there are some arguments as to whether the FDP is the degradation product that contain some fragments of FPA (fibrinopeptide A, that gets cleaved from fibrinogen during the conversion of fibrinogen to fibrin in clot formation process) [422, 423]. A more robust way of testing thrombus stability would be the D-dimer assay. The D-dimer is a unique fragment formed by digestion of highly cross-linked fibrin [424-426]. Though some inaccurate results were predicted with the FDP assay, good consistency and correlation was observed at 25 Gy in agreement with the previous high fibrin formation in the presence of conjugates under flow. Hence it may be worth in any future study if additional D-dimer assay was used as a further test to determine the thrombus stability where it can measure the released fibrin fragments from complex cross-linked fibrin digests.

In this study, human cerebral microvascular endothelial cells were used in the flow system rather than human AVM endothelial cells which may be considered a minor limitation of the study. The latter would be more physiologically relevant for our final goals of AVM targeting. While no specific surface markers of AVM endothelium have been identified, the literature reviewed in Chapter 1 highlighted the recognition that AVM endothelial cells do have an inherently different phenotype from normal endothelial cells [246, 247, 250]. This may suggest that AVM endothelial cells could potentially behave differently to normal endothelial cells in response to radiation, potentially altering their radiation-induced surface proteome. This has not to date been tested given the difficulties in establishing sufficient AVM-derived cells for

analysis, but establishing the ability of radiation to induce expression of the novel targets in these AVM-derived cells would be of value, to validate the utility of the proposed targets in the human AVM context and further, to examine whether the AVM endothelial phenotype has any inherent differences in thrombotic reaction. This would be of considerable interest and useful to test the conjugate effect using irradiated human AVM endothelial cells, but considered not essential at this stage since this is more preliminary work to understand the combined effect of radiation and developed conjugate in achieving selective thrombosis under flow. However future studies may consider isolation and use of these cells within system.

5.5 Other options for targeted delivery

Further important development that could be assessed in ongoing studies could be the use of nanotechnology constructs to increase the payload of conjugates. Attaching multiple ligands and multiple effector molecules to some sort of nanoparticle might improve the efficacy and safe delivery of the pro-thrombotic molecule. Attention has been focused recently on the development of nanoconjugates with various antibodies and effector drugs developed to create multi-drug delivery platforms for the treatment of various diseases [427-429]. Although not included in this thesis due to preliminary testing, a hexagonal flat nanodisk provided by Binyang Shi [430] was used as a base for conjugation of multiple annexin V and thrombin molecules through click biochemistry conjugation (performed by Zhenjun Zhao; as described in Chapter 3) for testing on irradiated hCMEC/D3 cells (25 Gy) under the developed *in vitro* flow using EBM-2 medium. The results showed greater binding of the auto-fluorescent nanoconjugate on irradiated cells compared to non-irradiated control cells under flow (Figure 5.2). This was not done using whole blood since it was an initial testing designed to better understand the ability of the designed nanoconjugate to interact with irradiated cells under flow compared to non-irradiated cells, but again shows the utility of the system for testing both target expression and ligand and conjugate efficacy in a simple defined way that can

predetermine conjugate formulations that may be the best to take to the next stage of animal studies. This work will be further extended in future by attaching more target molecules and effector molecules in defined ratios and testing in the *in vitro* flow system. Before proceeding to any animal work, it is important to analyse the best target molecule, and doses to achieve high selectivity and stability in treating AVM patients.

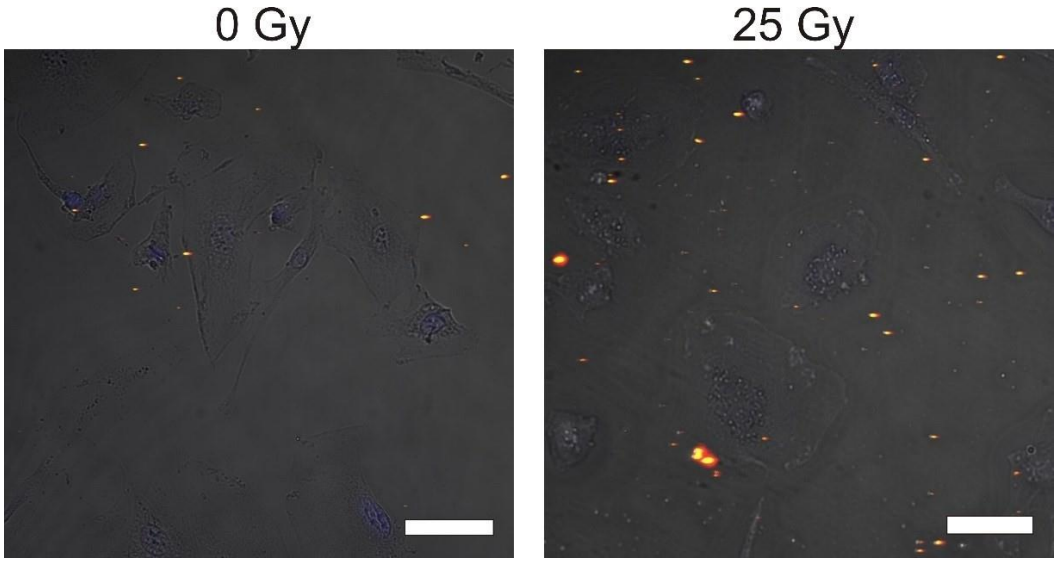

Figure 5.2: Binding specificity of nanodisks conjugated to annexin V and-thrombin to irradiated endothelial cells under flow. Representative confocal images of nanodisk (reddish yellow) on irradiated endothelial cells (25 Gy) in the parallel-plate flow chamber at day 1; post -irradiation or sham. Cell nuclei were pre-stained post-flow with Hoechst 33342 (blue). Bar = 50 µm; magnification = 200×. Original images.

5.6 Progression to pre-clinical studies

Before proceeding to human patients, the future work will focus on animal studies for further validation of doses using the *in vitro* data. Our group has an established animal model of AVM that can be treated with localised radiosurgery [129, 243, 255, 284]. The current *in vitro* studies will definitely help to analyse the proper dose range to be tested in this model, since the blood volume used in the flow (~12 mL) is near to the whole blood volume of rats used in this model. However, it will be important to consider the interaction of conjugate with endothelium of the whole animal as well as filtration through the liver and kidneys that will affect the *in vivo* dose

range, which might suggest a slightly higher dose would be required, but this *in vitro* system gives us a range for initial *in vivo* testing. Animal studies in the AVM model will be important for establishing the specificity of conjugate binding *in vivo* and will also establish whether we can induce sufficient thrombosis in appropriately sized vessels to induce complete occlusion, which will be required in the clinical setting.

What must also be established prior to giving thrombotic conjugates to patients, is the level and specificity of target expression in humans. For PS, the identified targets were observed both *in vitro* [256] and *in vivo* [255] prior to developing the conjugate to make sure it was well expressed in both human cell line and an AVM animal model. PS has been previously analysed in many human pathological conditions where it has been reported to get exposed under some stress condition compared to normal conditions [293, 296, 417, 431]. High level of PS exposure was identified in tumour cell lines compared to normal cells thereby suggesting it as a novel target for diagnosis and therapy in cancer [431]. To date, no studies have investigated the PS translocation in human AVMs in response to radiation, but initial studies would first require imaging of endothelial PS exposure in non-irradiated and irradiated human AVMs or indeed imaging for any other potential targets and their specificity in the body within the irradiated zone. This is the reason for validation and development of multiple targets and associated conjugates, as species-specific and AVM-specific differences may eliminate various targets along the drug development pipeline, so that it will be highly useful in future to screen the best target molecules that are highly expressed in agreement with the previous findings. Overall, the significant outcome of this project will be translated to animal work before advancing it for human trials.

5.7 Application of radiation-guided-vascular targeting for non-AVM treatment

Apart from treating AVMs, this radiation-guided, vascular targeting strategy could potentially also be used to treat any type of bodily lesion that could be defined by radiosurgery. Various other lesions such as primary or metastatic brain tumours may be amenable to this approach using pro-thrombotic agents to block tumour vessels, where there are limited therapeutic treatment options and relatively low efficacy of drug delivery to these types of target lesions [432-434]. Other groups have considered this approach for radiation-guided delivery of chemotherapeutic drugs (Refs). Another type of vascular lesion that may be amenable to this approach is cerebral cavernomas malformations or CCMs ([1, 54, 435]). These present as clusters of abnormal blood vessels that cause stroke and seizures and where successful surgical resection is doubtful due to location and size of the lesion [436, 437]. The overall treatment goal for these lesions is similar to that of AVMs in causing vessel occlusion. Hence, using radiation as a priming tool and targeting the endothelial surface more selectively with the vascular targeting agents would also be of potential benefit in these lesion types and could be considered in future.

5.8 Final Summary

Effective and stable thrombosis was successfully achieved on irradiated endothelial cells in the presence of both annexin V-thrombin and anti-CRYAB-thrombin conjugate using the established *in vitro* parallel-plate flow chamber system. The system proved a simple and reproducible tool with cost-effective screening of various molecular targets possible in the future using different combined doses of radiation and conjugate. This technique will be useful in understanding whether future constructed conjugates binds well with the expressed target on irradiated cells under near physiological flow conditions, where the selected conjugates with

its optimised dose conditions will be tested using AVM animal models before advancing it to AVM patients.

References

References

1. McCormick WF. The pathology of vascular ("arteriovenous") malformations. *J Neurosurg*. 1966;**24**:807-16.

2. Choi JH, Mohr JP. Brain arteriovenous malformations in adults. *Lancet Neurol*. 2005;**4**:299-308.

3. Yamada S, Brauer FS, Colohan AR, Won DJ, Siddiqi J, Johnson WD, Yamada SM, Rouse GA, Lonser RR, Iacono RP, Mandybur GT. Concept of arteriovenous malformation compartments and surgical management. *Neurol Res*. 2004;**26**:288-300.

4. Fleetwood IG, Steinberg GK. Arteriovenous malformations. *Lancet*. 2002;**359**:863-73.

5. Wong JH, Awad IA, Kim JH. Ultrastructural pathological features of cerebrovascular malformations: a preliminary report. *Neurosurgery*. 2000;**46**:1454-9.

6. Hermanto Y, Takagi Y, Yoshida K, Ishii A, Kikuchi T, Funaki T, Mineharu Y, Miyamoto S. Histopathological Features of Brain Arteriovenous Malformations in Japanese Patients. *Neurol Med Chir (Tokyo)*. 2016;**56**:340-4.

7. Nishijima M, Takaku A, Endo S, Kuwayama N, Koizumi F, Sato H, Owada K. Etiological evaluation of dural arteriovenous malformations of the lateral and sigmoid sinuses based on histopathological examinations. *J Neurosurg*. 1992;**76**:600-6.

8. Willinsky RA, Lasjaunias P, Terbrugge K, Burrows P. Multiple cerebral arteriovenous malformations (AVMs). Review of our experience from 203 patients with cerebral vascular lesions. *Neuroradiology*. 1990;**32**:207-10.

9. Nornes H, Grip A. Hemodynamic aspects of cerebral arteriovenous malformations. *J Neurosurg*. 1980;**53**:456-64.

10. Lawton MT, Jacobowitz R, Spetzler RF. Redefined role of angiogenesis in the pathogenesis of dural arteriovenous malformations. *J Neurosurg*. 1997;**87**:267-74.

11. Morgan MK, Johnston I, Besser M, Baines D. Cerebral arteriovenous malformations, steal, and the hypertensive breakthrough threshold. An experimental study in rats. *J Neurosurg*. 1987;**66**:563-7.

12. Herman JM, Spetzler RF, Bederson JB, Kurbat JM, Zabramski JM. Genesis of a dural arteriovenous malformation in a rat model. *J Neurosurg*. 1995;**83**:539-45.

13. Farhat HI. Cerebral arteriovenous malformations. *Dis Mon*. 2011;**57**:625-37.

14. Graf CJ, Perret GE, Torner JC. Bleeding from cerebral arteriovenous malformations as part of their natural history. *J Neurosurg*. 1983;**58**:331-7.

15. Mast H, Young WL, Koennecke HC, Sciacca RR, Osipov A, Pile-Spellman J, Hacein-Bey L, Duong H, Stein BM, Mohr JP. Risk of spontaneous haemorrhage after diagnosis of cerebral arteriovenous malformation. *Lancet*. 1997;**350**:1065-8.

16. Miyasaka Y, Yada K, Ohwada T, Kitahara T, Kurata A, Irikura K. An analysis of the venous drainage system as a factor in hemorrhage from arteriovenous malformations. *J Neurosurg*. 1992;**76**:239-43.

17. Alexander M, Patil AK, Mathew V, Sivadasan A, Chacko G, Mani SE. Recurrent craniospinal subarachnoid hemorrhage in cerebral amyloid angiopathy. *Ann Indian Acad Neurol*. 2013;**16**:97-9.

18. Fujimura M, Shimizu H, Mugikura S, Tominaga T. Delayed intracerebral hemorrhage after superficial temporal artery-middle cerebral artery anastomosis in a patient with moyamoya disease: possible involvement of cerebral hyperperfusion and increased vascular permeability. *Surg Neurol*. 2009;**71**:223-7; discussion 7.

19. Kader A, Young WL, Pile-Spellman J, Mast H, Sciacca RR, Mohr JP, Stein BM. The influence of hemodynamic and anatomic factors on hemorrhage from cerebral arteriovenous malformations. *Neurosurgery*. 1994;**34**:801-7; discussion 7-8.

20. Deruty R, Mottolese C, Soustiel JF, Pelissou-Guyotat I. Association of cerebral arteriovenous malformation and cerebral aneurysm. Diagnosis and management. *Acta Neurochir (Wien)*. 1990;**107**:133-9.

21. da Costa L, Wallace MC, Ter Brugge KG, O'Kelly C, Willinsky RA, Tymianski M. The natural history and predictive features of hemorrhage from brain arteriovenous malformations. *Stroke*. 2009;**40**:100-5.

22. Greene AK, Orbach DB. Management of arteriovenous malformations. *Clin Plast Surg*. 2011;**38**:95-106.

23. Fareed MM, Amro AA, Bayoumi Y, Orz YI, Tunio M, Maklad A, Riaz K. LINAC Stereotactic Radiosurgery for brain arteriovenous malformation: a single institutional experience from Saudi Arabia. *Neuroscience Discovery*. 2013;**1**:1.

24. Mullan S, Mojtahedi S, Johnson DL, Macdonald RL. Embryological basis of some aspects of cerebral vascular fistulas and malformations. *J Neurosurg*. 1996;**85**:1-8.

25. Houtteville JP. Brain cavernoma: a dynamic lesion. *Surg Neurol*. 1997;**48**:610-4.

26. Stevens J, Leach JL, Abruzzo T, Jones BV. De novo cerebral arteriovenous malformation: case report and literature review. *AJNR Am J Neuroradiol*. 2009;**30**:111-2.

27. Song JK, Niimi Y, Kupersmith MJ, Berenstein A. Postnatal growth and development of a cerebral arteriovenous malformation on serial magnetic resonance imaging in a child with hemangiomatosis. Case report. *J Neurosurg*. 2007;**106**:384-7.

28. Schmit BP, Burrows PE, Kuban K, Goumnerova L, Scott RM. Acquired cerebral arteriovenous malformation in a child with moyamoya disease. Case report. *J Neurosurg*. 1996;**84**:677-80.

29. Gonzalez LF, Bristol RE, Porter RW, Spetzler RF. De novo presentation of an arteriovenous malformation. Case report and review of the literature. *J Neurosurg*. 2005;**102**:726-9.

30. Bulsara KR, Alexander MJ, Villavicencio AT, Graffagnino C. De novo cerebral arteriovenous malformation: case report. *Neurosurgery*. 2002;**50**:1137-40; discussion 40-1.

31. Achrol AS, Guzman R, Varga M, Adler JR, Steinberg GK, Chang SD. Pathogenesis and radiobiology of brain arteriovenous malformations: implications for risk stratification in natural history and posttreatment course. *Neurosurg Focus*. 2009;**26**:E9.

32. Achrol AS, Pawlikowska L, McCulloch CE, Poon KY, Ha C, Zaroff JG, Johnston SC, Lee C, Lawton MT, Sidney S, Marchuk DA, Kwok PY, Young WL. Tumor necrosis factor-alpha-238G>A promoter polymorphism is associated with increased risk of new hemorrhage in the natural course of patients with brain arteriovenous malformations. *Stroke*. 2006;**37**:231-4.

33. Hashimoto T, Lam T, Boudreau NJ, Bollen AW, Lawton MT, Young WL. Abnormal balance in the angiopoietin-tie2 system in human brain arteriovenous malformations. *Circ Res*. 2001;**89**:111-3.

34. Tuente W. [CLINICAL ASPECTS AND GENETICS OF OSLER'S DISEASE]. *Z Mensch Vererb Konstitutionsl*. 1963;**37**:221-50.

35. Porteous ME, Burn J, Proctor SJ. Hereditary haemorrhagic telangiectasia: a clinical analysis. *J Med Genet*. 1992;**29**:527-30.

36. Garland HG, Anning ST. Hereditary haemorrhagic telangiectasia: a genetic and bibliographical study. *Br J Dermatol Syph*. 1950;**62**:289-310.

37. Perret G, Nishioka H. Report on the cooperative study of intracranial aneurysms and subarachnoid hemorrhage. Section VI. Arteriovenous malformations. An analysis of 545 cases of cranio-cerebral arteriovenous malformations and fistulae reported to the cooperative study. *J Neurosurg*. 1966;**25**:467-90.

38. Frugoni P, Mingrino S, Giammusso V. Association of cerebral vascualr malformations. Coexistence of arteriovenous malformations angioma and persistent carotid-basilar anastosis (primitive trigeminal artery). *Neurochirurgia (Stuttg)*. 1963;**6**:74-81.

39. Zellem RT, Buchheit WA. Multiple intracranial arteriovenous malformations: case report. *Neurosurgery*. 1985;**17**:88-93.

40. Putman CM, Chaloupka JC, Fulbright RK, Awad IA, White RI, Jr., Fayad PB. Exceptional multiplicity of cerebral arteriovenous malformations associated with hereditary hemorrhagic telangiectasia (Osler-Weber-Rendu syndrome). *AJNR Am J Neuroradiol*. 1996;**17**:1733-42.

41. Facini C, Pavlidis E, Turco EC, Pisani F. Hereditary Hemorrhagic Telangiectasia presenting as migraine: a case report. *Brain Dev*. 2015;**37**:974-7.

42. Robert T, Blanc R, Botta D, Ciccio G, Smajda S, Redjem H, Fahed R, Piotin M. Management of multiple cerebral arteriovenous malformations in a non-pediatric population. *Acta Neurochir (Wien)*. 2016;**158**:1019-25.

43. Roman G, Fisher M, Perl DP, Poser CM. Neurological manifestations of hereditary hemorrhagic telangiectasia (Rendu-Osler-Weber disease): report of 2 cases and review of the literature. *Ann Neurol*. 1978;**4**:130-44.

44. Letteboer TG, Mager HJ, Snijder RJ, Lindhout D, Ploos van Amstel HK, Zanen P, Westermann KJ. Genotype-phenotype relationship for localization and age distribution of telangiectases in hereditary hemorrhagic telangiectasia. *Am J Med Genet A*. 2008;**146a**:2733-9.

45. Krings T, Chng SM, Ozanne A, Alvarez H, Rodesch G, Lasjaunias PL. Hereditary haemorrhagic telangiectasia in children. Endovascular treatment of neurovascular malformations. Results in 31 patients. *Interv Neuroradiol*. 2005;**11**:13-23.

46. Maher CO, Piepgras DG, Brown RD, Jr., Friedman JA, Pollock BE. Cerebrovascular manifestations in 321 cases of hereditary hemorrhagic telangiectasia. *Stroke*. 2001;**32**:877-82.

47. Lux A, Salway F, Dressman HK, Kroner-Lux G, Hafner M, Day PJ, Marchuk DA, Garland J. ALK1 signalling analysis identifies angiogenesis related genes and reveals disparity between TGF-beta and constitutively active receptor induced gene expression. *BMC Cardiovasc Disord*. 2006;**6**:13.

48. Wooderchak-Donahue WL, McDonald J, O'Fallon B, Upton PD, Li W, Roman BL, Young S, Plant P, Fulop GT, Langa C, Morrell NW, Botella LM, Bernabeu C, Stevenson DA, Runo JR, Bayrak-Toydemir P. BMP9 mutations cause a vascular-anomaly syndrome with phenotypic overlap with hereditary hemorrhagic telangiectasia. *Am J Hum Genet*. 2013;**93**:530-7.

49. Goumans MJ, Lebrin F, Valdimarsdottir G. Controlling the angiogenic switch: a balance between two distinct TGF-b receptor signaling pathways. *Trends Cardiovasc Med*. 2003;**13**:301-7.

50. Bernabeu C, Blanco FJ, Langa C, Garrido-Martin EM, Botella LM. Involvement of the TGF-β superfamily signalling pathway in hereditary haemorrhagic telangiectasia. *Journal of Applied Biomedicine*. 2010;**8**:169-77.

51. Shoemaker LD, Fuentes LF, Santiago SM, Allen BM, Cook DJ, Steinberg GK, Chang SD. Human brain arteriovenous malformations express lymphatic-associated genes. *Ann Clin Transl Neurol*. 2014;**1**:982-95.

52. Jabbour MN, Elder JB, Samuelson CG, Khashabi S, Hofman FM, Giannotta SL, Liu CY. Aberrant angiogenic characteristics of human brain arteriovenous malformation endothelial cells. *Neurosurgery*. 2009;**64**:139-46; discussion 46-8.

53. Hashimoto T, Mesa-Tejada R, Quick CM, Bollen AW, Joshi S, Pile-Spellman J, Lawton MT, Young WL. Evidence of increased endothelial cell turnover in brain arteriovenous malformations. *Neurosurgery*. 2001;**49**:124-31; discussion 31-2.

54. Sure U, Butz N, Schlegel J, Siegel AM, Wakat JP, Mennel HD, Bien S, Bertalanffy H. Endothelial proliferation, neoangiogenesis, and potential de novo generation of cerebrovascular malformations. *J Neurosurg*. 2001;**94**:972-7.

55. Sonstein WJ, Kader A, Michelsen WJ, Llena JF, Hirano A, Casper D. Expression of vascular endothelial growth factor in pediatric and adult cerebral arteriovenous malformations: an immunocytochemical study. *J Neurosurg*. 1996;**85**:838-45.

56. Seker A, Yildirim O, Kurtkaya O, Sav A, Gunel M, Pamir MN, Kilic T. Expression of integrins in cerebral arteriovenous and cavernous malformations. *Neurosurgery*. 2006;**58**:159-68; discussion -68.

57. Gridley T. Notch signaling in vascular development and physiology. *Development*. 2007;**134**:2709-18.

58. Gridley T. Notch signaling during vascular development. *Proc Natl Acad Sci U S A*. 2001;**98**:5377-8.

59. Shutter JR, Scully S, Fan W, Richards WG, Kitajewski J, Deblandre GA, Kintner CR, Stark KL. Dll4, a novel Notch ligand expressed in arterial endothelium. *Genes Dev*. 2000;**14**:1313-8.

60. Uyttendaele H, Marazzi G, Wu G, Yan Q, Sassoon D, Kitajewski J. Notch4/int-3, a mammary proto-oncogene, is an endothelial cell-specific mammalian Notch gene. *Development*. 1996;**122**:2251-9.

61. Shirayoshi Y, Yuasa Y, Suzuki T, Sugaya K, Kawase E, Ikemura T, Nakatsuji N. Proto-oncogene of int-3, a mouse Notch homologue, is expressed in endothelial cells during early embryogenesis. *Genes Cells*. 1997;**2**:213-24.

62. ZhuGe Q, Wu Z, Huang L, Zhao B, Zhong M, Zheng W, GouRong C, Mao X, Xie L, Wang X, Jin K. Notch4 is activated in endothelial and smooth muscle cells in human brain arteriovenous malformations. *J Cell Mol Med*. 2013;**17**:1458-64.

63. Krebs LT, Starling C, Chervonsky AV, Gridley T. Notch1 activation in mice causes arteriovenous malformations phenocopied by ephrinB2 and EphB4 mutants. *Genesis*. 2010;**48**:146-50.

64. Kim H, Su H, Weinsheimer S, Pawlikowska L, Young WL. Brain arteriovenous malformation pathogenesis: a response-to-injury paradigm. *Acta Neurochir Suppl*. 2011;**111**:83-92.

65. Kim H, Hysi PG, Pawlikowska L, Poon A, Burchard EG, Zaroff JG, Sidney S, Ko NU, Achrol AS, Lawton MT, McCulloch CE, Kwok PY, Young WL. Common variants in interleukin-1-Beta gene are associated with intracranial hemorrhage and susceptibility to brain arteriovenous malformation. *Cerebrovasc Dis*. 2009;**27**:176-82.

66. Pawlikowska L, Tran MN, Achrol AS, McCulloch CE, Ha C, Lind DL, Hashimoto T, Zaroff J, Lawton MT, Marchuk DA, Kwok PY, Young WL. Polymorphisms in genes involved in inflammatory and angiogenic pathways and the risk of hemorrhagic presentation of brain arteriovenous malformations. *Stroke*. 2004;**35**:2294-300.

67. Achrol AS, Kim H, Pawlikowska L, Trudy Poon KY, McCulloch CE, Ko NU, Johnston SC, McDermott MW, Zaroff JG, Lawton MT, Kwok PY, Young WL. Association of tumor necrosis factor-alpha-238G>A and apolipoprotein E2 polymorphisms with intracranial hemorrhage after brain arteriovenous malformation treatment. *Neurosurgery*. 2007;**61**:731-9; discussion 40.

68. Sturiale CL, Puca A, Sebastiani P, Gatto I, Albanese A, Di Rocco C, Maira G, Pola R. Single nucleotide polymorphisms associated with sporadic brain arteriovenous malformations: where do we stand? *Brain*. 2013;**136**:665-81.

69. ApSimon HT, Reef H, Phadke RV, Popovic EA. A population-based study of brain arteriovenous malformation: long-term treatment outcomes. *Stroke*. 2002;**33**:2794-800.

70. Brown RD, Jr., Wiebers DO, Torner JC, O'Fallon WM. Incidence and prevalence of intracranial vascular malformations in Olmsted County, Minnesota, 1965 to 1992. *Neurology*. 1996;**46**:949-52.

71. Berman MF, Sciacca RR, Pile-Spellman J, Stapf C, Connolly ES, Jr., Mohr JP, Young WL. The epidemiology of brain arteriovenous malformations. *Neurosurgery*.2000;**47**:389-96; discussion 97.

72. Crawford PM, West CR, Chadwick DW, Shaw MD. Arteriovenous malformations of the brain: natural history in unoperated patients. *J Neurol Neurosurg Psychiatry*. 1986;**49**:1-10.

73. Pellettieri L, Carlsson CA, Grevsten S, Norlen G, Uhlemann C. Surgical versus conservative treatment of intracranial arteriovenous malformations: a study in surgical decision-making. *Acta Neurochir Suppl (Wien)*. 1979;**29**:1-86.

74. Abad JM, Alvarez F, Manrique M, Garcia-Blazquez M. Cerebral arteriovenous malformations. Comparative results of surgical vs conservative treatment in 112 cases. *J Neurosurg Sci*. 1983;**27**:203-10.

75. Ondra SL, Troupp H, George ED, Schwab K. The natural history of symptomatic arteriovenous malformations of the brain: a 24-year follow-up assessment. *J Neurosurg*. 1990;**73**:387-91.

76. Brown Jr RD, Wiebers DO, Forbes G, O'Fallon WM, Piepgras DG, Marsh WR, Maciunas RJ. The natural history of unruptured intracranial arteriovenous malformations. *Journal of neurosurgery*. 1988;**68**:352-7.

77. Zhao J, Wang S, Li J, Qi W, Sui D, Zhao Y. Clinical characteristics and surgical results of patients with cerebral arteriovenous malformations. *Surgical neurology*. 2005;**63**:156-61.

78. Hofmeister C, Stapf C, Hartmann A, Sciacca R, Mansmann U, Lasjaunias P, Mohr J, Mast H, Meisel J. Demographic, morphological, and clinical characteristics of 1289 patients with brain arteriovenous malformation. *Stroke*. 2000;**31**:1307-10.

79. Hladky J-P, Lejeune J-P, Blond S, Pruvo J-P, Dhellemmes P. Cerebral arteriovenous malformations in children: report on 62 cases. *Child's Nervous System*. 1994;**10**:328-33.

80. Crawford P, West C, Chadwick D, Shaw M. Arteriovenous malformations of the brain: natural history in unoperated patients. *Journal of Neurology, Neurosurgery & Psychiatry*. 1986;**49**:1-10.

81. Parkinson D, Bachers G. Arteriovenous malformations: summary of 100 consecutive supratentorial cases. *Journal of neurosurgery*. 1980;**53**:285-99.

82. Ellis JA, Mejia Munne JC, Lavine SD, Meyers PM, Connolly ES, Jr., Solomon RA. Arteriovenous malformations and headache. *J Clin Neurosci*. 2016;**23**:38-43.

83. Kendall B, Claveria L. The use of computed axial tomography (CAT) for the diagnosis and management of intracranial angiomas. *A Journal Devoted to Neuroimaging and Interventional Neuroradiology*. 1976;**12**:141-60.

84. Leblanc R, Feindel W, Ethier R. Epilepsy from cerebral arteriovenous malformations. *Canadian Journal of Neurological Sciences/Journal Canadien des Sciences Neurologiques*. 1983;**10**:91-5.

85. Spetzler RF, Martin NA. A proposed grading system for arteriovenous malformations. *J Neurosurg*. 1986;**65**:476-83.

86. Heros RC, Korosue K, Diebold PM. Surgical excision of cerebral arteriovenous malformations: late results. *Neurosurgery*. 1990;**26**:570-7; discussion 7-8.

87. Pik JH, Morgan MK. Microsurgery for small arteriovenous malformations of the brain: results in 110 consecutive patients. *Neurosurgery*. 2000;**47**:571-5; discussion 5-7.

88. Sisti MB, Kader A, Stein BM. Microsurgery for 67 intracranial arteriovenous malformations less than 3 cm in diameter. *J Neurosurg*. 1993;**79**:653-60.

89. Hamilton MG, Spetzler RF. The prospective application of a grading system for arteriovenous malformations. *Neurosurgery*. 1994;**34**:2-6; discussion -7.

90. Morgan MK, Johnston IH, Hallinan JM, Weber NC. Complications of surgery for arteriovenous malformations of the brain. *J Neurosurg*. 1993;**78**:176-82.

91. Lawton MT, Kim H, McCulloch CE, Mikhak B, Young WL. A supplementary grading scale for selecting patients with brain arteriovenous malformations for surgery. *Neurosurgery*. 2010;**66**:702-13; discussion 13.

92. Lawton MT. Spetzler-Martin Grade III arteriovenous malformations: surgical results and a modification of the grading scale. *Neurosurgery*. 2003;**52**:740-8; discussion 8-9.

93. Han PP, Ponce FA, Spetzler RF. Intention-to-treat analysis of Spetzler-Martin grades IV and V arteriovenous malformations: natural history and treatment paradigm. *J Neurosurg*. 2003;**98**:3-7.

94. Jeon HJ, Park KY, Kim SY, Lee JW, Huh SK, Lee KC. Surgical outcomes after classifying Grade III arteriovenous malformations according to Lawton's modified Spetzler-Martin grading system. *Clin Neurol Neurosurg*. 2014;**124**:72-80.

95. Neidert MC, Lawton MT, Mader M, Seifert B, Valavanis A, Regli L, Bozinov O, Burkhardt JK. The AVICH Score: A Novel Grading System to Predict Clinical Outcome in Arteriovenous Malformation-Related Intracerebral Hemorrhage. *World Neurosurg*. 2016;**92**:292-7.

96. Jiao Y, Lin F, Wu J, Li H, Wang L, Jin Z, Wang S, Cao Y. A supplementary grading scale combining lesion-to-eloquence distance for predicting surgical outcomes of patients with brain arteriovenous malformations. *J Neurosurg*. 2018;**128**:530-40.

97. Dumont TM, Kan P, Snyder KV, Hopkins LN, Siddiqui AH, Levy EI. A proposed grading system for endovascular treatment of cerebral arteriovenous malformations: Buffalo score. *Surg Neurol Int*. 2015;**6**:3.

98. Pollock BE, Brown RD, Jr. Use of the Modified Rankin Scale to assess outcome after arteriovenous malformation radiosurgery. *Neurology*. 2006;**67**:1630-4.

99. Pollock BE, Flickinger JC. Modification of the radiosurgery-based arteriovenous malformation grading system. *Neurosurgery*. 2008;**63**:239-43; discussion 43.

100. Milker-Zabel S, Kopp-Schneider A, Wiesbauer H, Schlegel W, Huber P, Debus J, Zabel-du Bois A. Proposal for a new prognostic score for linac-based radiosurgery in cerebral arteriovenous malformations. *Int J Radiat Oncol Biol Phys*. 2012;**83**:525-32.

101. Starke RM, Yen CP, Ding D, Sheehan JP. A practical grading scale for predicting outcome after radiosurgery for arteriovenous malformations: analysis of 1012 treated patients. *J Neurosurg*. 2013;**119**:981-7.

102. Hattangadi-Gluth JA, Chapman PH, Kim D, Niemierko A, Bussiere MR, Stringham A, Daartz J, Ogilvy C, Loeffler JS, Shih HA. Single-fraction proton beam stereotactic radiosurgery for cerebral arteriovenous malformations. *Int J Radiat Oncol Biol Phys*. 2014;**89**:338-46.

103. Pollock BE, Storlie CB, Link MJ, Stafford SL, Garces YI, Foote RL. Comparative analysis of arteriovenous malformation grading scales in predicting outcomes after stereotactic radiosurgery. *J Neurosurg*. 2017;**126**:852-8.

104. Spetzler RF, Martin NA. A proposed grading system for arteriovenous malformations. *Journal of neurosurgery*. 1986;**65**:476-83.

105. Krivoshapkin AL, Melidy EG. Microsurgery for cerebral arteriovenous malformation management: a Siberian experience. *Neurosurgical review*. 2005;**28**:124-30.

106. Wang S, Liu L, Zhao Y, Zhang D, Yang M, Zhao J. Evaluation of surgical microscope-integrated intraoperative near-infrared indocyanine green videoangiography during aneurysm surgery. *Neurosurgical review*. 2011;**34**:209-15.

107. Zhao J, Yu T, Wang S, Zhao Y, Yang WY. Surgical treatment of giant intracranial arteriovenous malformations. *Neurosurgery*. 2010;**67**:1359-70; discussion 70.

108. Friedlander RM. Arteriovenous malformations of the brain. *New England Journal of Medicine*. 2007;**356**:2704-12.

109. Elsenousi A, Aletich VA, Alaraj A. Neurological outcomes and cure rates of embolization of brain arteriovenous malformations with n-butyl cyanoacrylate or Onyx: a meta-analysis. *Journal of neurointerventional surgery*. 2014:neurintsurg-2014-011427.

110. Gailloud P. Endovascular treatment of cerebral arteriovenous malformations. *Tech Vasc Interv Radiol*. 2005;**8**:118-28.

111. Hartmann A, Mast H, Mohr JP, Pile-Spellman J, Connolly ES, Sciacca RR, Khaw A, Stapf C. Determinants of staged endovascular and surgical treatment outcome of brain arteriovenous malformations. *Stroke*. 2005;**36**:2431-5.

112. Elsenousi A, Aletich VA, Alaraj A. Neurological outcomes and cure rates of embolization of brain arteriovenous malformations with n-butyl cyanoacrylate or Onyx: a meta-analysis. *J Neurointerv Surg*. 2016;**8**:265-72.

113. Kalani MY, Albuquerque FC, Fiorella D, McDougall CG. Endovascular treatment of cerebral arteriovenous malformations. *Neuroimaging Clin N Am*. 2013;**23**:605-24.

114. Howington JU, Kerber CW, Hopkins LN. Liquid embolic agents in the treatment of intracranial arteriovenous malformations. *Neurosurg Clin N Am*. 2005;**16**:355-63, ix-x.

115. Lasjaunias P, Manelfe C, Terbrugge K, Ibor LL. Endovascular treatment of cerebral arteriovenous malformations. *Neurosurgical review*. 1986;**9**:265-75.

116. Donya M, Radford M, ElGuindy A, Firmin D, Yacoub MH. Radiation in medicine: Origins, risks and aspirations. *Glob Cardiol Sci Pract*. 2014;**2014**:437-48.

117. Huang Q, Li F, Liu X, Li W, Shi W, Liu FF, O'Sullivan B, He Z, Peng Y, Tan AC, Zhou L, Shen J, Han G, Wang XJ, Thorburn J, Thorburn A, Jimeno A, Raben D, Bedford JS, Li CY. Caspase 3-mediated stimulation of tumor cell repopulation during cancer radiotherapy. *Nat Med*. 2011;**17**:860-6.

118. Najafi M, Motevaseli E, Shirazi A, Geraily G, Rezaeyan A, Norouzi F, Rezapoor S, Abdollahi H. Mechanisms of inflammatory responses to radiation and normal tissues toxicity: clinical implications. *Int J Radiat Biol*. 2018:1-22.

119. Leksell L. Stereotactic radiosurgery. *Journal of Neurology, Neurosurgery & Psychiatry*. 1983;**46**:797-803.

120. Sun DQ, Carson KA, Raza SM, Batra S, Kleinberg LR, Lim M, Huang J, Rigamonti D. The radiosurgical treatment of arteriovenous malformations: obliteration, morbidities, and performance status. *International Journal of Radiation Oncology* Biology* Physics*. 2011;**80**:354-61.

121. See AP, Raza S, Tamargo RJ, Lim M. Stereotactic radiosurgery of cranial arteriovenous malformations and dural arteriovenous fistulas. *Neurosurgery clinics of North America*. 2012;**23**:133-46.

122. Souhami L, Seiferheld W, Brachman D, Podgorsak EB, Werner-Wasik M, Lustig R, Schultz CJ, Sause W, Okunieff P, Buckner J, Zamorano L, Mehta MP, Curran WJ, Jr. Randomized comparison of stereotactic radiosurgery followed by conventional radiotherapy with carmustine to conventional radiotherapy with carmustine for patients with glioblastoma multiforme: report of Radiation Therapy Oncology Group 93-05 protocol. *Int J Radiat Oncol Biol Phys*. 2004;**60**:853-60.

123. Steiner L, Lindquist C, Steiner M. Radiosurgery. *Adv Tech Stand Neurosurg*. 1992;**19**:19-102.

124. Schneider BF, Eberhard DA, Steiner LE. Histopathology of arteriovenous malformations after gamma knife radiosurgery. *Journal of neurosurgery*. 1997;**87**:352-7.

125. Szeifert G, Timperley W, Forster D, Kemeny A. Histopathological changes in cerebral arteriovenous malformations following Gamma Knife radiosurgery. Radiosurgery and Pathological Fundamentals. 20: Karger Publishers; 2007. p. 212-9.

126. Steiner L, Leksell L, Forster DM, Greitz T, Backlund EO. Stereotactic radiosurgery in intracranial arterio-venous malformations. *Acta Neurochir (Wien)*. 1974;**Suppl 21**:195-209.

127. Szeifert GT, Major O, Kemeny AA. Ultrastructural changes in arteriovenous malformations after gamma knife surgery: an electron microscopic study. *J Neurosurg*. 2005;**102**:289-92.

128. Tu J, Stoodley MA, Morgan MK, Storer KP. Responses of arteriovenous malformations to radiosurgery: ultrastructural changes. *Neurosurgery*. 2006;**58**:749-58; discussion -58.

129. Karunanyaka A, Tu J, Watling A, Storer KP, Windsor A, Stoodley MA. Endothelial molecular changes in a rodent model of arteriovenous malformation. *J Neurosurg*. 2008;**109**:1165-72.

130. Goldin-Lang P, Niebergall F, Antoniak S, Szotowski B, Rosenthal P, Pels K, Schultheiss HP, Rauch U. Ionizing radiation induces upregulation of cellular procoagulability and tissue factor expression in human peripheral blood mononuclear cells. *Thromb Res*. 2007;**120**:857-64.

131. Friedman WA, Bova FJ, Bollampally S, Bradshaw P. Analysis of factors predictive of success or complications in arteriovenous malformation radiosurgery. *Neurosurgery*. 2003;**52**:296-307; discussion -8.

132. Karlsson B, Lindquist C, Steiner L. Prediction of obliteration after gamma knife surgery for cerebral arteriovenous malformations. *Neurosurgery*. 1997;**40**:425-30; discussion 30-1.

133. Maruyama K, Kawahara N, Shin M, Tago M, Kishimoto J, Kurita H, Kawamoto S, Morita A, Kirino T. The risk of hemorrhage after radiosurgery for cerebral arteriovenous malformations. *N Engl J Med*. 2005;**352**:146-53.

134. Zabel-du Bois A, Milker-Zabel S, Huber P, Schlegel W, Debus J. Stereotactic linac-based radiosurgery in the treatment of cerebral arteriovenous malformations located deep, involving corpus callosum, motor cortex, or brainstem. *Int J Radiat Oncol Biol Phys*. 2006;**64**:1044-8.

135. Kurita H, Kawamoto S, Suzuki I, Sasaki T, Tago M, Terahara A, Kirino T. Control of epilepsy associated with cerebral arteriovenous malformations after radiosurgery. *J Neurol Neurosurg Psychiatry*. 1998;**65**:648-55.

136. Pollock BE, Gorman DA, Brown PD. Radiosurgery for arteriovenous malformations of the basal ganglia, thalamus, and brainstem. *J Neurosurg*. 2004;**100**:210-4.

137. Nagy G, Major O, Rowe JG, Radatz MW, Hodgson TJ, Coley SC, Kemeny AA. Stereotactic radiosurgery for arteriovenous malformations located in deep critical regions. *Neurosurgery*. 2011;**70**:1458-71.

138. Zhao B, Cao Y, Zhao Y, Wu J, Wang S. Functional MRI-guided microsurgery of intracranial arteriovenous malformations: study protocol for a randomised controlled trial. *BMJ Open*. 2014;**4**:e006618.

139. Vinuela F, Dion JE, Duckwiler G, Martin NA, Lylyk P, Fox A, Pelz D, Drake CG, Girvin JJ, Debrun G. Combined endovascular embolization and surgery in the management of cerebral arteriovenous malformations: experience with 101 cases. *J Neurosurg*. 1991;**75**:856-64.

140. Mathis JA, Barr JD, Horton JA, Jungreis CA, Lunsford LD, Kondziolka DS, Vincent D, Pentheny S. The efficacy of particulate embolization combined with stereotactic radiosurgery for treatment of large arteriovenous malformations of the brain. *AJNR Am J Neuroradiol*. 1995;**16**:299-306.

141. Henkes H, Nahser HC, Berg-Dammer E, Weber W, Lange S, Kuhne D. Endovascular therapy of brain AVMs prior to radiosurgery. *Neurol Res*. 1998;**20**:479-92.

142. Fournier D, TerBrugge KG, Willinsky R, Lasjaunias P, Montanera W. Endovascular treatment of intracerebral arteriovenous malformations: experience in 49 cases. *J Neurosurg*. 1991;**75**:228-33.

143. Germano IM, Davis RL, Wilson CB, Hieshima GB. Histopathological follow-up study of 66 cerebral arteriovenous malformations after therapeutic embolization with polyvinyl alcohol. *J Neurosurg*. 1992;**76**:607-14.

144. Purdy PD, Samson D, Batjer HH, Risser RC. Preoperative embolization of cerebral arteriovenous malformations with polyvinyl alcohol particles: experience in 51 adults. *AJNR Am J Neuroradiol*. 1990;**11**:501-10.

145. Hartmann A, Pile-Spellman J, Stapf C, Sciacca RR, Faulstich A, Mohr JP, Schumacher HC, Mast H. Risk of endovascular treatment of brain arteriovenous malformations. *Stroke*. 2002;**33**:1816-20.

146. Crowley RW, Ducruet AF, McDougall CG, Albuquerque FC. Endovascular advances for brain arteriovenous malformations. *Neurosurgery*. 2014;**74**:S74-S82.

147. Taylor CL, Dutton K, Rappard G, Pride GL, Replogle R, Purdy PD, White J, Giller C, Kopitnik TA, Jr., Samson DS. Complications of preoperative embolization of cerebral arteriovenous malformations. *J Neurosurg*. 2004;**100**:810-2.

148. Haw CS, terBrugge K, Willinsky R, Tomlinson G. Complications of embolization of arteriovenous malformations of the brain. *J Neurosurg*. 2006;**104**:226-32.

149. Raymond J, Iancu D, Weill A, Guilbert F, Bahary JP, Bojanowski M, Roy D. Embolization as one modality in a combined strategy for the management of cerebral arteriovenous malformations. *Interv Neuroradiol*. 2005;**11**:57-62.

150. Friedman WA, Bova FJ, Mendenhall WM. Linear accelerator radiosurgery for arteriovenous malformations: the relationship of size to outcome. *J Neurosurg*. 1995;**82**:180-9.

151. Altay T. Management of arteriovenous malformations related to Spetzler-Martin grading system. *J Neurol Surg A Cent Eur Neurosurg*. 2012;**73**:307-19.

152. Yamamoto M, Ban S, Ide M, Jimbo M. A diffuse white matter ischemic lesion appearing 7 years after stereotactic radiosurgery for cerebral arteriovenous malformations: case report. *Neurosurgery*. 1997;**41**:1405-9.

153. Yamamoto M, Hara M, Ide M, Ono Y, Jimbo M, Saito I. Radiation-related adverse effects observed on neuro-imaging several years after radiosurgery for cerebral arteriovenous malformations. *Surg Neurol*. 1998;**49**:385-97; discussion 97-8.

154. Yamamoto M, Jimbo M, Hara M, Saito I, Mori K. Gamma knife radiosurgery for arteriovenous malformations: long-term follow-up results focusing on complications occurring more than 5 years after irradiation. *Neurosurgery*. 1996;**38**:906-14.

155. Friedman WA. Stereotactic radiosurgery of intracranial arteriovenous malformations. *Neurosurg Clin N Am*. 2013;**24**:561-74.

156. Engenhart R, Wowra B, Debus J, Kimmig BN, Hover KH, Lorenz W, Wannenmacher M. The role of high-dose, single-fraction irradiation in small and large intracranial arteriovenous malformations. *Int J Radiat Oncol Biol Phys*. 1994;**30**:521-9.

157. Karlsson B, Lindquist C, Steiner L. Effect of Gamma Knife surgery on the risk of rupture prior to AVM obliteration. *Minim Invasive Neurosurg*. 1996;**39**:21-7.

158. Pollock BE, Flickinger JC, Lunsford LD, Bissonette DJ, Kondziolka D. Hemorrhage risk after stereotactic radiosurgery of cerebral arteriovenous malformations. *Neurosurgery*. 1996;**38**:652-9; discussion 9-61.

159. Levy RP, Fabrikant JI, Frankel KA, Phillips MH, Lyman JT. Charged-particle radiosurgery of the brain. *Neurosurg Clin N Am*. 1990;**1**:955-90.

160. Friedman WA, Blatt DL, Bova FJ, Buatti JM, Mendenhall WM, Kubilis PS. The risk of hemorrhage after radiosurgery for arteriovenous malformations. *J Neurosurg*. 1996;**84**:912-9.

161. Kihlstrom L, Guo WY, Karlsson B, Lindquist C, Lindqvist M. Magnetic resonance imaging of obliterated arteriovenous malformations up to 23 years after radiosurgery. *J Neurosurg*. 1997;**86**:589-93.

162. Loeffler JS, Siddon RL, Wen PY, Nedzi LA, Alexander E, 3rd. Stereotactic radiosurgery of the brain using a standard linear accelerator: a study of early and late effects. *Radiother Oncol*. 1990;**17**:311-21.

163. Flickinger JC. An integrated logistic formula for prediction of complications from radiosurgery. *Int J Radiat Oncol Biol Phys*. 1989;**17**:879-85.

164. Schultheiss TE, Orton CG, Peck RA. Models in radiotherapy: volume effects. *Med Phys*. 1983;**10**:410-5.

165. Schultheiss TE, Stephens LC. The pathogenesis of radiation myelopathy: wideningthe circle. *Int J Radiat Oncol Biol Phys*. 1992;**23**:1089-91; discussion 93-4.

166. Flickinger JC, Pollock BE, Kondziolka D, Lunsford LD. A dose-response analysis of arteriovenous malformation obliteration after radiosurgery. *Int J Radiat Oncol Biol Phys*. 1996;**36**:873-9.

167. Flickinger JC, Kondziolka D, Pollock BE, Maitz AH, Lunsford LD. Complications from arteriovenous malformation radiosurgery: multivariate analysis and risk modeling. *Int J Radiat Oncol Biol Phys*. 1997;**38**:485-90.

168. Niranjan A, Flickinger JC. Dose fractionated gamma knife radiosurgery for large arteriovenous malformations. *Neurol India*. 2017;**65**:697-8.

169. Flickinger JC, Kondziolka D, Maitz AH, Lunsford LD. An analysis of the dose-response for arteriovenous malformation radiosurgery and other factors affecting obliteration. *Radiother Oncol*. 2002;**63**:347-54.

170. O'Reilly MS, Holmgren L, Shing Y, Chen C, Rosenthal RA, Moses M, Lane WS, Cao Y, Sage EH, Folkman J. Angiostatin: a novel angiogenesis inhibitor that mediates the suppression of metastases by a Lewis lung carcinoma. *Cell*. 1994;**79**:315-28.

171. Carmeliet P. Mechanisms of angiogenesis and arteriogenesis. *Nat Med*. 2000;**6**:389-95.

172. Zou X, Zhang L, Yuan J, Yang C, Wu Z, Song J, Zhu W, Mao Y, Chen L. Endogenous hormone 2-methoxyestradiol suppresses venous hypertension-induced angiogenesis through up- and down-regulating p53 and id-1. *J Cell Mol Med*. 2018;**22**:957-67.

173. Colletti G, Dalmonte P, Moneghini L, Ferrari D, Allevi F. Adjuvant role of anti-angiogenic drugs in the management of head and neck arteriovenous malformations. *Med Hypotheses*. 2015;**85**:298-302.

174. Thiery-Vuillemin A, Theodore C, Jacobasch L, Schmitz J, Papandreou C, Guillot A, Emmanouilides C, Slimane K, Kelkouli N, Kim S, Nguyen Tan Hon T. Efficacy and Safety of Sequential Use of Everolimus in Patients With Metastatic Renal Cell Carcinoma Previously Treated With Bevacizumab With or Without Interferon Therapy: Results From the European AVATOR Study. *Clin Genitourin Cancer*. 2015;**13**:231-8.

175. Simpson DR, Mell LK, Cohen EE. Targeting the PI3K/AKT/mTOR pathway in squamous cell carcinoma of the head and neck. *Oral Oncol*. 2015;**51**:291-8.

176. Lee CZ, Yao JS, Huang Y, Zhai W, Liu W, Guglielmo BJ, Lin E, Yang GY, Young WL. Dose-response effect of tetracyclines on cerebral matrix metalloproteinase-9 after vascular endothelial growth factor hyperstimulation. *J Cereb Blood Flow Metab*. 2006;**26**:1157-64.

177. Hashimoto T, Matsumoto MM, Li JF, Lawton MT, Young WL. Suppression of MMP-9 by doxycycline in brain arteriovenous malformations. *BMC Neurol*. 2005;**5**:1.

178. Ferrara N, Hillan KJ, Novotny W. Bevacizumab (Avastin), a humanized anti-VEGF monoclonal antibody for cancer therapy. *Biochem Biophys Res Commun*. 2005;**333**:328-35.

179. Ferrara N, Hillan KJ, Gerber HP, Novotny W. Discovery and development of bevacizumab, an anti-VEGF antibody for treating cancer. *Nat Rev Drug Discov*. 2004;**3**:391-400.

180. Walker EJ, Su H, Shen F, Degos V, Amend G, Jun K, Young WL. Bevacizumab attenuates VEGF-induced angiogenesis and vascular malformations in the adult mouse brain. *Stroke*. 2012;**43**:1925-30.

181. Herbst RS, O'Neill VJ, Fehrenbacher L, Belani CP, Bonomi PD, Hart L, Melnyk O, Ramies D, Lin M, Sandler A. Phase II study of efficacy and safety of bevacizumab in combination with chemotherapy or erlotinib compared with chemotherapy alone for treatment of recurrent or refractory non small-cell lung cancer. *J Clin Oncol*. 2007;**25**:4743-50.

182. Tanvetyanon T, Murtagh R, Bepler G. Rupture of a cerebral arteriovenous malformation in a patient treated with bevacizumab. *J Thorac Oncol*. 2009;**4**:268-9.

183. Gennari A, Salvadori B, Donati S, Bengala C, Orlandini C, Danesi R, Del Tacca M, Bruzzi P, Conte PF. Cardiotoxicity of epirubicin/paclitaxel-containing regimens: role of cardiac risk factors. *J Clin Oncol*. 1999;**17**:3596-602.

184. Cathomas R, Klingbiel D, Geldart TR, Mead GM, Ellis S, Wheater M, Simmonds P, Nagaraj N, von Moos R, Fehr M. Relevant risk of carboplatin underdosing in cancer patients

with normal renal function using estimated GFR: lessons from a stage I seminoma cohort. *Ann Oncol*. 2014;**25**:1591-7.

185. Maestraggi Q, Bouattour M, Toquet S, Jaussaud R, Kianmanesh R, Durand F, Servettaz A. Bevacizumab to Treat Cholangiopathy in Hereditary Hemorrhagic Telangiectasia: Be Cautious: A Case Report. *Medicine (Baltimore)*. 2015;**94**:e1966.

186. Stein KP, Wanke I, Forsting M, Oezkan N, Huetter BO, Sandalcioglu IE, Sure U. Associated Aneurysms in Infratentorial Arteriovenous Malformations: Role of Aneurysm Size and Comparison with Supratentorial Lesions. *Cerebrovasc Dis*. 2016;**41**:219-25.

187. Redekop G, TerBrugge K, Montanera W, Willinsky R. Arterial aneurysms associated with cerebral arteriovenous malformations: classification, incidence, and risk of hemorrhage. *J Neurosurg*. 1998;**89**:539-46.

188. Hayashi S, Arimoto T, Itakura T, Fujii T, Nishiguchi T, Komai N. The association of intracranial aneurysms and arteriovenous malformation of the brain. Case report. *J Neurosurg*. 1981;**55**:971-75.

189. Al-Jehani H, Tampieri D, Cortes M, Melancon D. Re-growth of a posterior inferior cerebellar artery aneurysm after resection of the associated posterior fossa arteriovenous malformation. *Interv Neuroradiol*. 2014;**20**:61-6.

190. Reynolds MR, Arias EJ, Chatterjee AR, Chicoine MR, Cross DT, 3rd. Acute rupture of a feeding artery aneurysm after embolization of a brain arteriovenous malformation. *Interv Neuroradiol*. 2015;**21**:613-9.

191. Rammos SK, Gardenghi B, Bortolotti C, Cloft HJ, Lanzino G. Aneurysms Associated with Brain Arteriovenous Malformations. *AJNR Am J Neuroradiol*. 2016.

192. Eliava S, Dmitriev A, Shekhtman O, Yakovlev S, Kheireddin A, Pilipenko Y. Treatment of Brain Arteriovenous Malformations with Hemodynamic Aneurysms: A Series of 131 Consecutive Cases. *World Neurosurg*. 2017.

193. Narayanan M, Atwal GS, Nakaji P. Multimodality management of cerebral arteriovenous malformations. *Handb Clin Neurol*. 2017;**143**:85-96.

194. Lee CC, Chen CJ, Ball B, Schlesinger D, Xu Z, Yen CP, Sheehan J. Stereotactic radiosurgery for arteriovenous malformations after Onyx embolization: a case-control study. *J Neurosurg*. 2015;**123**:126-35.

195. Zhao J, Wang C, Wang S, Li J, Sui D, Zhao Y. Combination of intraoperative embolization with surgical resection for treatment of giant cerebral arteriovenous malformation. *Chin Med J (Engl)*. 1999;**112**:273-7.

196. Caldarelli M, Di Rocco C, Iannelli A, Rollo M, Tamburrini G, Velardi F. Combined management of intracranial vascular malformations in children. *J Neurosurg Sci*. 1997;**41**:315-24.

197. Nerva JD, Mantovani A, Barber J, Kim LJ, Rockhill JK, Hallam DK, Ghodke BV, Sekhar LN. Treatment outcomes of unruptured arteriovenous malformations with a subgroup analysis of ARUBA (A Randomized Trial of Unruptured Brain Arteriovenous Malformations)-eligible patients. *Neurosurgery*. 2015;**76**:563-70; discussion70; quiz 70.

198. Stapf C. The rationale behind "A Randomized Trial of Unruptured Brain AVMs" (ARUBA). *Acta Neurochir Suppl*. 2010;**107**:83-5.

199. Halim AX, Johnston SC, Singh V, McCulloch CE, Bennett JP, Achrol AS, Sidney S, Young WL. Longitudinal risk of intracranial hemorrhage in patients with arteriovenous malformation of the brain within a defined population. *Stroke*. 2004;**35**:1697-702.

200. Stapf C, Mast H, Sciacca RR, Choi JH, Khaw AV, Connolly ES, Pile-Spellman J, Mohr JP. Predictors of hemorrhage in patients with untreated brain arteriovenous malformation. *Neurology*. 2006;**66**:1350-5.

201. Cockroft KM. Unruptured brain arteriovenous malformations should be treated conservatively: no. *Stroke*. 2007;**38**:3310-1.

202. Brown RD, Jr. Unruptured brain AVMs: to treat or not to treat. *Lancet Neurol*. 2008;**7**:195-6.

203. Davis SM, Donnan GA. Unruptured brain arteriovenous malformations: another asymptomatic conundrum. *Stroke*. 2007;**38**:3312.

204. Knopman J, Stieg PE. Management of unruptured brain arteriovenous malformations. *Lancet*. 2014;**383**:581-3.

205. Wong J, Slomovic A, Ibrahim G, Radovanovic I, Tymianski M. Microsurgery for ARUBA Trial (A Randomized Trial of Unruptured Brain Arteriovenous Malformation)-Eligible Unruptured Brain Arteriovenous Malformations. *Stroke*. 2017;**48**:136-44.

206. Weiner GM, Grandhi R, Friedlander RM. Conservative management vs intervention for unruptured brain arteriovenous malformations. *Jama*. 2014;**312**:1057-8.

207. Cockroft KM, Jayaraman MV, Amin-Hanjani S, Derdeyn CP, McDougall CG, Wilson JA. A perfect storm: how a randomized trial of unruptured brain arteriovenous malformations' (ARUBA's) trial design challenges notions of external validity. *Stroke*. 2012;**43**:1979-81.

208. Fiehler J, Stapf C. ARUBA--beating natural history in unruptured brain AVMs by intervention. *Neuroradiology*. 2008;**50**:465-7.

209. Rutledge WC, Abla AA, Nelson J, Halbach VV, Kim H, Lawton MT. Treatment and outcomes of ARUBA-eligible patients with unruptured brain arteriovenous malformations at a single institution. *Neurosurg Focus*. 2014;**37**:E8.

210. Al-Shahi Salman R, White PM, Counsell CE, du Plessis J, van Beijnum J, Josephson CB, Wilkinson T, Wedderburn CJ, Chandy Z, St George EJ, Sellar RJ, Warlow CP. Outcome after conservative management or intervention for unruptured brain arteriovenous malformations. *Jama*. 2014;**311**:1661-9.

211. Mohr JP. Results of ARUBA are applicable to most patients with nonruptured arteriovenous malformations. *Stroke*. 2014;**45**:1541-2.

212. Bambakidis NC, Cockroft K, Connolly ES, Amin-Hanjani S, Morcos J, Meyers PM, Alexander MJ, Friedlander RM. Preliminary results of the ARUBA study. *Neurosurgery*. 2013;**73**:E379-81.

213. Mohr JP, Parides MK, Stapf C, Moquete E, Moy CS, Overbey JR, Al-Shahi Salman R, Vicaut E, Young WL, Houdart E, Cordonnier C, Stefani MA, Hartmann A, von Kummer R, Biondi A, Berkefeld J, Klijn CJ, Harkness K, Libman R, Barreau X, Moskowitz AJ. Medical management with or without interventional therapy for unruptured brain arteriovenous malformations (ARUBA): a multicentre, non-blinded, randomised trial. *Lancet*. 2014;**383**:614-21.

214. Tong X, Wu J, Lin F, Cao Y, Zhao Y, Wang S, Zhao J. Cerebellar Arteriovenous Malformations: Clinical Feature, Risk of Hemorrhage and Predictors of Posthemorrhage Outcome. *World Neurosurg*. 2016;**92**:206-17.

215. Javadpour M, Al-Mahfoudh R, Mitchell PS, Kirollos R. Outcome of microsurgical excision of unruptured brain arteriovenous malformations in ARUBA-eligible patients. *Br J Neurosurg*. 2016;**30**:619-22.

216. Potts MB, Lau D, Abla AA, Kim H, Young WL, Lawton MT. Current surgical results with low-grade brain arteriovenous malformations. *J Neurosurg*. 2015;**122**:912-20.

217. Brack SS, Dinkelborg LM, Neri D. Molecular targeting of angiogenesis for imaging and therapy. *Eur J Nucl Med Mol Imaging*. 2004;**31**:1327-41.

218. Thorpe PE. Vascular targeting agents as cancer therapeutics. *Clin Cancer Res*. 2004;**10**:415-27.

219. Juweid M, Neumann R, Paik C, Perez-Bacete MJ, Sato J, van Osdol W, Weinstein JN. Micropharmacology of monoclonal antibodies in solid tumors: direct experimental evidence for a binding site barrier. *Cancer Res*. 1992;**52**:5144-53.

220. Jain RK. Transport of molecules in the tumor interstitium: a review. *Cancer Res*. 1987;**47**:3039-51.

221. Jain RK, Baxter LT. Mechanisms of heterogeneous distribution of monoclonal antibodies and other macromolecules in tumors: significance of elevated interstitial pressure. *Cancer Res*. 1988;**48**:7022-32.

222. Epenetos AA, Snook D, Durbin H, Johnson PM, Taylor-Papadimitriou J. Limitations of radiolabeled monoclonal antibodies for localization of human neoplasms. *Cancer Res*. 1986;**46**:3183-91.

223. Denekamp J. Endothelial cell proliferation as a novel approach to targeting tumour therapy. *Br J Cancer*. 1982;**45**:136-9.

224. Thorpe PE, Burrows FJ. Antibody-directed targeting of the vasculature of solid tumors. *Breast Cancer Res Treat*. 1995;**36**:237-51.

225. Wang JM, Kumar S, Pye D, van Agthoven AJ, Krupinski J, Hunter RD. A monoclonal antibody detects heterogeneity in vascular endothelium of tumours and normal tissues. *Int J Cancer*. 1993;**54**:363-70.

226. Burrows FJ, Derbyshire EJ, Tazzari PL, Amlot P, Gazdar AF, King SW, Letarte M, Vitetta ES, Thorpe PE. Up-regulation of endoglin on vascular endothelial cells in human solid tumors: implications for diagnosis and therapy. *Clin Cancer Res*. 1995;**1**:1623-34.

227. Wakai Y, Matsui J, Koizumi K, Tsunoda S, Makimoto H, Ohizumi I, Taniguchi K, Kaiho S, Saito H, Utoguchi N, Tsutsumi Y, Nakagawa S, Ohsugi Y, Mayumi T. Effective cancer targeting using an anti-tumor tissue vascular endothelium-specific monoclonal antibody (TES-23). *Jpn J Cancer Res*. 2000;**91**:1319-25.

228. Ran S, Gao B, Duffy S, Watkins L, Rote N, Thorpe PE. Infarction of solid Hodgkin's tumors in mice by antibody-directed targeting of tissue factor to tumor vasculature. *Cancer Res*. 1998;5**8**:4646-53.

229. Kaczmarek J, Castellani P, Nicolo G, Spina B, Allemanni G, Zardi L. Distribution of oncofetal fibronectin isoforms in normal, hyperplastic and neoplastic human breast tissues. *Int J Cancer*. 1994;**59**:11-6.

230. Kosmehl H, Berndt A, Strassburger S, Borsi L, Rousselle P, Mandel U, Hyckel P, Zardi L, Katenkamp D. Distribution of laminin and fibronectin isoforms in oral mucosa and oral squamous cell carcinoma. *Br J Cancer*. 1999;**81**:1071-9.

231. Birchler MT, Milisavlijevic D, Pfaltz M, Neri D, Odermatt B, Schmid S, Stoeckli SJ. Expression of the extra domain B of fibronectin, a marker of angiogenesis, in head and neck tumors. *Laryngoscope*. 2003;**113**:1231-7.

232. Sipkins DA, Cheresh DA, Kazemi MR, Nevin LM, Bednarski MD, Li KC. Detection of tumor angiogenesis in vivo by alphaVbeta3-targeted magnetic resonance imaging. *Nat Med*. 1998;**4**:623-6.

233. Brooks PC, Montgomery AM, Rosenfeld M, Reisfeld RA, Hu T, Klier G, Cheresh DA. Integrin alpha v beta 3 antagonists promote tumor regression by inducing apoptosis of angiogenic blood vessels. *Cell*. 1994;**79**:1157-64.

234. Curnis F, Sacchi A, Corti A. Improving chemotherapeutic drug penetration in tumors by vascular targeting and barrier alteration. *J Clin Invest*. 2002;**110**:475-82.

235. Schliemann C, Neri D. Antibody-based targeting of the tumor vasculature. *Biochim Biophys Acta*. 2007;**1776**:175-92.

236. Thorpe PE, Chaplin DJ, Blakey DC. The first international conference on vascular targeting: meeting overview. *Cancer Res*. 2003;**63**:1144-7.

237. Bernardes GJ, Casi G, Trussel S, Hartmann I, Schwager K, Scheuermann J, Neri D. A traceless vascular-targeting antibody-drug conjugate for cancer therapy. *Angew Chem Int Ed Engl*. 2012;**51**:941-4.

238. Halin C, Rondini S, Nilsson F, Berndt A, Kosmehl H, Zardi L, Neri D. Enhancement of the antitumor activity of interleukin-12 by targeted delivery to neovasculature. *Nat Biotechnol*. 2002;**20**:264-9.

239. Carnemolla B, Borsi L, Balza E, Castellani P, Meazza R, Berndt A, Ferrini S, Kosmehl H, Neri D, Zardi L. Enhancement of the antitumor properties of interleukin-2 by its targeted delivery to the tumor blood vessel extracellular matrix. *Blood*. 2002;**99**:1659-65.

240. Nilsson F, Kosmehl H, Zardi L, Neri D. Targeted delivery of tissue factor to the ED-B domain of fibronectin, a marker of angiogenesis, mediates the infarction of solid tumors in mice. *Cancer Res*. 2001;**61**:711-6.

241. Bieker R, Kessler T, Schwoppe C, Padro T, Persigehl T, Bremer C, Dreischaluck J, Kolkmeyer A, Heindel W, Mesters RM, Berdel WE. Infarction of tumor vessels by NGR-peptide-directed targeting of tissue factor: experimental results and first-in-man experience. *Blood*. 2009;**113**:5019-27.

242. Huang ZJ, Zhao Y, Luo WY, You J, Li SW, Yi WC, Wang SY, Yan JH, Luo Q. Targeting the vasculature of colorectal carcinoma with a fused protein of (RGD)(3)-tTF. *ScientificWorldJournal*. 2013;**2013**:637086.

243. Storer K, Tu J, Karunanayaka A, Smee R, Short R, Thorpe P, Stoodley M. Coadministration of low-dose lipopolysaccharide and soluble tissue factor inducesthrombosis after radiosurgery in an animal arteriovenous malformation model. *Neurosurgery*. 2007;**61**:604-10; discussion 10-1.

244. Boscolo E, Pavesi G, Zampieri P, Conconi MT, Calore C, Scienza R, Parnigotto PP, Folin M. Endothelial cells from human cerebral aneurysm and arteriovenous malformation release ET-1 in response to vessel rupture. *Int J Mol Med*. 2006;**18**:813-9.

245. Matsubara S, Bourdeau A, Wallace C, Letarte M. Analysis of endoglin expression in normal brain tissue and in cerebral arteriovenous malformations. *Stroke*. 2000;**31**:2653-60.

246. Lim M, Cheshier S, Steinberg GK. New vessel formation in the central nervous system during tumor growth, vascular malformations, and Moyamoya. *Curr Neurovasc Res*. 2006;**3**:237-45.

247. Moftakhar P, Hauptman JS, Malkasian D, Martin NA. Cerebral arteriovenous malformations. Part 1: cellular and molecular biology. *Neurosurg Focus*. 2009;**26**:E10.

248. Arthur HM, Ure J, Smith AJ, Renforth G, Wilson DI, Torsney E, Charlton R, Parums DV, Jowett T, Marchuk DA, Burn J, Diamond AG. Endoglin, an ancillary TGFbeta receptor, is required for extraembryonic angiogenesis and plays a key role in heart development. *Dev Biol*. 2000;**217**:42-53.

249. Tual-Chalot S, Oh SP, Arthur HM. Mouse models of hereditary hemorrhagic telangiectasia: recent advances and future challenges. *Front Genet*. 2015;**6**:25.

250. Storer KP, Tu J, Karunanayaka A, Morgan MK, Stoodley MA. Inflammatory molecule expression in cerebral arteriovenous malformations. *J Clin Neurosci*. 2008;**15**:179-84.

251. Guo W, Karlsson B, Ericson K, Lindqvist M. Even the smallest remnant of an AVM constitutes a risk of further bleeding. *Acta neurochirurgica*. 1993;**121**:212-5.

252. Reddy R, Duong TT, Fairhall JM, Smee RI, Stoodley MA. Durable thrombosis in a rat model of arteriovenous malformation treated with radiosurgery and vascular targeting. *J Neurosurg*. 2014;**120**:113-9.

253. Storer KP, Tu J, Karunanayaka A, Morgan MK, Stoodley MA. Thrombotic molecule expression in cerebral vascular malformations. *J Clin Neurosci*. 2007;**14**:975-80.

254. Liu S, Sammons V, Fairhall J, Reddy R, Tu J, Duong TT, Stoodley M. Molecular responses of brain endothelial cells to radiation in a mouse model. *J Clin Neurosci*. 2012;**19**:1154-8.

255. Raoufi Rad N, McRobb LS, Zhao Z, Lee VS, Patel NJ, Qureshi AS, Grace M, McHattan JJ, Amal Raj JV, Duong H, Kashba SR, Stoodley MA. Phosphatidylserine Translocation after

Radiosurgery in an Animal Model of Arteriovenous Malformation. *Radiat Res*. 2017;**187**:701-7.

256. Zhao Z, Johnson MS, Chen B, Grace M, Ukath J, Lee VS, McRobb LS, Sedger LM, Stoodley MA. Live-cell imaging to detect phosphatidylserine externalization in brain endothelial cells exposed to ionizing radiation: implications for the treatment of brain arteriovenous malformations. *J Neurosurg*. 2016;**124**:1780-7.

257. Fishman AP. Endothelium: a distributed organ of diverse capabilities. *Ann N Y Acad Sci*. 1982;**401**:1-8.

258. Sammons V, Davidson A, Tu J, Stoodley MA. Endothelial cells in the context of brain arteriovenous malformations. *J Clin Neurosci*. 2011;**18**:165-70.

259. Aird WC. Phenotypic heterogeneity of the endothelium: I. Structure, function, and mechanisms. *Circ Res*. 2007;**100**:158-73.

260. Hennig B, Chow CK. Lipid peroxidation and endothelial cell injury: implications in atherosclerosis. *Free Radic Biol Med*. 1988;**4**:99-106.

261. Smits KM, Melotte V, Niessen HE, Dubois L, Oberije C, Troost EG, Starmans MH, Boutros PC, Vooijs M, van Engeland M, Lambin P. Epigenetics in radiotherapy: where are we heading? *Radiother Oncol*. 2014;**111**:168-77.

262. Miousse IR, Kutanzi KR, Koturbash I. Effects of ionizing radiation on DNA methylation: from experimental biology to clinical applications. *Int J Radiat Biol*. 2017;**93**:457-69.

263. Willson RL, Dunster CA, Forni LG, Gee CA, Kittridge KJ. Organic free radicals and proteins in biochemical injury: electron- or hydrogen-transfer reactions? *Philos Trans R Soc Lond B Biol Sci*. 1985;**311**:545-63.

264. Gilbert BC, King DM, Thomas CB. The oxidation of some polysaccharides by the hydroxyl radical: an e.s.r. investigation. *Carbohydr Res*. 1984;**125**:217-35.

265. Eldor A, Vlodavsky I, HyAm E, Atzmon R, Fuks Z. The effect of radiation on prostacyclin (PGI2) production by cultured endothelial cells. *Prostaglandins*. 1983;**25**:263-79.

266. Raymond J, Yoon SC, Ts'ao CH. Stimulation of radiation-impaired plasminogen activator release by phorbol ester in aortic endothelial cells. *Proc Soc Exp Biol Med*. 1990;**195**:213-7.

267. Sporn LA, Rubin P, Marder VJ, Wagner DD. Irradiation induces release of von Willebrand protein from endothelial cells in culture. *Blood*. 1984;**64**:567-70.

268. McRobb LS, McKay MJ, Gamble JR, Grace M, Moutrie V, Santos ED, Lee VS, Zhao Z, Molloy MP, Stoodley MA. Ionizing radiation reduces ADAM10 expression in brain microvascular endothelial cells undergoing stress-induced senescence. *Aging (Albany NY)*. 2017;**9**:1248-68.

269. Iliakis G, Wang Y, Guan J, Wang H. DNA damage checkpoint control in cells exposed to ionizing radiation. *Oncogene*. 2003;**22**:5834-47.

270. Azzam EI, Jay-Gerin JP, Pain D. Ionizing radiation-induced metabolic oxidativestress and prolonged cell injury. *Cancer Lett*. 2012;**327**:48-60.

271. Li L, Story M, Legerski RJ. Cellular responses to ionizing radiation damage. *Int J Radiat Oncol Biol Phys*. 2001;**49**:1157-62.

272. Kulkarni S, Wang TC, Guha C. Stromal Progenitor Cells in Mitigation of Non-Hematopoietic Radiation Injuries. *Curr Pathobiol Rep*. 2016;**4**:221-30.

273. Meziani L, Mondini M, Petit B, Boissonnas A, Thomas de Montpreville V, Mercier O, Vozenin MC, Deutsch E. CSF1R inhibition prevents radiation pulmonary fibrosis by depletion of interstitial macrophages. *Eur Respir J*. 2018;**51**.

274. Fajardo LF, Berthrong M. Vascular lesions following radiation. *Pathol Annu*. 1988;**23 Pt 1**:297-330.

275. Slauson DO, Hahn FF, Benjamin SA, Chiffelle TL, Jones RK. Inflammatory sequences in acute pulmonary radiation injury. *Am J Pathol*. 1976;**82**:549-72.

276. Oh CW, Bump EA, Kim JS, Janigro D, Mayberg MR. Induction of a senescence-like phenotype in bovine aortic endothelial cells by ionizing radiation. *Radiat Res*. 2001;**156**:232-40.

277. Belyakov OV, Mitchell SA, Parikh D, Randers-Pehrson G, Marino SA, Amundson SA, Geard CR, Brenner DJ. Biological effects in unirradiated human tissue induced by radiation damage up to 1 mm away. *Proc Natl Acad Sci U S A*. 2005;**102**:14203-8.

278. Brenner DJ, Doll R, Goodhead DT, Hall EJ, Land CE, Little JB, Lubin JH, Preston DL, Preston RJ, Puskin JS, Ron E, Sachs RK, Samet JM, Setlow RB, Zaider M. Cancer risks attributable to low doses of ionizing radiation: assessing what we really know. *Proc Natl Acad Sci U S A*. 2003;**100**:13761-6.

279. Molla M, Panes J, Casadevall M, Salas A, Conill C, Biete A, Anderson DC, Granger DN, Pique JM. Influence of dose-rate on inflammatory damage and adhesion molecule expression after abdominal radiation in the rat. *Int J Radiat Oncol Biol Phys*. 1999;**45**:1011-8.

280. Hallahan D, Clark ET, Kuchibhotla J, Gewertz BL, Collins T. E-selectin gene induction by ionizing radiation is independent of cytokine induction. *Biochem Biophys Res Commun*. 1995;**217**:784-95.

281. Hallahan D, Kuchibhotla J, Wyble C. Cell adhesion molecules mediate radiation-induced leukocyte adhesion to the vascular endothelium. *Cancer research*. 1996;**56**:5150-5.

282. Pober JS, Sessa WC. Evolving functions of endothelial cells in inflammation. *Nature reviews Immunology*. 2007;**7**:803.

283. Bombeli T, Karsan A, Tait JF, Harlan JM. Apoptotic vascular endothelial cells become procoagulant. *Blood*. 1997;**89**:2429-42.

284. Raoufi-Rad N, McRobb LS, Lee VS, Bervini D, Grace M, Ukath J, McHattan J, Sreenivasan VKA, Duong TTH, Zhao Z, Stoodley MA. In vivo imaging of endothelial cell adhesion molecule expression after radiosurgery in an animal model of arteriovenous malformation. *PLoS One*. 2017;**12**:e0185393.

285. Vance JE, Tasseva G. Formation and function of phosphatidylserine and phosphatidylethanolamine in mammalian cells. *Biochim Biophys Acta*. 2013;**1831**:543-54.

286. Leventis PA, Grinstein S. The distribution and function of phosphatidylserine in cellular membranes. *Annu Rev Biophys*. 2010;**39**:407-27.

287. Bevers EM, Comfurius P, Zwaal RF. Changes in membrane phospholipid distribution during platelet activation. *Biochim Biophys Acta*. 1983;**736**:57-66.

288. Thiagarajan P, Tait JF. Collagen-induced exposure of anionic phospholipid in platelets and platelet-derived microparticles. *J Biol Chem*. 1991;**266**:24302-7.

289. Fadok VA, Voelker DR, Campbell PA, Cohen JJ, Bratton DL, Henson PM. Exposure of phosphatidylserine on the surface of apoptotic lymphocytes triggers specific recognition and removal by macrophages. *J Immunol*. 1992;**148**:2207-16.

290. Kagan VE, Gleiss B, Tyurina YY, Tyurin VA, Elenstrom-Magnusson C, Liu SX, Serinkan FB, Arroyo A, Chandra J, Orrenius S, Fadeel B. A role for oxidative stress in apoptosis: oxidation and externalization of phosphatidylserine is required for macrophage clearance of cells undergoing Fas-mediated apoptosis. *J Immunol*. 2002;**169**:487-99.

291. Fadok VA, de Cathelineau A, Daleke DL, Henson PM, Bratton DL. Loss of phospholipid asymmetry and surface exposure of phosphatidylserine is required for phagocytosis of apoptotic cells by macrophages and fibroblasts. *J Biol Chem*. 2001;**276**:1071-7.

292. Fadok VA, Bratton DL, Rose DM, Pearson A, Ezekewitz RA, Henson PM. A receptor for phosphatidylserine-specific clearance of apoptotic cells. *Nature*. 2000;**405**:85-90.

293. Rimon G, Bazenet CE, Philpott KL, Rubin LL. Increased surface phosphatidylserine is an early marker of neuronal apoptosis. *J Neurosci Res*. 1997;**48**:563-70.

294. Barroso G, Taylor S, Morshedi M, Manzur F, Gavino F, Oehninger S. Mitochondrial membrane potential integrity and plasma membrane translocation of phosphatidylserine as early apoptotic markers: a comparison of two different sperm subpopulations. *Fertil Steril*. 2006;**85**:149-54.

295. Huynh ML, Fadok VA, Henson PM. Phosphatidylserine-dependent ingestion of apoptotic cells promotes TGF-beta1 secretion and the resolution of inflammation. *J Clin Invest*. 2002;**109**:41-50.

296. Ran S, Thorpe PE. Phosphatidylserine is a marker of tumor vasculature and a potential target for cancer imaging and therapy. *Int J Radiat Oncol Biol Phys*. 2002;**54**:1479-84.

297. Utsugi T, Schroit AJ, Connor J, Bucana CD, Fidler IJ. Elevated expression of phosphatidylserine in the outer membrane leaflet of human tumor cells and recognition by activated human blood monocytes. *Cancer Res*. 1991;**51**:3062-6.

298. Boersma HH, Kietselaer BL, Stolk LM, Bennaghmouch A, Hofstra L, Narula J, Heidendal GA, Reutelingsperger CP. Past, present, and future of annexin A5: from protein discovery to clinical applications. *J Nucl Med*. 2005;**46**:2035-50.

299. Rao LV, Tait JF, Hoang AD. Binding of annexin V to a human ovarian carcinoma cell line (OC-2008). Contrasting effects on cell surface factor VIIa/tissue factor activity and prothrombinase activity. *Thromb Res*. 1992;**67**:517-31.

300. Zhao J, Zhou Q, Wiedmer T, Sims PJ. Level of expression of phospholipid scramblase regulates induced movement of phosphatidylserine to the cell surface. *J Biol Chem*. 1998;**273**:6603-6.

301. Audo R, Hua C, Hahne M, Combe B, Morel J, Daien CI. Phosphatidylserine Outer Layer Translocation Is Implicated in IL-10 Secretion by Human Regulatory B Cells. *PLoS One*. 2017;**12**:e0169755.

302. Vermes I, Haanen C, Steffens-Nakken H, Reutelingsperger C. A novel assay for apoptosis. Flow cytometric detection of phosphatidylserine expression on early apoptotic cells using fluorescein labelled Annexin V. *J Immunol Methods*. 1995;**184**:39-51.

303. van Engeland M, Nieland LJ, Ramaekers FC, Schutte B, Reutelingsperger CP. Annexin V-affinity assay: a review on an apoptosis detection system based on phosphatidylserine exposure. *Cytometry*. 1998;**31**:1-9.

304. McRobb LS, Lee VS, Simonian M, Zhao Z, Thomas SG, Wiedmann M, Raj JV, Grace M, Moutrie V, McKay MJ, Molloy MP, Stoodley MA. Radiosurgery Alters the Endothelial Surface Proteome: Externalized Intracellular Molecules as Potential Vascular Targets in Irradiated Brain Arteriovenous Malformations. *Radiat Res*. 2017;**187**:66-78.

305. Munn LL, Melder RJ, Jain RK. Analysis of cell flux in the parallel plate flow chamber: implications for cell capture studies. *Biophys J*. 1994;**67**:889-95.

306. Huesa C, Helfrich MH, Aspden RM. Parallel-plate fluid flow systems for bone cell stimulation. *J Biomech*. 2010;**43**:1182-9.

307. Nauman EA, Risic KJ, Keaveny TM, Satcher RL. Quantitative assessment of steady and pulsatile flow fields in a parallel plate flow chamber. *Ann Biomed Eng*. 1999;**27**:194-9.

308. Martines E, McGhee K, Wilkinson C, Curtis A. A parallel-plate flow chamber to study initial cell adhesion on a nanofeatured surface. *IEEE Trans Nanobioscience*. 2004;**3**:90-5.

309. Frangos JA, McIntire LV, Eskin SG. Shear stress induced stimulation of mammalian cell metabolism. *Biotechnol Bioeng*. 1988;**32**:1053-60.

310. Levesque MJ, Nerem RM. The elongation and orientation of cultured endothelial cells in response to shear stress. *J Biomech Eng*. 1985;**107**:341-7.

311. Davies PF, Dull RO. How does the arterial endothelium sense flow? Hemodynamic forces and signal transduction. *Adv Exp Med Biol*. 1990;**273**:281-93.

312. Helmlinger G, Geiger RV, Schreck S, Nerem RM. Effects of pulsatile flow on cultured vascular endothelial cell morphology. *J Biomech Eng*. 1991;**113**:123-31.

313. Levesque MJ, Nerem RM, Sprague EA. Vascular endothelial cell proliferation in culture and the influence of flow. *Biomaterials*. 1990;**11**:702-7.

314. Para AN, Ku DN. A low-volume, single pass in-vitro system of high shear thrombosis in a stenosis. *Thromb Res*. 2013;**131**:418-24.

315. O'Brien S, Kent NJ, Lucitt M, Ricco AJ, McAtamney C, Kenny D, Meade G. Effective hydrodynamic shaping of sample streams in a microfluidic parallel-plate flow-assay device: matching whole blood dynamic viscosity. *IEEE Trans Biomed Eng*. 2012;**59**:374-82.

316. Lincoln B, Ricco AJ, Kent NJ, Basabe-Desmonts L, Lee LP, MacCraith BD, Kenny D, Meade G. Integrated system investigating shear-mediated platelet interactions with von Willebrand factor using microliters of whole blood. *Anal Biochem*. 2010;**405**:174-83.

317. Jain A, van der Meer AD, Papa AL, Barrile R, Lai A, Schlechter BL, Otieno MA, Louden CS, Hamilton GA, Michelson AD, Frelinger AL, 3rd, Ingber DE. Assessment of whole blood thrombosis in a microfluidic device lined by fixed human endothelium. *Biomed Microdevices*. 2016;**18**:73.

318. Westein E, de Witt S, Lamers M, Cosemans JM, Heemskerk JW. Monitoring in vitro thrombus formation with novel microfluidic devices. *Platelets*. 2012;**23**:501-9.

319. Van Kruchten R, Cosemans JM, Heemskerk JW. Measurement of whole blood thrombus formation using parallel-plate flow chambers - a practical guide. *Platelets*. 2012;**23**:229-42.

320. Dewey CF, Jr., Bussolari SR, Gimbrone MA, Jr., Davies PF. The dynamic response of vascular endothelial cells to fluid shear stress. *J Biomech Eng*. 1981;**103**:177-85.

321. Jain A, Graveline A, Waterhouse A, Vernet A, Flaumenhaft R, Ingber DE. A shear gradient-activated microfluidic device for automated monitoring of whole blood haemostasis and platelet function. *Nat Commun*. 2016;**7**:10176.

322. Dahlback B. Blood coagulation. *Lancet*. 2000;**355**:1627-32.

323. Dahlback B. Coagulation and inflammation--close allies in health and disease. *Semin Immunopathol*. 2012;**34**:1-3.

324. Spronk HM, Govers-Riemslag JW, ten Cate H. The blood coagulation system as a molecular machine. *Bioessays*. 2003;**25**:1220-8.

325. Furie B, Furie BC. The molecular basis of blood coagulation. *Cell*. 1988;**53**:505-18.

326. Mann KG, Lorand L. Introduction: blood coagulation. *Methods Enzymol*. 1993;**222**:1-10.

327. Ruggeri ZM. Mechanisms of shear-induced platelet adhesion and aggregation. *Thromb Haemost*. 1993;**70**:119-23.

328. Ruggeri ZM, Orje JN, Habermann R, Federici AB, Reininger AJ. Activation-independent platelet adhesion and aggregation under elevated shear stress. *Blood*. 2006;**108**:1903-10.

329. Orvim U, Barstad RM, Stormorken H, Brosstad F, Sakariassen KS. Immunologic quantification of fibrin deposition in thrombi formed in flowing native human blood. *Br J Haematol*. 1996;**95**:389-98.

330. Weisel JW. Structure of fibrin: impact on clot stability. *J Thromb Haemost*. 2007;**5 Suppl 1**:116-24.

331. Doolittle RF. Structural aspects of the fibrinogen to fibrin conversion. *Adv Protein Chem*. 1973;**27**:1-109.

332. Macfarlane RG. An enzyme cascade in the blood clotting mechanism, and its function as a biochemical amplifier. *Nature*. 1964;**202**:498-9.

333. Davie EW, Ratnoff OD. Waterfall sequence for intrinsic blood clotting. *Science*. 1964;**145**:1310-2.

334. Hoffman M, Monroe DM, 3rd. A cell-based model of hemostasis. *Thromb Haemost*. 2001;**85**:958-65.

335. Oliver JA, Monroe DM, Roberts HR, Hoffman M. Thrombin activates factor XI on activated platelets in the absence of factor XII. *Arterioscler Thromb Vasc Biol*. 1999;**19**:170-7.

336. Baglia FA, Walsh PN. Prothrombin is a cofactor for the binding of factor XI to the platelet surface and for platelet-mediated factor XI activation by thrombin. *Biochemistry*. 1998;**37**:2271-81.

337. Grover SP, Mackman N. Tissue Factor: An Essential Mediator of Hemostasis and Trigger of Thrombosis. *Arterioscler Thromb Vasc Biol*. 2018.

338. Furie B, Furie BC. Molecular and cellular biology of blood coagulation. *N Engl J Med*. 1992;**326**:800-6.

339. Davie EW. Biochemical and molecular aspects of the coagulation cascade. *Thromb Haemost*. 1995;**74**:1-6.

340. Zhang C, Neelamegham S. Application of microfluidic devices in studies of thrombosis and hemostasis. *Platelets*. 2017;**28**:434-40.

341. Resnick N, Yahav H, Shay-Salit A, Shushy M, Schubert S, Zilberman LC, Wofovitz E. Fluid shear stress and the vascular endothelium: for better and for worse. *Prog Biophys Mol Biol*. 2003;**81**:177-99.

342. Cunningham KS, Gotlieb AI. The role of shear stress in the pathogenesis of atherosclerosis. *Lab Invest*. 2005;**85**:9-23.

343. Malek AM, Alper SL, Izumo S. Hemodynamic shear stress and its role in atherosclerosis. *Jama*. 1999;**282**:2035-42.

344. Tateshima S, Murayama Y, Villablanca JP, Morino T, Nomura K, Tanishita K, Vinuela F. In vitro measurement of fluid-induced wall shear stress in unruptured cerebral aneurysms harboring blebs. *Stroke*. 2003;**34**:187-92.

345. Kabinejadian F, Ghista DN, Su B, Nezhadian MK, Chua LP, Yeo JH, Leo HL. Invitro measurements of velocity and wall shear stress in a novel sequential anastomotic graft design model under pulsatile flow conditions. *Med Eng Phys*. 2014;**36**:1233-45.

346. Conant CG, Nevill JT, Zhou Z, Dong JF, Schwartz MA, Ionescu-Zanetti C. Using well-plate microfluidic devices to conduct shear-based thrombosis assays. *J Lab Autom*. 2011;**16**:148-52.

347. Matsunari Y, Sugimoto M, Doi M, Matsui H, Kawaguchi M. Functional characterization of tissue factor in von Willebrand factor-dependent thrombus formation under whole blood flow conditions. *Int J Hematol*. 2016;**104**:661-8.

348. Casa LDC, Ku DN. Thrombus Formation at High Shear Rates. *Annu Rev Biomed Eng*. 2017;**19**:415-33.

349. Wain RAJ, Smith DJ, Hammond DR, Whitty JPM. Influence of microvascular sutures on shear strain rate in realistic pulsatile flow. *Microvasc Res*. 2018.

350. Asakura T, Karino T. Flow patterns and spatial distribution of atherosclerotic lesions in human coronary arteries. *Circ Res*. 1990;**66**:1045-66.

351. Pedersen EM, Agerbaek M, Kristensen IB, Yoganathan AP. Wall shear stress and early atherosclerotic lesions in the abdominal aorta in young adults. *Eur J Vasc Endovasc Surg*. 1997;**13**:443-51.

352. Schafer M, Kheyfets VO, Barker AJ, Stenmark K, Hunter KS, McClatchey PM, Buckner JK, Reece TB, Jazaeri O, Fenster BE. Reduced shear stress and associated aortic deformation in the thoracic aorta of patients with chronic obstructive pulmonary disease. *J Vasc Surg*. 2017.

353. Rossitti S, Svendsen P. Shear stress in cerebral arteries supplying arteriovenous malformations. *Acta Neurochir (Wien)*. 1995;**137**:138-45, discussion 45.

354. Errill EW. Rheology of blood. *Physiol Rev*. 1969;**49**:863-88.

355. Lok CE, Appleton D, Bhola C, Khoo B, Richardson RM. Trisodium citrate 4%--an alternative to heparin capping of haemodialysis catheters. *Nephrol Dial Transplant*. 2007;**22**:477-83.

356. Betjes MG, van Oosterom D, van Agteren M, van de Wetering J. Regional citrate versus heparin anticoagulation during venovenous hemofiltration in patients at low risk for bleeding: similar hemofilter survival but significantly less bleeding. *J Nephrol*. 2007;**20**:602-8.

357. Strazza M, Maubert ME, Pirrone V, Wigdahl B, Nonnemacher MR. Co-culture model consisting of human brain microvascular endothelial and peripheral blood mononuclear cells. *J Neurosci Methods*. 2016;**269**:39-45.

358. Urich E, Lazic SE, Molnos J, Wells I, Freskgard PO. Transcriptional profiling of human brain endothelial cells reveals key properties crucial for predictive in vitro blood-brain barrier models. *PLoS One*. 2012;**7**:e38149.

359. Weksler B, Romero IA, Couraud PO. The hCMEC/D3 cell line as a model of the human blood brain barrier. *Fluids Barriers CNS*. 2013;**10**:16.

360. Daniels BP, Cruz-Orengo L, Pasieka TJ, Couraud PO, Romero IA, Weksler B, Cooper JA, Doering TL, Klein RS. Immortalized human cerebral microvascular endothelial cells maintain the properties of primary cells in an in vitro model of immune migration across the blood brain barrier. *J Neurosci Methods*. 2013;**212**:173-9.

361. Jacob A, Potin S, Saubamea B, Crete D, Scherrmann JM, Curis E, Peyssonnaux C, Decleves X. Hypoxia interferes with aryl hydrocarbon receptor pathway in hCMEC/D3 human cerebral microvascular endothelial cells. *J Neurochem*. 2015;**132**:373-83.

362. Richards J, Larson L, Yang J, Guzman R, Tomooka Y, Osborn R, Imagawa W, Nandi S. Method for culturing mammary epithelial cells in a rat tail collagen gel matrix. *Methods in Cell Science*. 1983;**8**:31-6.

363. Engler C, Kelliher C, Speck CL, Jun AS. Assessment of attachment factors for primary cultured human corneal endothelial cells. *Cornea*. 2009;**28**:1050-4.

364. Echahdi H, El Hasbaoui B, El Khorassani M, Agadr A, Khattab M. Von Willebrand's disease: case report and review of literature. *Pan Afr Med J*. 2017;**27**:147.

365. Clemetson KJ. Platelets and primary haemostasis. *Thromb Res*. 2012;**129**:220-4.

366. Quarmby S, Kumar P, Wang J, Macro JA, Hutchinson JJ, Hunter RD, Kumar S. Irradiation induces upregulation of CD31 in human endothelial cells. *Arterioscler Thromb Vasc Biol*. 1999;**19**:588-97.

367. Hernandez-Segura A, Nehme J, Demaria M. Hallmarks of Cellular Senescence. *Trends Cell Biol*. 2018.

368. Eriksson D, Stigbrand T. Radiation-induced cell death mechanisms. *Tumour Biol*. 2010;**31**:363-72.

369. Studencka M, Schaber J. Senoptosis: non-lethal DNA cleavage as a route to deep senescence. *Oncotarget*. 2017;**8**:30656-71.

370. von Zglinicki T, Saretzki G, Ladhoff J, d'Adda di Fagagna F, Jackson SP. Human cell senescence as a DNA damage response. *Mech Ageing Dev*. 2005;**126**:111-7.

371. Roninson IB. Tumor cell senescence in cancer treatment. *Cancer Res*. 2003;**63**:2705-15.

372. Harfouche G, Martin MT. Response of normal stem cells to ionizing radiation: a balance between homeostasis and genomic stability. *Mutat Res*. 2010;**704**:167-74.

373. Tu J, Hu Z, Chen Z. Endothelial gene expression and molecular changes in response to radiosurgery in in vitro and in vivo models of cerebral arteriovenous malformations. *Biomed Res Int*. 2013;**2013**:408253.

374. Storer KP, Tu J, Stoodley MA, Smee RI. Expression of endothelial adhesion molecules after radiosurgery in an animal model of arteriovenous malformation. *Neurosurgery*. 2010;**67**:976-83; discussion 83.

375. Lunsford LD, Kondziolka D, Flickinger JC, Bissonette DJ, Jungreis CA, Maitz AH, Horton JA, Coffey RJ. Stereotactic radiosurgery for arteriovenous malformations of the brain. *J Neurosurg*. 1991;**75**:512-24.

376. Monaco EA, 3rd, Niranjan A, Kano H, Flickinger JC, Kondziolka D, Lunsford LD. Management of adverse radiation effects after radiosurgery for arteriovenous malformations. *Prog Neurol Surg*. 2013;**27**:107-18.

377. Warkentin TE, Powling MJ, Hardisty RM. Measurement of fibrinogen binding to platelets in whole blood by flow cytometry: a micromethod for the detection of platelet activation. *Br J Haematol*. 1990;**76**:387-94.

378. Lindahl TL, Festin R, Larsson A. Studies of fibrinogen binding to platelets by flow cytometry: an improved method for studies of platelet activation. *Thromb Haemost*. 1992;**68**:221-5.

379. Ashford TP, Freiman DG. Platelet aggregation at sites of minimal endothelial injury. An electron microscopic study. *Am J Pathol*. 1968;**53**:599-607.

380. Bouma BN, Meijers JC. New insights into factors affecting clot stability: A role for thrombin activatable fibrinolysis inhibitor (TAFI; plasma procarboxypeptidase B, plasma procarboxypeptidase U, procarboxypeptidase R). *Semin Hematol*. 2004;**41**:13-9.

381. Collen D, Lijnen HR. Basic and clinical aspects of fibrinolysis and thrombolysis. *Blood*. 1991;**78**:3114-24.

382. Bourey RE, Santoro SA. Interactions of exercise, coagulation, platelets, and fibrinolysis--a brief review. *Med Sci Sports Exerc*. 1988;**20**:439-46.

383. Magari Y, Mizunaga S, Ito M, Shibata T, Ito H. [Molecular marker for detecting hypercoagulable state]. *Rinsho Byori*. 1994;**42**:22-33.

384. Sakai Y, Maeda M, Takei F, Matsumoto T, Nishijima Y, Nakamura K. Determination of FDP in human plasma by a novel latex immunoassay. *Thromb Res*. 1988;**50**:469-79.

385. Moresco RN, Junior RH, Claudio Rosa Vargas L, Mariano da Rocha Silla L. Association between plasma levels of D-dimer and fibrinogen/fibrin degradation products (FDP) for exclusion of thromboembolic disorders. *J Thromb Thrombolysis*. 2006;**21**:199-202.

386. Psuja P, Zozulinska M, Turowiecka Z, Cieslikowski W, Vinazzer H, Zawilska K. Plasma markers of hypercoagulability in patients with serious infections and risk of septic shock. *Clin Appl Thromb Hemost*. 2002;**8**:225-30.

387. Thompson JA, Motzer R, Molina AM, Choueiri TK, Heath EI, Kollmannsberger CK, Redman BG, Sangha RS, Ernst DS, Pili R. Phase I studies of anti-ENPP3 antibody drug conjugates (ADCs) in advanced refractory renal cell carcinomas (RRCC). American Society of Clinical Oncology; 2015.

388. Shimada K, Uzawa K, Kato M, Endo Y, Shiiba M, Bukawa H, Yokoe H, Seki N, Tanzawa H. Aberrant expression of RAB1A in human tongue cancer. *Br J Cancer*. 2005;**92**:1915-21.

389. Kim DS, Hubbard SL, Peraud A, Salhia B, Sakai K, Rutka JT. Analysis of mammalian septin expression in human malignant brain tumors. *Neoplasia*. 2004;**6**:168-78.

390. Ramos FS, Serino LT, Carvalho CM, Lima RS, Urban CA, Cavalli IJ, Ribeiro EM. PDIA3 and PDIA6 gene expression as an aggressiveness marker in primary ductal breast cancer. *Genet Mol Res*. 2015;**14**:6960-7.

391. Sala A, Bettuzzi S, Pucci S, Chayka O, Dews M, Thomas-Tikhonenko A. Regulation of CLU gene expression by oncogenes and epigenetic factors implications for tumorigenesis. *Adv Cancer Res*. 2009;**105**:115-32.

392. Shannan B, Seifert M, Leskov K, Boothman D, Pfohler C, Tilgen W, Reichrath J. Clusterin (CLU) and melanoma growth: CLU is expressed in malignant melanoma and 1,25-dihydroxyvitamin D3 modulates expression of CLU in melanoma cell lines in vitro. *Anticancer Res*. 2006;**26**:2707-16.

393. Kristiansen G, Pilarsky C, Wissmann C, Stephan C, Weissbach L, Loy V, Loening S, Dietel M, Rosenthal A. ALCAM/CD166 is up-regulated in low-grade prostate cancer and progressively lost in high-grade lesions. *Prostate*. 2003;**54**:34-43.

394. Tachezy M, Effenberger K, Zander H, Minner S, Gebauer F, Vashist YK, Sauter G, Pantel K, Izbicki JR, Bockhorn M. ALCAM (CD166) expression and serum levels are markers for poor survival of esophageal cancer patients. *Int J Cancer*. 2012;**131**:396-405.

395. Qin H, Ni Y, Tong J, Zhao J, Zhou X, Cai W, Liang J, Yao X. Elevated expression of CRYAB predicts unfavorable prognosis in non-small cell lung cancer. *Med Oncol*. 2014;**31**:142.

396. Tian XC, Wang QY, Li DD, Wang ST, Yang ZQ, Guo B, Yue ZP. Differential expression and regulation of Cryab in mouse uterus during preimplantation period. *Reproduction*. 2013;**145**:577-85.

397. Raman B, Ramakrishna T, Rao CM. Temperature dependent chaperone-like activity of alpha-crystallin. *FEBS Lett*. 1995;**365**:133-6.

398. Takemoto L, Emmons T, Horwitz J. The C-terminal region of alpha-crystallin: involvement in protection against heat-induced denaturation. *Biochem J*. 1993;**294 (Pt 2)**:435-8.

399. Iwaki T, Iwaki A, Miyazono M, Goldman JE. Preferential expression of alpha B-crystallin in astrocytic elements of neuroectodermal tumors. *Cancer*. 1991;**68**:2230-40.

400. Iwaki T, Tateishi J. Immunohistochemical demonstration of alphaB-crystallin in hamartomas of tuberous sclerosis. *Am J Pathol*. 1991;**139**:1303-8.

401. Duguid JR, Rohwer RG, Seed B. Isolation of cDNAs of scrapie-modulated RNAs by subtractive hybridization of a cDNA library. *Proc Natl Acad Sci U S A*. 1988;**85**:5738-42.

402. Iwaki T, Iwaki A, Tateishi J, Sakaki Y, Goldman JE. Alpha B-crystallin and 27-kd heat shock protein are regulated by stress conditions in the central nervous system and accumulate in Rosenthal fibers. *Am J Pathol*. 1993;**143**:487-95.

403. Dubin R, Wawrousek E, Piatigorsky J. Expression of the murine alpha B-crystallin gene is not restricted to the lens. *Molecular and cellular biology*. 1989;**9**:1083-91.

404. Pollice AA, McCoy JP, Jr., Shackney SE, Smith CA, Agarwal J, Burholt DR, Janocko LE, Hornicek FJ, Singh SG, Hartsock RJ. Sequential paraformaldehyde and methanol fixation for simultaneous flow cytometric analysis of DNA, cell surface proteins, and intracellular proteins. *Cytometry*. 1992;**13**:432-44.

405. Hovanessian AG, Puvion-Dutilleul F, Nisole S, Svab J, Perret E, Deng JS, Krust B. The cell-surface-expressed nucleolin is associated with the actin cytoskeleton. *Exp Cell Res*. 2000;**261**:312-28.

406. Lanier LL, Warner NL. Paraformaldehyde fixation of hematopoietic cells for quantitative flow cytometry (FACS) analysis. *J Immunol Methods*. 1981;**47**:25-30.

407. Pollack A, Ciancio G. Cell cycle phase-specific analysis of cell viability using Hoechst 33342 and propidium iodide after ethanol preservation. *Methods Cell Biol*. 1990;**33**:19-24.

408. van de Winkel JG, Anderson CL. Biology of human immunoglobulin G Fc receptors. *J Leukoc Biol*. 1991;**49**:511-24.

409. Kaneko Y, Nimmerjahn F, Ravetch JV. Anti-inflammatory activity of immunoglobulin G resulting from Fc sialylation. *Science*. 2006;**313**:670-3.

410. Chang T-C, Shirato H, Aoyama H, Ushikoshi S, Kato N, Kuroda S, Ishikawa T, Houkin K, Iwasaki Y, Miyasaka K. Stereotactic irradiation for intracranial arteriovenous malformation using stereotactic radiosurgery or hypofractionated stereotactic radiotherapy. *International Journal of Radiation Oncology* Biology* Physics*. 2004;**60**:861-70.

411. Chang SD, Shuster DL, Steinberg GK, Levy RP, Frankel K. Stereotactic radiosurgery of arteriovenous malformations: pathologic changes in resected tissue. *Clin Neuropathol*. 1997;**16**:111-6.

412. Tu J, Hu Z, Chen Z. A combination of radiosurgery and soluble tissue factor enhances vascular targeting for experimental glioblastoma. *BioMed research international*. 2013;**2013**.

413. Sharma R, Huang X, Brekken RA, Schroit AJ. Detection of phosphatidylserine-positive exosomes for the diagnosis of early-stage malignancies. *Br J Cancer*. 2017;**117**:545-52.

414. Hoffman M. A cell-based model of coagulation and the role of factor VIIa. *Blood Rev*. 2003;**17 Suppl 1**:S1-5.

415. Schwoppe C, Kessler T, Persigehl T, Liersch R, Hintelmann H, Dreischaluck J, Ring J, Bremer C, Heindel W, Mesters RM, Berdel WE. Tissue-factor fusion proteins induce occlusion of tumor vessels. *Thromb Res*. 2010;**125 Suppl 2**:S143-50.

416. Kessler T, Bieker R, Padro T, Schwoppe C, Persigehl T, Bremer C, Kreuter M, Berdel WE, Mesters RM. Inhibition of tumor growth by RGD peptide-directed delivery of truncated tissue factor to the tumor vasculature. *Clin Cancer Res*. 2005;**11**:6317-24.

417. Zwaal RF, Comfurius P, Bevers EM. Surface exposure of phosphatidylserine in pathological cells. *Cell Mol Life Sci*. 2005;**62**:971-88.

418. Ohnishi S, Garfein ES, Karp SJ, Frangioni JV. Radiolabeled and near-infrared fluorescent fibrinogen derivatives create a system for the identification and repair of obscure gastrointestinal bleeding. *Surgery*. 2006;**140**:785-92.

419. Mardel SN, Saunders FM, Allen H, Menezes G, Edwards CM, Ollerenshaw L, Baddeley D, Kennedy A, Ibbotson RM. Reduced quality of clot formation with gelatin-based plasma substitutes. *Br J Anaesth*. 1998;**80**:204-7.

420. Astrup T. The biological significance of fibrinolysis. *Lancet*. 1956;**271**:565-8.

421. Gaffney PJ. Fibrin degradation products. A review of structures found in vitro and in vivo. *Ann N Y Acad Sci*. 2001;**936**:594-610.

422. Nieuwenhuizen W, Hoegee-De Nobel E, Laterveer R. A rapid monoclonal antibody-based enzyme immunoassay (EIA) for the quantitative determination of soluble fibrin in plasma. *Thromb Haemost*. 1992;**68**:273-7.

423. Koppert PW, Kuipers W, Hoegee-de Nobel B, Brommer EJ, Koopman J, Nieuwenhuizen W. A quantitative enzyme immunoassay for primary fibrinogenolysis products in plasma. *Thromb Haemost*. 1987;**57**:25-8.

424. Gaffney PJ. Fibrin Degradation Products. *Annals of the New York Academy of Sciences*. 2001;**936**:594-610.

425. Gaffney P. Subunit relationships between fibrinogen and fibrin degradation products. *Thrombosis Research*. 1973;**2**:201-17.

426. Kopeć M, Teisseyre E, Dudek-Wojciechowska G, Kloczewiak M, Pankiewicz A, Latallo Z. Studies on the “double D” fragment from stabilized bovine fibrin. *Thrombosis Research*. 1973;**2**:283-91.

427. Ljubimova JY, Fujita M, Ljubimov AV, Torchilin VP, Black KL, Holler E. Poly(malic acid) nanoconjugates containing various antibodies and oligonucleotides for multitargeting drug delivery. *Nanomedicine (Lond)*. 2008;**3**:247-65.

428. Muthu MS, Agrawal P, Singh S. Theranostic nanomedicine of gold nanoclusters: an emerging platform for cancer diagnosis and therapy. *Nanomedicine (Lond)*. 2016;**11**:327-30.

429. Varshosaz J, Sadeghi-aliabadi H, Ghasemi S, Behdadfar B. Use of magnetic folate-dextran-retinoic acid micelles for dual targeting of doxorubicin in breast cancer. *Biomed Res Int*. 2013;**2013**:680712.

430. Zhou B, Shi B, Jin D, Liu X. Controlling upconversion nanocrystals for emerging applications. *Nat Nanotechnol*. 2015;**10**:924-36.

431. Riedl S, Rinner B, Asslaber M, Schaider H, Walzer S, Novak A, Lohner K, Zweytick D. In search of a novel target - phosphatidylserine exposed by non-apoptotic tumor cells and metastases of malignancies with poor treatment efficacy. *Biochim Biophys Acta*. 2011;**1808**:2638-45.

432. Kemper EM, Boogerd W, Thuis I, Beijnen JH, van Tellingen O. Modulation of the blood-brain barrier in oncology: therapeutic opportunities for the treatment of brain tumours? *Cancer Treat Rev*. 2004;**30**:415-23.

433. Swerdlow AJ, Reddingius RE, Higgins CD, Spoudeas HA, Phipps K, Qiao Z, Ryder WD, Brada M, Hayward RD, Brook CG, Hindmarsh PC, Shalet SM. Growth hormone treatment of children with brain tumors and risk of tumor recurrence. *J Clin Endocrinol Metab*. 2000;**85**:4444-9.

434. Behin A, Hoang-Xuan K, Carpentier AF, Delattre JY. Primary brain tumours in adults. *Lancet*. 2003;**361**:323-31.

435. Motegi H, Kuroda S, Ishii N, Aoyama H, Terae S, Shirato H, Iwasaki Y. De novo formation of cavernoma after radiosurgery for adult cerebral arteriovenous malformation--case report. *Neurol Med Chir (Tokyo)*. 2008;**48**:397-400.

436. Vaquero J, Leunda G, Martinez R, Bravo G. Cavernomas of the brain. *Neurosurgery*. 1983;**12**:208-10.

437. Vaquero J, Salazar J, Martinez R, Martinez P, Bravo G. Cavernomas of the central nervous system: clinical syndromes, CT scan diagnosis, and prognosis after surgical treatment in 25 cases. *Acta Neurochir (Wien)*. 1987;**85**:29-33.

438. Nadine Herr, Maximillian Mauler, Christoph Bode, Daniel Duerschmied. Intravital microscopy of leukocyte-endothelial and platelet-leukocyte interactions in mesenterial veins in mice. *J Vis Exp.* 2015;**102**:53077.